Instituto Tecnológico y de Estudios Superiores de Monterrey

Campus Monterrey

School of Engineering and Sciences

Characterization of Arc Extinction in Direct Current Residential Circuit Breakers

A thesis presented by

Julio César Bautista Cruz

Submitted to the
School of Engineering and Sciences
in partial fulfillment of the requirements for the degree of

Master of Science
In
Energy Engineering

Monterrey Nuevo León. May 15th, 2018

Instituto Tecnológico y de Estudios Superiores de Monterrey

Campus Monterrey

School of Engineering and Sciences

The committee members, hereby, certify that have read the thesis presented by Julio César Bautista Cruz and that it is fully adequate in scope and quality as a partial requirement for the degree *of Master of Science in Energy Engineering.*

Thesis Committee:

Federico Ángel Viramontes Brown, PhD
Tecnológico de Monterrey
Principal Advisor

Carlos Iván Rivera Solorio, PhD
Tecnológico de Monterrey
Committee Member

José Carlos Suarez Guevara, M.SC
Schneider-Electric
Committee Member

Efrain Gutierrez Villanueva, M.SC
Schneider-Electric
Committee Member

Ruben Morales Menéndez, PhD
Dean of Graduate Studies
School of Engineering and Sciences

Tecnológico de Monterrey
21 MAY 2018
Dirección Nacional de Posgrado
Dr. Rubén Morales Menéndez

Monterrey Nuevo León. May 15th, 2018

Declaration of Authorship

I, Julio César Bautista Cruz, declare that this thesis titled, "*Characterization of Arc Extinction in Direct Current Residential Circuit Breakers*" and the work presented in it are my own. I confirm that:

- This work was done wholly while in candidature for the degree of Master of Science at this University.
- Where I have consulted the published work of others, this is always clearly attributed.
- Where I have quoted from the work of others, the source is always given. With the exception of such quotations, this thesis is entirely my own work.
- I have acknowledged all main sources of help.
- I have given credence to the contributions of the co-authors.

Julio César Bautista Cruz
Monterrey Nuevo León, May 2018

Dedication

To Yahveh my Lord, who has given me the life and has allowed me to consummate my master's degree, providing me the cleverness, talent, resources and especially wonderful people who motivated me to move forward.

Acknowledgment

To Osvaldo Micheloud and Federico Viramontes for calling me to be part of the *Industrial Consortium to Foster Applied Research in Mexico* and for allowing me to join this great research group.

To my advisor Federico Viramontes, for his support and advice at each stage of the project, his constant motivation despite all the obstacles encountered and mainly by all the classes taught by him, always interesting, challenging and with a well-founded purpose.

To Carlos Rivera, for his advice, suggestions, collaboration on this project, and for the careful revision of the manuscript and useful discussion.

To Efraín Gutiérrez, Mauricio Diaz, José Suarez, José Valerio, of Schneider-Electric, for supporting me in different means, in addition to the resources for carrying out this research, review of the manuscript and constant motivation.

To all my professors, since each one of their teaching were vital during the development of this research.

Everything I have accomplished, beyond my effort,
has been the result of my patience.

Julio Bautista

Contents

Abstract i
Resumen iii
List of Figures v
List of Tables ix
Lexicon xi
1. CHAPTER I 1
1.1. Introduction 1
1.2. Problem Statement 2
1.3. Objectives 2
1.4. Justification 2
1.5. Research questions 3
1.6. Scope and Limitations 3
1.7. Thesis structure 3
2. CHAPTER II 5
2.1. Characteristics of the electric arc 5
2.2. Low voltage circuit breakers 7
Interruption in LVCB 7
2.3. The Limiter Circuit Breaker 9
2.3.1 Arc breaking 9
2.3.2 Kind of breaking in established currents 10
2.3.3 Arc breaking with limitation 11
2.4. Consequences of Arcing 11
2.4.1 Contact Erosion 11
2.5. Components of CB 12
2.5.1 Frame 12
2.5.2 Contacts 13
2.5.3 Arc Chute Assembly 13
2.5.4 Operating Mechanism 14
2.5.5 Trip Unit 14

2.6. Arc manipulation 15
2.6.1. Open Gap 15
2.6.2. Arc Runner 15
2.6.3. Blowout Coils 16
2.6.4. Puffer 16
2.7. Theory of Multi-physical Fields in a Fault Arc 17
2.8. Fluid Models Magnetohydrodynamic description 19
2.9. Simulation tool. 20
2.9.1 Ansys-Fluent. 20
2.9.2 ANSYS-Maxwell. 21
2.9.3 Altair-Flux 22
3. Chapter III 25
3.1. Methodology for simulation 25
3.2. Description model 27
3.2.1 Geometry model 27
3.2.2 Mesh 27
3.2.3 Plasma properties as UDF 30
3.2.4 Interfaces and boundary conditions 33
3.2.5 Parametrization 35
3.3. Software Set-up 35
3.3.1 Set up in MHD module 35
4. Chapter IV 45
4.1. Simulations cases 45
4.2. Case A: Justification analysis 46
4.3. Case B: Base Model 47
4.4. Case C: Coupling Maxwell-Fluent 47
4.5. Case D: Coupling Flux-Fluent 48
4.6. Case E: Comparative analysis 48
5. Chapter V 49
5.1. Case A1. Justification analysis ($3D_S$ model) 49
5.2. Case A2. Justification analysis ($3D_F$ model) 51
Comparison case A1 vs case A2 52

5.3. Case B1. Base Model (laminar regimen) 53
5.4. Case B2. Base Model (turbulent regimen) 60
Comparison case B1 vs case B2 67
5.5. Case C1. Coupling Maxwell-Fluent 68
5.6. Case D1. Coupling Flux-Fluent 72
Comparison case C1 vs case D2 73
5.7. Case E1. Comparative analysis 74
Comparison case B2 vs case E1 79
6. Chapter VI 81
7. Chapter VII 85
Bibliography 87
A. Appendix A. The Physics of Electric Arc. 91
B. Appendix B. The MHD module of Ansys-Fluent. 93
C. Appendix C. User Define Functions (UDFs) 97
D. Annex D 101
E. Annex E 107
Vita 109

Characterization of Arc Extinction in Direct Current Residential Circuit Breakers

By

Julio César Bautista Cruz

Abstract.

Break the current in a direct current (DC) network is a challenging theme, since the current does not exhibit a zero crossing point, making it difficult to interrupt. Recent researches show promising results in the development of Circuit Breakers (CB) for DC, with different configurations to achieve an artificial zero crossing. However, regardless of the method, the physical effect of switching is the formation of an electric arc, causing high levels of temperature, strong magnetic fields, current of several tens of KA, added to mechanical stress and overpressure on the walls.

Due to this reason, physical phenomena should be studied to determine a suitable design. This thesis aim is to provide a methodology for the modeling and the comprehension of the physics that governs electric arc and the role of each component within the CB. To reach this, the thesis starts by understanding the arc in alternating current (AC), then proceeds to DC. A theoretical description of the electric arc is outlined, based on plasma physics.

The Magneto-Hydrodynamic (MHD) model is proposed, which allows modeling a plasma as an electric fluid, allowing coupling the equations of fluid mechanics and magnetic fields. The scope of the model is the macroscopic scale of the arc dynamics as a conducting, compressible, viscid fluid, driven by electromagnetic forces and pressure gradients. Some analysis are performed in different software and a comparative analysis is accomplished. Finally, the aim of this thesis is to provide to Schneider-Electric Company the background for this kind of analysis in DC CB.

Resumen

Interrumpir el voltaje en una red de corriente directa (DC) es un tema retador, debido a que la corriente no exhibe un cruce por cero natural, lo que dificulta la interrupción. Investigaciones recientes muestran resultados prometedores en el desarrollo de Circuit Breakers (CB) para CD, con diferentes configuraciones para lograr un cruce por cero artificial. Sin embargo, independientemente del método que se use, el efecto de la interrupción es la formación de un arco eléctrico, causando incrementos de temperatura, fuertes campos magnéticos, corrientes de varias decenas de KA, sumado a los esfuerzos mecánicos provocados por la presión en las paredes.

Por estas razones, estos fenómenos físicos deben estudiarse para determinar un diseño adecuado. Esta tesis tiene como finalidad proporcionar una metodología para el modelado y la comprensión de la física que rige el fenómeno de arco eléctrico y el papel de cada componente dentro del CB. Para llegar a esto, la tesis comienza explicando el fenómeno en corriente alterna (AC), y luego se procede en CD. Además, se describe la teórica del arco eléctrico basada en la física del plasma.

Para esto, se propone el modelo Magneto-hidrodinámico (MHD) en ANSYS-Fluent, que permite modelar un plasma como un fluido eléctrico, permitiendo el acoplamiento de las ecuaciones de la mecánica de fluidos y los campos magnéticos. El alcance del modelo es un análisis macroscópico, viendo al arco como un fluido conductor, compresible y viscoso, impulsado por fuerzas electromagnéticas y gradientes de presión. Algunos análisis se realizan en diferentes programas y se realiza un análisis comparativo entre ellos. Finalmente, el objetivo de esta tesis es proporcionar a la compañía Schneider-Electric las bases para este tipo de estudios en Circuit Brakers de CD.

List of Figures

Figure 2-1: Cathode fall [16] 5
Figure 2-2: Anode fall [16] 6
Figure 2-3 Double break rotary contact, Patent number: 8,159,319 B2. 8
Figure 2-4 the electric arc, composition of the arc column. [28] 9
Figure 2-5 Arc in extinguishing condition. a- in DC. voltage b- in AC. voltage with Ur of same sign as Ua at the time of zero current [28]. 10
Figure 2-6 equivalent circuit in a short circuit fault. 10
Figure 2-7 Frame of a Circuit Breaker [31]. 12
Figure 2-8 Straight through contacts and bow apart contacts [30]. 13
Figure 2-9 Arc chute assembly [30]. 14
Figure 2-10 Operating mechanism, a) ON position, b) OFF position [30]. 14
Figure 2-11 Thermal-Magnetic trip unit [30]. 15
Figure 2-12 Assembling of arc runners [32]. 16
Figure 2-13 Blowout coils assembling [34]. 16
Figure 2-14 Puffer type SF6 CB, a) ON position, b) OFF position [35]. 17
Figure 2-15 Interaction of physical processes in the arc column [9]. 23
Figure 3-1 Toolbox of Fluent. 25
Figure 3-2 Geometry with dimensions. 27
Figure 3-3 Overview of the full mesh (a), detailed (b). 29
Figure 3-4 Skewness of $3D_F$ mesh. 29
Figure 3-5 Orthogonal quality of $3D_F$ mesh. 29
Figure 3-6 Skewness of $3D_S$ mesh. 30
Figure 3-7 Orthogonal quality of $3D_S$ mesh. 30
Figure 3-8 Density for high temperature air [42], a) plot in TI-Nspire CX CAS software, b) plot in Excel. 31
Figure 3-9 Specific Heat for high temperature air [42], a) plot in TI Nspire CX CAS software, b) plot in Excel. 31
Figure 3-10 Thermal Conductivity for high temperature air [42], a) plot in TI-Nspire CX CAS software, b) plot in Excel. 31
Figure 3-11 Viscosity for high temperature air [42], a) plot in TI-Nspire CX CAS software, b) plot in Excel. 32
Figure 3-12 Electric Conductivity for high temperature air [42], a) plot in TI-Nspire CX CAS software, b) plot in Excel. 32
Figure 3-13 Boundary conditions on the model. 34
Figure 3-14 Modules of ANSYS Fluent. 36
Figure 3-15 Set-up MHD module. 36
Figure 3-16 Set-up of transient simulation, P1 radiation model and turbulent analysis. 37
Figure 3-17 Compilation of plasma properties. 37
Figure 3-18 Loading material properties. 37
Figure 3-19 Set-up cell zone condition. 37
Figure 3-20 Configuration of limits of the simulation. 38
Figure 3-21 Advance configurations for the solution controls. 38
Figure 3-22 Solution Methods Set-up Fluent. 38
Figure 3-23 Solution Controls Set-up Fluent. 38
Figure 3-24 Set-up of Run Calculation. 39
Figure 3-25 Toolbox of Maxwell. 39
Figure 3-26 Assignation of each zone in the geometry 39
Figure 3-27 Set-up of Magnetostatic simulation and assign of direction current in Maxwell. 40

Figure 3-28 Set-up Mesh length in Maxwell. 40
Figure 3-29 Configuration of Fluent conductivity coupling. 41
Figure 3-30 Validation check of the set-up. 41
Figure 3-31 Geometry imported from the modeler context. 41
Figure 3-32 Mesh model of the CB. 42
Figure 3-33 Configuration of the formulation model in Transient Magnetic 3D application. 42
Figure 3-34 Current applied to the model in the circuit dedicated context. 42
Figure 3-35 Importing material from material manager. 43
Figure 3-36 Assignment terminals to solid conductors. 43
Figure 3-37 Scenario to solve the MCCB extinction module model. 44
Figure 5-1 Arc movement, expressed by temperature for case A1. 50
Figure 5-2 Maximum temperature in air for case A1. 50
Figure 5-3 Arc movement, expressed by temperature for case A2. 51
Figure 5-4 Maximum temperature in air for case A2. 52
Figure 5-5 Arc movement, expressed by temperature and current density for case B1. 53
Figure 5-6 Maximum electric potential for case B1. 54
Figure 5-7 Maximum temperature in air for case B1. 55
Figure 5-8 Maximum temperature in Anode and Cathode for case B1. 56
Figure 5-9 Maximum temperature in splitter for case B1. 56
Figure 5-10 Maximum radiation temperature for walls for case B1. 57
Figure 5-11 Maximum current density in air for case B1. 58
Figure 5-12 Maximum current density at the splitter for case B1. 58
Figure 5-13 Maximum absolute pressure for case B1. 59
Figure 5-14 Arc movement, expressed by temperature and current density for case B2. 61
Figure 5-15 Maximum electric potential for case B2. 62
Figure 5-16 Maximum temperature in air for case B2. 63
Figure 5-17 Maximum temperature in Anode and Cathode for case B2. 63
Figure 5-18 Maximum temperature in splitter for case B2. 64
Figure 5-19 Maximum radiation temperature for walls for case B2. 64
Figure 5-20 Maximum current density in the air for case B2. 65
Figure 5-21 Maximum current density at the splitter for case B2. 66
Figure 5-22 Maximum absolute pressure for case B2. 66
Figure 5-23 Arc movement, expressed by temperature (left) and current density (right) for case C1. 68
Figure 5-24 Maximum temperature in Air for case C1. 69
Figure 5-25 Arc movement, expressed by Magnetic Flux Density for case C1. 70
Figure 5-26 Maximum magnetic flux density for case C1. 71
Figure 5-27 Arc movement, expressed by geometry for case D1. 72
Figure 5-28 Maximum magnetic flux density for case D1. 73
Figure 5-29 Arc movement, expressed by temperature and current density for case E1. 74
Figure 5-30 Maximum temperature in Air for case E1. 75
Figure 5-31 Maximum temperature in Anode and Cathode for case E1. 76
Figure 5-32 Maximum current density in the air for case E1. 76
Figure 5-33 Maximum current density at the splitter for case E1. 77
Figure 5-34 Maximum electric potential for case E1. 77
Figure 5-35 Maximum radiation temperature for walls for case E1. 78
Figure 5-36 Maximum absolute pressure for case E1. 79
Figure A-1 Electron trajectory in a homogeneous electric field. The trajectory is interrupted by elastic collisions with neutral atoms.[45] 92
Figure B-1 Modules of ANSYS Fluent. 95

Figure C-1 Grid components [41]. *98*
Figure C-2 Example of UDF codification. *99*
Figure D-1 Arc movement images from reference [9]. *101*
Figure D-2 Arc movement, (temperature and current density) for case B1. ..... *102*
Figure D-3 Arc movement, (temperature and current density) for case B2. ..... *103*
Figure D-4 Arc movement, (temperature and current density) for case C1. ..... *104*
Figure D-5 Arc movement, (temperature and current density) for case E1. ..... *105*

List of Tables

Table 2-1 Minimum voltage and current in different materials 6
Table 3-1 Description of the $3D_F$ mesh 28
Table 3-2 Description of the $3D_S$ mesh. 28
Table 3-3 Boundary conditions applied in the model 33
Table 4-1 Cases analyzed 45
Table B-1 User-Define Scalars in MHD Model 95
Table C-1 Grid nomenclature. 98

Lexicon

2D. Bi-dimensional
3D. Tri-dimensional
$3D_F$. Tridimensional analysis full
$3D_S$. Tridimensional analysis simplified
AC. Alternating current
Arc chute. Series of plates in the path of that arc that split it up into smaller segments
Arc column. Region where the ions and electrons circulate through a column of ionized gases and metallic vapors, this zone is considered as quasi-neutral fluid.
Arc root. Short segment of the electric arc, where the arc surges from the cathode or the anode.
B. Magnetic flux density
CB. Circuit Breaker
CFD. Computerized Fluid Dynamics.
Contact. Static or dynamic elements, which allow current to flow between them.
DC. Direct current
Drift velocity. Average velocity that a particle, such as an electron, attains in a material due Electric arc
HVCB. High Voltage Circuit Breaker.
Ionization. Process by which an atom or a molecule acquires a negative or positive charge by gaining or losing electrons to form ions.
J. Current density
Lorentz force. Combination of electric and magnetic force on a point charge due to electromagnetic fields.
LTE. Local Thermic Equilibrium.
LVCB. Low Voltage Circuit Breaker.
MCCB. Molded Case Circuit Breaker.
MVCB. Medium Voltage Circuit Breaker
P. Pressure
Plasma. Fourth state of the matter, created by the ionization of a gas.
T. Temperature
Terminals. Extreme of the current path in the circuit breaker.
Trip unit. Module of a circuit breaker that sends a signal to interrupt the current through the circuit.

CHAPTER I

1.1. Introduction

At present, it is well known that the growth in the generation of electric power systems, the emergence of renewable sources and the need for reliable power distribution systems have caused to reconsider the use of direct current (DC) instead of alternating current (AC). This new approach is taken because of the different benefits of the DC distribution and interconnection with renewable energy sources, control systems, train systems and construction industry, to name a few.

On the other hand, DC-based systems are defenseless against faults in the transmission and distribution lines, which can lead to the destruction of electronic devices instantly [1], [2]. For this reason, it is necessary to detect faults in the network to achieve a quick interruption of high levels of currents. To make the rapid detection and interruption of current, devices known as Circuit Breakers (CB) are used, which can detect overcurrent levels and open immediately to stop the current.

However, achieving this interruption in a DC line can be complicated, since the key to carry through this is an absent primordial element, which is zero crossing point. Given that this element does not exist in DC, procedures to force this artificially cross must be implemented. Fortunately for voltages at residential levels (120V in AC), the CB just must generate and maintain an arc voltage which in turn causes the arc to collapse and interrupt the current.

In the case of voltages over the residential level, there are several papers referred to DCCB, which have developed different methods to switch current, some are: current injection in reverse through parallel capacitor [3]; Ballistic CB with resistors in series to distribute the arc [4]; mechanical contacts with high speed actuators [5]; interruption of arc by transverse or axial magnetic fields [6], [7]; use of inductors for automatic detection of arcs [8], to mention a few of the most recent methods used.

Regardless of the method, the physical effect of switching is the formation of an electric arc within the CB, causing high levels of temperature, strong magnetic fields, current of several tens of KA, added to mechanical stress and overpressure on the walls. Due to these reasons, physical phenomena should be studied to determine a suitable design.

For the purpose of this project, the electric arc will be modeling through a Computational Fluid Dynamics (CFD) software, coupling the Maxwell equations for electromagnetic fields and the Navier Stokes equations. For this coupling, the software of ANSYS (Fluent, Maxwell) and ALTAIR-FLUX will be used. Important research about arc modeling have been studying in [9], [10], [11], where the simulation processes are explained in great detail, exposing results such as voltages, currents, pressures and temperatures. In the case of [9] experimental tests are also carried out.

1.2. Problem Statement

Currently there is a lot of information related to modeling the electric arc, however, nowhere is the simulation process that need to be followed for the correct characterization. For this reason, it is necessary to give an answer and propose the methodology to follow for the correct simulation related to the interruption of a DC short circuit fault, detailing the steps and the initial and boundary conditions in the model. The simulation must include the levels due to temperatures and pressures in the CB.

1.3. Objectives

The main objective here involves the simulation of the thermal and magnetic phenomena produced by the interruption process during a short circuit fault in a DC CB.

Particularly objectives are intended to cover the following points:

- Development of a suitable methodology to characterize the electric arc using the MHD module of Fluent.
- Perform a coupling between Maxwell-Fluent and Flux-Fluent to obtain the magnetic flux density (**B**).
- Determine the maximum values of temperature and overpressure reached within the CB. Conduct a comparison of results with [9].
- Use the MHD methodology in a static model (no electrodes movement) using a simplified CB geometry.

The thesis mentioned in reference [9] has been chosen as a comparison, since it offers a geometry easy to analyze, the methodology and boundary conditions are presented in detail, as well as offering simulation results together with experimental tests.

1.4. Justification

It is necessary to know the physics that governs the electric arc phenomenon. Also, it is expected to know the interaction of the components and meet the performance of the CB during an arc extinction, which requires the application of specialized software that allows characterizing such phenomena.

This thesis proposal is made to develop a project raised by Schneider Electric Company, which previously has been tested successfully for adaptations of CB from AC to DC at medium voltage level (Compact NSX DC & DC PV model), however, now the purpose is in residential level (low voltage). Considering that nowadays they have a functional design of an AC CB (QO model), this is a standard thermal-magnetic to 15 and 20 amperes CB, which can provide overload and short-circuit protection for conductors [12].

It is expected that the results of this thesis can help to understand the electric arc phenomenon and the improvement of a DC CB at residential level.

1.5. Research questions

1. What is an electric arc and what are the physical properties that it presents (electrical conductivity, viscosity, density, etc.)?
2. What is a Breaker, features and components?
3. What are the consequences of arc extinction within a Breaker?
4. What are the main factors that intervene during the formation of an electric (temperatures, current levels) arc and how an electric arc can be modeled?

1.6. Scope and Limitations

The scope of this investigation begins by understanding the physical phenomena in CB for AC (bibliographic research), then proceed in DC, this includes equations that govern the electric arc, modeling of the magnetic forces, arc power, thermal energy and fluid flow. Once these points were covered, the simulation of a static CB is done (2D and 3D). Verifying its correct performance, through comparisons with the results from [9].

Some of the most critical limitations of the project are, the LVCB is the most difficult to simulate [13], because current is difficult to maintain during simulations. Here, further phenomena such as arc motion along rail electrodes, arc birth, eddy currents, and the interaction between the arc and the external circuit have not been considered (as a simplification). In addition, all effects are strongly coupled and cannot be validated separately, unfortunately, there is not good arc simulation tool available on the market. Industrial researchers typically couple different tools, Fluent + electromagnetic solver, for example: Fluent + MpCCI + ANSYS EMAG [14]. Therefore, the biggest limiting will be achieving a good coupling of the different tools for modeling the arc.

1.7. Thesis structure

This thesis is divided into 7 chapters. Chapter 1 describes the justification, objectives, and scope of the project. Chapter 2 deals with the characteristics of the electric arc, consequences of interruption, explanation of CBs, as well as their operation. Subsequent to this, the theory for the modeling of the electric arc is also described, as well as the necessary simplifications.

In Chapter 3, the methodology for the simulation is explained. The model to be used is defined, such as geometry, mesh, and boundary conditions. Also, the setup is explicated for each of the software used. In chapter 4 all the cases to be analyzed are described, where the modifications of each one are exposed and what is expected to be obtained. After that, in chapter 5 the results of the simulations are presented, the results are described in addition to the variations with respect to each case. Here the results are presented in terms of graphs and contours.

In chapter 6 the conclusions of this thesis are presented, starting with a summary of chapter 1-4 and later highlighting the most important results of chapter 5. Finally, in chapter 7 the future works are presented based on what was developed in this thesis.

CHAPTER II

2.1. Characteristics of the electric arc

The internal arc fault is a very severe short-circuit fault that can occur in electrical equipment [15]. In a conventional way, the current flows in a solid conductor; when **an** arc fault occurs, this current flows through the air between two conductors (anode-cathode).

In one side the cathode contact provides the electrons to allow the arc to continue between the contacts (Figure 2-1). The cathode region can be described with a high electric field of 10^8-10^9 volts/meter. In general, the electron emission involves a combination of thermally enhanced field emission (T-F emission) and the effects of ion bombardment. In the cathode fall region, about 90% of the current is carried by electron and 10% is carried by ions. The voltage drop in the cathode fall is approximately 15 volts. Cathode temperature is comparable the boiling point of contact material. The high electron emission is produced by heat and enhanced field emission. The current density of the spot is about 10^3-10^6 A/cm^2 [16].

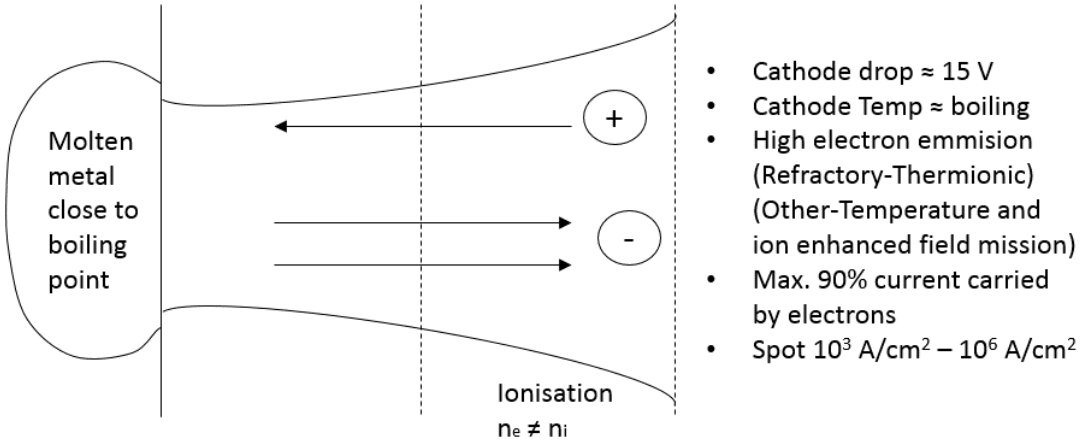

Figure 2-1: Cathode fall [16]

The arc column has the characteristics of a plasma. The density of the electrons and ions are equal. In addition, the temperature of the electron and ions are equal to the gas temperature [16].

On the other hand, the anode region serves to collect**s** the electrons carrying the current from the arc column (Figure 2-2). The thermal boundary layer between the arc column and the anode surface is small. The electron density gradients are high so that electron diffusion flow exists. The anode fall voltages can be close to zero and as high as 15-20 volts. The anode fall temperature is about 200-degrees C up to the boiling point of the contact material. The current is carried by electrons and anode spot current density is less than that of the cathode spot.

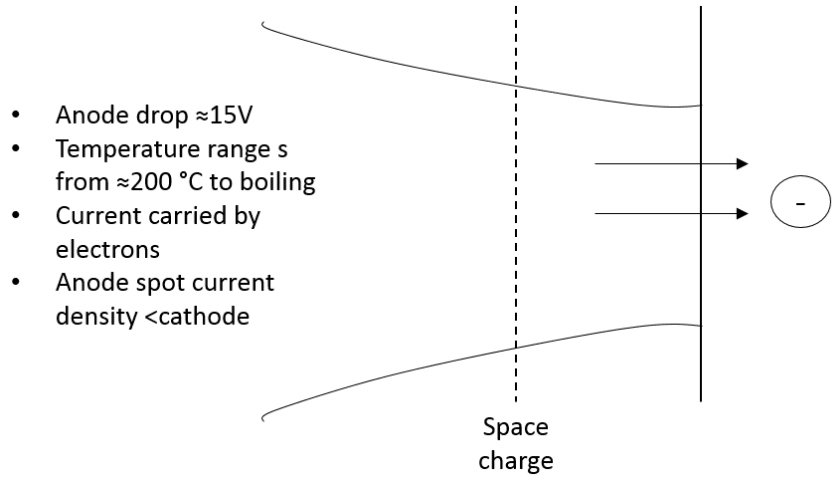

Figure 2-2: Anode fall [16]

When a fault is detected in an AC network, the CB starts to open to break the current, during this process an electric arc is built between opening contacts, which must be maintained to achieve a successful current interruption.

Nevertheless, many conditions are necessary to attain this. Thus, the arc is ignited. The arc cannot exist if the arc current is lower than the minimum arc current. The value of this is a characteristic of the contact material, [16]. When the arc starts, the arc voltage must have a minimum value, this can be determined by the current magnitude, the gap width, and the orientations of electrodes [17].

An already established arc requires a continuous flow of electrons from the cathode to be sustained. Below some minimum value $I_A \leq I_{min}$, the energy losses will exceed the introduced energy to the cathode and the arc will be extinguished.

A minimum voltage, U_{min}, is also required across the open contacts to sustain the arc. The electric arc would at least require a voltage that corresponds to the ionization potential of the gas, V_i, and the work function voltage, U_ϕ, of the cathode contact. It is, therefore, reasonable to assume that [18]:

$$U_{min} \approx V_i + U_\phi$$

Calculated values for $V_i + U_\phi$ is compared to measured value for U_{min} and I_{min} for different contact materials in Table 2-1.

Table 2-1 Minimum voltage and current in different materials

	V_i *(volts)*	V_ϕ *(volts)*	$V_i + V_\phi$ *(volts)*	V_{min} *(volts)*	I_{min} *(Amperes)*
Al	5.98	4.10	10.08	11.2	0.4
Ag	7.57	4.74	12.31	12	0.4
Cu	7.72	4.72	12.19	13	0.4
Fe	7.90	4.63	12.53	12.5	0.45

During a circuit fault, the CB is turned off or is tripped, this interrupts the flow of current by separating its contacts. The current through the conductors of the CB generates a magnetic field in the arc chamber.

The electromagnetic and thermal forces of the arc are supplemented to force the arc away from the contact region along arc runners and directly into the arc chutes. This assembly is made up of several "U" shaped steel plates that surround the contacts. As the arc develops, it is drawn into the arc chute where it is divided into smaller arcs, which are extinguished faster. Minimizing the arc is important for two reasons. First, arcing can damage the contacts. Second, the arc ionizes gases inside the molded case [15].

In turn, the current is reduced. Therefore, the arc cannot be maintained. The resistance of the arc and the arc voltage can be varied by increasing the length of the arc, cooling the arc and splitting the arc into a number of series arcs [16]. For more information about the arc physics, consult annex A.

2.2. Low voltage circuit breakers

A circuit breaker is a device designed not only to protect the load and cables but also for safety and security of the human life. All circuit breakers protect the circuit conductors mainly by detecting and interrupting the overcurrent [19]–[23].

The opening of the circuit breaker is a reaction to situations of transient current, such as short circuits or faults in the electrical system. The circuit breakers are classified according to the available interruption capacity and the nominal direct current (Low-voltage circuit breakers, Molded Case Circuit Breakers, (MCCB), Low Voltage Power Circuit Breakers (LVPCB), Isolated Circuit Breakers (ICCB), Mini Circuit Breakers (MCB) to mention a few) [24].

The interrupting capacity of a circuit breaker is the maximum short-circuit current that the circuit breaker can safely interrupt at a defined voltage. This short-circuit current described by current magnitude and its value is in symmetrical amperes rms. The amount of current that a circuit breaker can transmit until it reaches the overload conditions and opens the circuit is defined as the DC classification [25], [26],[27].

Interruption in LVCB

At low voltage, the LVCBs are the most important devices for the extinction of electric arc. Most of them are very similar in layout design and structure, even though some differences exist. This way, the general layout of a conventional LVCB can be seen in Figure 2-3, including the following components:

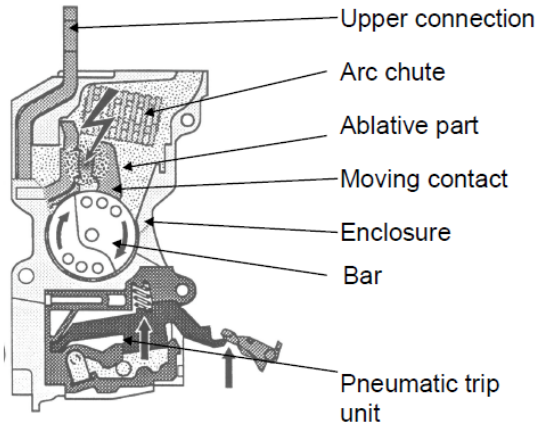

Figure 2-3 Double break rotary contact, Patent number: 8,159,319 B2.

- Upper connection: To connect the circuit breaker with the electrical circuit.
- Fixed and movable contacts: where the electric arc is formed when these contacts separate physically.
- Arc chamber and splitter plates stack: it is constituted by several plates, arranged in parallel between them. The aim is to split the arc into smaller arcs, in order to lengthen and extinguish it. In some references, the arc chamber is also known as arc chute.

Talking about conventional CB, generally use air for current interruption, with little differences in details and components, the general construction is showed in Figure 2-3, includes: the main contacts designed to carry the current under normal operating conditions, the arcing contacts (also called rails) the arc chamber, enclosure and the trip unit. In many cases, the geometry of the current carrying parts produces a magnetic force that moves the arc into the chamber. This way, some designs use coils for increasing the magnetic force, while others help the arc by blowing air [9].

The typical sequence in a LV conventional air circuit breaker is the following:

- The main contacts open while the arc contacts remain closed.
- The arcing contacts open and the arc starts to move along their length.
- The magnetic force produced by the arc current or by blowing coils moves the arc to the arc chamber.
- The arc is divided into several small arcs in series, by the plates of the arc chamber.
- The arc chamber allows cooling the arc, lengthening and narrowing its section until the current is interrupted.
- The arc chamber enables the ionization products to be dissipated or absorbed, restoring the dielectric strength in the air space between the contacts.

The conventional LVCBs described establish the arc in the interrupting medium, air in most LV switches, and maintain it until the next natural zero current for AC cases or until the voltage drop of the arc rises above circuit's voltage for DC cases. Then, the arc is extinguished [9].

2.3. The Limiter Circuit Breaker

As was mentioned below, to achieve a successful interruption, a CB must generate an arc voltage which in turn causes the arc to collapse. This kind of CB is known as Limiting Circuit-Breaker. A current limitation is achieved by making use of the arc voltage under fault conditions. This arc must be well managed, that is to say:

- The arc voltage must be sufficient value to facilitate high limitation and rapid extinction,
- Dielectric regeneration properties when the arc current reaches zero.

Further, the limiting CB must exhibit several properties under high short-circuit currents:

- A minimum current to ensure contact repulsion
- A transitive energy value,
- A short arc voltage duration,
- A maximum value of arc voltage, which is independent of the fault current.

The model also must take into account the external parameters of electric network being considered: voltage, frequency, short-circuit level, number of phases, etc. [28].

2.3.1 Arc breaking

The arc corresponds to a 4th physical condition: plasma. As soon as two contacts separate, one of them (cathode) transmits electrons and the other one (anode) receives them, and since electronic emission is by its very nature energy generating, the cathode will be hot (Figure 2-4). Resulting in arc stagnation which can give rise to metallic vapors. These vapors and the ambient gas will then be ionized, hence [28]:

- more free electrons;
- creation of positive ions which drop back on the cathode, thus maintaining its high temperature;
- creation of negative ions which bombard the anode causing temperature to rise.

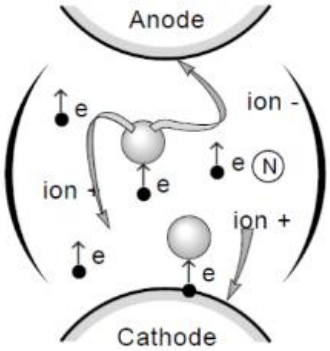

Figure 2-4 the electric arc, composition of the arc column. [28]

This natural phenomenon, once controlled, proved to be an irreplaceable intermediary for current breaking. Breaking control must relate to at least two specific arc-related aspects:

- Arc voltage helps reduce current strength and,
- Arc extinguishing conditions when the current moves to zero are met if dielectric regeneration is quickly achieved.

This regeneration must take place despite the presence of mains voltage and of the overvoltage phenomenon due to the circuit stray capacity (transient recovery voltage or TRV). The Figure 2-5 shows the TRV on breaking of DC and AC current. Consult annex A for more details about the arc physics.

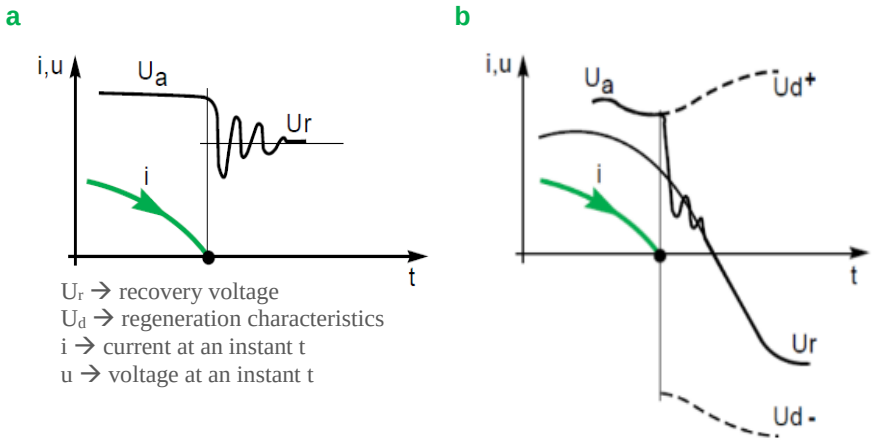

Figure 2-5 Arc in extinguishing condition. **a**- in DC. voltage **b**- in AC. voltage with Ur of same sign as Ua at the time of zero current [28].

2.3.2 Kind of breaking in established currents

In both cases considered below (AC or DC), the current is in steady state before breaking.

In a DC voltage

As soon as the contacts open, an arc voltage appears and the current will start to decrease. The equation governing the circuit becomes:

$$U_r(t) - Ri - L\frac{di}{dt} - U_a(t) = 0 \qquad Ec.\ 2\text{-}1$$

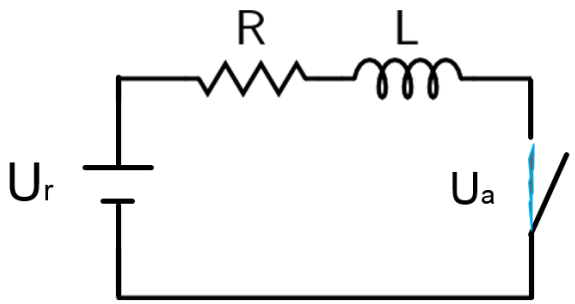

Figure 2-6 equivalent circuit in a short circuit fault.

It appears that current *i* cannot be forced to 0 unless arc voltage U_a becomes and remains greater than mains voltage *E*. Since the arc voltage is greater than mains voltage when the current is canceled, the resulting dielectric regeneration is problem free. Figure 2-6 shows an equivalent short-circuit fault.

In an AC voltage

In this case, the steady state current passes regularly via the zero value. The first condition to be reached is thus the quick dielectric regeneration of the arc when the current passes to zero, despite the presence of the mains voltage. Successful breaking is in practice a competition of speed between dielectric regeneration and evolution of mains voltage.

2.3.3 Arc breaking with limitation

"With limitation" means that measures are taken to prevent the short-circuit current having the time to reach its maximum value, (about 63% of maximum fault current).

This current limitation will be obtained if arc voltage U_a quickly becomes greater than mains voltage and remains so until the current is canceled. In point of fact, the generalized Ohm´s law, (*n* is the number of splitters in the arc chamber and U_a is around 25-30 V [18]:

$$U_r - Ri - L\frac{di}{dt} - n \cdot U_a(t) = 0 \qquad Ec.\ 2\text{-}2$$

The Ec. 2-2 shows that *di/dt* will change sign as soon as $U_a\,(t) > U_r\,(t)$ both in DC and AC voltage. Limitation devices are based on current effects beyond a certain threshold, the short-circuit current creates thermal effects (fuse) or electromagnetic effects (circuit breakers) and generates an arc voltage [29].

2.4. Consequences of Arcing

The presence of an electric arc has both positive and negative consequences. The positive aspect is that the arc allows for a smooth decrease to zero current. If the circuit current were to suddenly drop to zero at the moment of contact separation, the energy stored in the inductance, L, would cause an over-voltage given by [18]:

$$V = -L\frac{dI}{dt} \qquad Ec.\ 2\text{-}3$$

The presence of an electric arc usually limits the over-voltage to a maximum of two or three times the circuit voltage. Without this feature, switch designers would have to design to protect the circuit against large over-voltages.
However, other consequences of arcing could be devastating for the switching device and affect the design and choice of materials.

2.4.1 Contact Erosion

Since erosion of the contact material is one of the most important consequences of arcing and the design is directly relating to the lifetime of the device. It occurs because both the anode and cathode heats up to above the boiling temperature of the contact material. The

temperature of the arc is so high that erosion occurs even if the arc is moving across the contact surfaces. The amount of erosion depends on many parameters, for example:

- Circuit current
- Arcing time
- Open gap distance
- Contact material
- Size and shape of the contact
- Contact opening velocity
- Arc motion on the contacts
- Design of the arc chamber

2.5. Components of CB

Many of the principals used by circuit breaker engineers to analyze and design DC circuit breakers to interrupt DC currents are carried over from AC devices. The physics of open gap, arc runners, slot motors, reverse loops, and arc chutes also apply in DC systems. One might say that the use of these design strategies is even more demanding in DC circuit breakers due to the added burden of quenching the arc without the aid of a current crossing zero. The basic of circuit breaker design and construction, are created from the following five major components, Frame, Contacts, Arc Chute Assembly, Operating Mechanism and Trip Unit [1].

2.5.1 Frame

The frame provides an insulated housing to mount the circuit breaker components (Figure 2-7). The construction material is usually a thermal set plastic, such as glass-polymer. The construction material can be a factor in determining the interruption rating of the circuit breaker. Typical frame ratings include, maximum voltage, maximum ampere rating, and interrupting rating [30].

Figure 2-7 Frame of a Circuit Breaker [31].

2.5.2 Contacts

The current flowing in a circuit controlled by a circuit breaker flows through the circuit breaker's contacts. When a circuit breaker is turned off or is tripped by a fault current, the circuit breaker interrupts the flow of current by separating its contacts.

Contacts are of two types depending on the interrupting rating: Straight-Through Contacts and Blow-Apart Contacts [30].

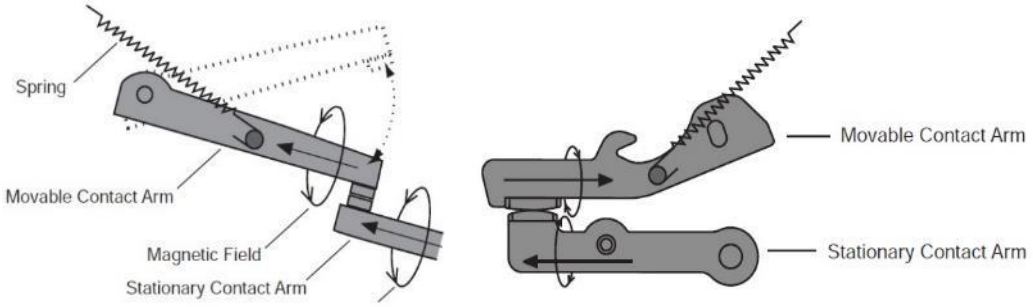

a) b)

Figure 2-8 Straight through contacts and bow apart contacts [30].

Straight-Through Contacts

Some circuit breakers use a straight-through contact arrangement, so called because the current flowing in one contact arm continues in a straight line through the other contact arm (Figure 2-8 a).

Blow-Apart Contacts

With this design, the two contact arms are positioned parallel to each other. As current flows through the contact arms, magnetic fields develop around each arm. Because the current flow in one arm is opposite in direction to the current flow in the other, the two magnetic fields oppose each other. Under normal conditions, the magnetic fields are not strong enough to force the contacts apart. When a fault develops, current increases rapidly causing the strength of the magnetic fields surrounding the contacts to increase as well (Figure 2-8 b).

2.5.3 Arc Chute Assembly

The arc is extinguished in this assembly. When a circuit breaker is turned off or is tripped by a fault current, the circuit breaker interrupts the flow of current by separating its contacts. This assembly is made up of several "U" shaped steel plates that surround the contacts (Figure 2-9). As the arc develops, it is drawn into the arc chute where it is divided into smaller arcs, which are extinguished faster [30].

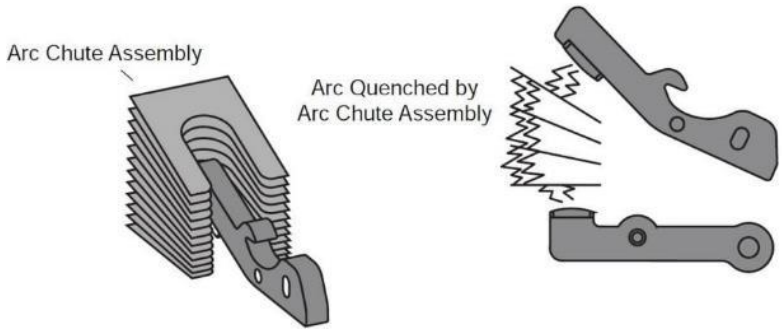

Figure 2-9 Arc chute assembly [30].

Minimizing the arc is important for two reasons. 1) Arcing can damage the contacts, 2) the arc ionizes gases inside the molded case. If the arc isn't extinguished quickly the pressure from the ionized gases can cause the molded case to rupture.

2.5.4 Operating Mechanism

The operating handle is connected to the moveable contact arm through an operating mechanism. In the following illustration, the operating handle is moved from the "OFF" to the "ON" position Figure 2-10. In this process, a spring begins to apply tension to the mechanism. When the handle is directly over the center, the tension in the spring is strong enough to snap the contacts closed. This means that the speed of the contact closing is independent of how fast the handle is operated [30].

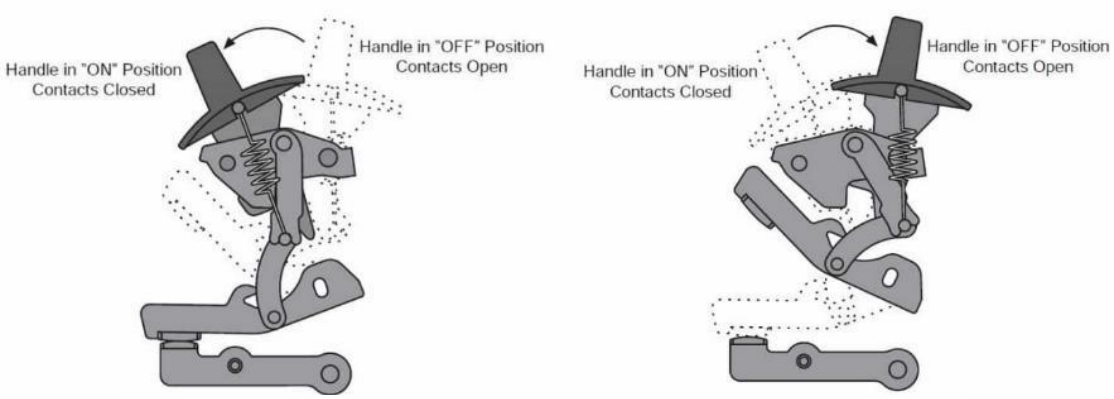

Figure 2-10 Operating mechanism, a) ON position, b) OFF position [30].

2.5.5 Trip Unit

In addition to providing a means to open and close its contacts manually, a circuit breaker must automatically open its contacts when an overcurrent is sensed. The trip unit (Figure 2-11), is the part of the circuit breaker that determines when the contacts will open automatically.

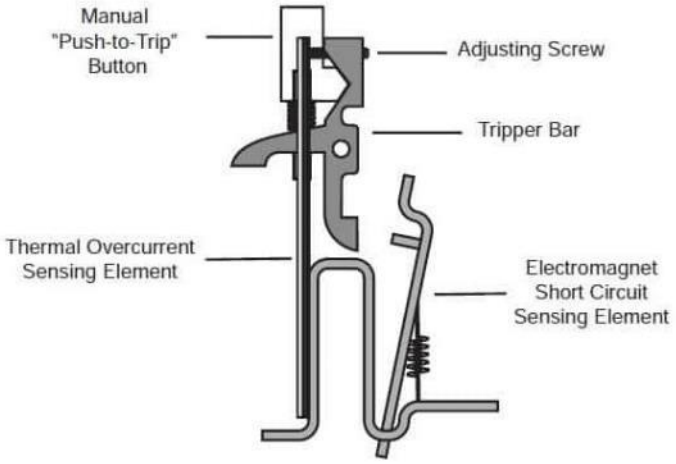

Figure 2-11 Thermal-Magnetic trip unit [30].

In a thermal-magnetic circuit breaker, the trip unit includes elements designed to sense the heat resulting from an overload condition and the high current resulting from a short circuit. In addition, some thermal-magnetic circuit breakers incorporate a “Push-to-Trip” button [30].

2.6. Arc manipulation

Perhaps the most difficult aspect of designing a circuit interrupter is manipulating the arc such that it moves into the arc chute where it can be extinguished quickly and reliably. This can be accomplished by employing a variety of technologies, some common to AC and DC and some unique to DC [1].

2.6.1. Open Gap

The simplest method of DC circuit interruption is to use a large open gap. The open gap of a circuit breaker is defined as the distance between the movable and stationary contacts when they are fully parted. Another means of increasing open gap in a DC breaker is to wire multiple poles in series [1].

2.6.2. Arc Runner

Shortly after the introduction of the arc chute system, it was found that other techniques were required to guide the arc into the arc chute. One such guide is the arc runner (Figure 2-12). The arc runner is closely coupled to the main contacts. It attracts the arc drawing on the arc runner. Once the arc has reached the runner, it will remain on the arc runner provided that no lower resistance path occurs. Electromagnetic forces move the arc along the runner towards the arc chute [1].

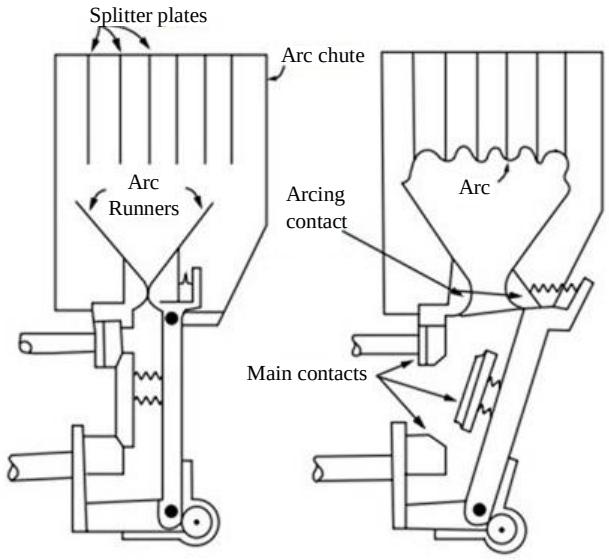

Figure 2-12 Assembling of arc runners [32].

2.6.3. Blowout Coils

This is a secondary copper coil in series with arcing contacts (Figure 2-13). The electromagnetic field helps move arc into arc chute. Contactors often incorporate magnetic blowout coils, for example, that push the arc away from the contacts as a means of more quickly cooling the arc [33].

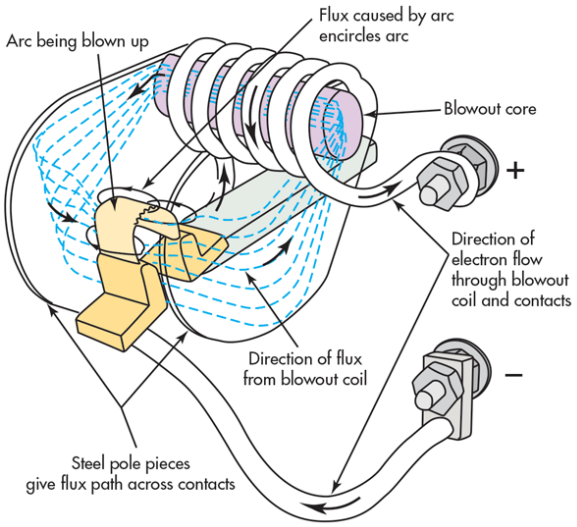

Figure 2-13 Blowout coils assembling [34].

2.6.4. Puffer

As illustrated in the Figure 2-14 the breaker has a cylinder and piston arrangement. Here the piston is fixed but the cylinder is movable. The cylinder is tied to the moving contact so that for opening the breaker the cylinder along with the moving contact moves away from the fixed contact. But due to the presence of fixed piston the SF6 gas inside the cylinder is

compressed. The compressed SF6 gas flows through the nozzle and over the electric arc in the axial direction. Due to heat convection and radiation, the arc radius reduces gradually and the arc is finally extinguished at current zero [33].

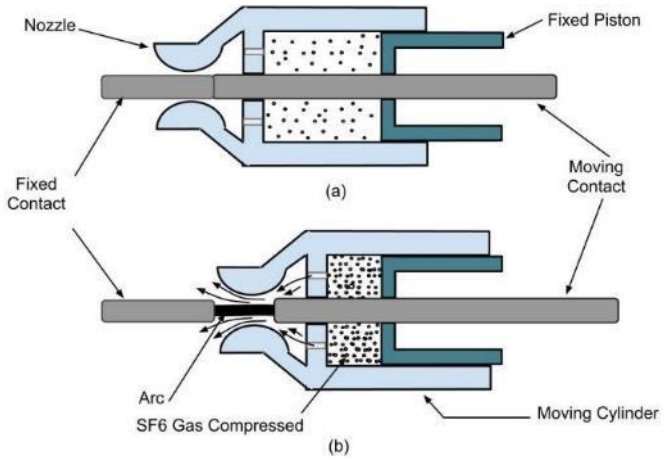

Figure 2-14 Puffer type SF6 CB, a) ON position, b) OFF position [35].

2.7. Theory of Multi-physical Fields in a Fault Arc

The temperature of an arc fault could be over 20000 K. This may destroy electrical equipment and threaten human life [36]. Also, an arc fault can reach high levels of temperature, strong magnetic fields, added to mechanical stress and overpressure.

In the present thesis, the multi-physical fields from the arc should be simulated to predict the complete phenomena in a simplified model of CB. To make this possible, the Magneto-Hydrodynamics (MHD) Theory will be used to simulate the interaction of the plasma and the magnetic field density.

The MHD refers to the interaction between an applied electromagnetic field and a flowing, electrically-conductive fluid. The MHD model allows analyzing the behavior of electrically conducting fluid flow under the influence of constant (DC) or oscillating (AC) electromagnetic fields [37].

With this approach, and with the current development of software tools, the physical processes that take place during the electric arc phenomenon is reproduced in detail. Even the methodology would can help us in the design and improvement of circuit breakers, being possible to study not only the parameters of the circuit, but also aspects directly related to the design, such as geometry, and main elements (as splitter plates or contacts), which are parameters studied by [24].

However, the major limitation of these models are:

- the limited accuracy in the resolution of the differential equations of the models,
- restriction in the computation time,

- need of a deep knowledge about the precise arc physical processes,
- knowledge of the physical properties of the extinguishing medium in a wide range of temperatures,
- also, test results from measurements of physical properties from the arc are needed to evaluate different parameters used, such as thermal conductivity, viscosity, electrical conductivity, specific heat or mass density,
- Geometry, mesh quality, resolution methods, convergence of results and experience of the engineer, also take an important role during the simulation process.

These aspects make the application of these type of models more difficult and determine the accuracy of the results provided by the model, [9].

With the MHD approach not only the equations of conservation of mass, momentum, and energy are considered in macroscopic elements, but also gas properties and empirical formulation to represent energy exchange mechanisms during the simulation. However, they all require applying simplifications in relation to the geometry and physical properties of the arc plasma. The thesis presented by [9] follows the next assumptions to adopt in current physical models:

- Arc plasma is electrically neutral and is represented as a mixture of gases at high temperature.
- There is a thermodynamic equation of state for each component of the plasma (electrons, ions, atoms and molecular species), but it is usually neglected in the macroscopic scale analysis.
- Physical properties of plasma (thermal conductivity, viscosity, density, specific heat, electrical conductivity) depend on its temperature and pressure conditions.
- The behavior of the gaseous mass is described by applying the Navier Stokes' (conservation of mass, momentum, and energy) and Maxwell's equations.
- Since plasma is electrically conductive, the corresponding term for the interaction with the magnetic field must be considered in the momentum equation. This magnetic field, depending on the degree of accuracy of the model, can be defined as external or self-induced by the current flowing through the arc. The second option is closer to reality.
- The magnetic field is calculated by applying Biot-Savart or by calculating the magnetic vector potential once the current distribution is known.
- The energy conservation equation is modified by considering additional terms that represent the generation of heat by Joule effect and the heat dissipation by radiation.
- In many cases, local thermal equilibrium (LTE) is assumed for the plasma, so that it is possible to set a temperature value which determines the degree of dissociation and ionization.
- The initialization of the arc is not achieved by the dynamic movement of the electrodes separation, as in reality, due to the complexity. The arc/electrode interaction is not considered in a microscopic way.

The last ~~one~~ considerations, make it possible to obtain the MHD equations for fluids under the influence of electromagnetic fields.

2.8. Fluid Models Magnetohydrodynamic description

The huge number of particles makes it impossible to solve Newton's equation for each of these particles. The magneto-hydrodynamic definition provides information about the behavior of the electric arc, by fluid dynamics and thermodynamic laws, at a macroscopic scale [9]. To understand the background of the MHD it is necessary to see the electric arc as a collection of particles.

- Electrons,
- Ions,
- Atoms and,
- Molecular species.

But the solution of all of them leads to a quite large mathematical problem. Accordingly, it is necessary to group all these particles into two categories, (or as two fluids):

- heavy particles (ions and neutrals) and
- light particles (electrons)

Each one is characterized by its own temperature: T_e (temperature of the electrons) and T_a (temperature of the heavy particles).

In the vicinity of the electrodes, (named cathode and anode regions), in a very thin surface layer, temperature falls from the value of the plasma column (typically around 25000K) to the value of the electrode (typically around 3000K). With that temperature of the electrode, the electrical conductivity value is close to zero, so that no current should flow, but the electrode is the main supplier of current to the plasma. This contradiction is solved taking into account that in unbalanced plasmas or without thermal equilibrium, the two previously mentioned temperatures appear. While the temperature of the heavy particles falls, the temperature of electrons is maintained at a high value, so that the plasma keeps being conductor in the situations described.

However, if extinction and reignition are not considered in the analysis, and the arc roots are macroscopically solved, it is possible to simulate the evolution of the arc at a macroscopic scale, by the approach called magneto-hydrodynamics. Which considers the plasma as a single fluid [9].

With the last considerations, the MHD method is used to calculate a plasma in Local Thermic equilibrium (LTE), in [9] are mentioned some considerations to assume this.

- Thermal equilibrium: the electrons temperature T_e, is equal to (or very similar) the heavy particles temperature T_a.
- Ionization equilibrium: the electron density, n_e, is equal or very similar to the density of electrons n_a that would exist in the plasma, with a unique temperature.
- Quasi-neutrality: the plasma is electrically neutral, both globally and locally.

Nevertheless, in the case of LV arcs the three above assumptions are not fulfilled in the arc roots, neither in the zero current when the arc is extinguished. For those reasons arc roots are not going to be analyzed deeply, just in a macroscopic way. Thus, adopting the LTE hypothesis and, therefore, adopting a single temperature field, "T", and a single average velocity field for the fluid "$\boldsymbol{u}$", for the whole plasma, that plasma can be reduced to a single fluid, simplifying the state equations of each particle [9].

Given the foregoing considerations, transport equations for the conservation of mass, momentum and energy of the plasma as a single fluid are defined, which are known as the modified Navier-Stokes equations, (Ec. 2-3 – Ec. 2-5).

2.9. Simulation tool.

The previous explanation gives the background about the behavior of an electric arc, now it is time to choose the computational tool to solve the problem. In this thesis were chosen the next software with some of their characteristics.

2.9.1 Ansys-Fluent.

ANSYS Fluent is a computer program for modeling fluid flow, heat transfer, and chemical reactions with complex geometries. Fluent uses the Volume of Fluid method (VOF), Mixture model or Eulerian model to solve the transport equations. The fluid flow conserves mass, momentum and energy are solved in ANSYS Fluent for a fluid flow.

The mass conservation equation can be written as follows: [36]

$$\frac{\partial \rho}{\partial t} + \nabla \cdot (\rho \boldsymbol{V}) = 0 \qquad \textit{Ec. 2-4} \quad [9]$$

- Change rate of density in the control volume
- Difference between the incoming and outgoing mass flow in the control volume

The momentum conservation is described by:

$$\rho \frac{\partial (\boldsymbol{V})}{\partial t} + \rho(\boldsymbol{V} \cdot \nabla)\boldsymbol{V} = -\nabla p + \frac{4}{3}\nabla\mu(\nabla \cdot \boldsymbol{V}) - \nabla x \mu(\nabla x \boldsymbol{V}) + \boldsymbol{F} + \rho \boldsymbol{g} \qquad \textit{Ec. 2-5} \quad [9]$$

- Change rate of momentum in the volume control
- Momentum difference in the incoming and outgoing flow in the control volumen
- Pressure gradient
- Surface forces on the control volume
- Lorentz force. Interaction term with the magnetic field.
- Accelerating gravity force

The equation for energy conservation is given by

$$\rho \frac{\partial}{\partial t}(H) + \rho(\boldsymbol{V} \cdot \nabla)H - \frac{\partial p}{\partial t} - (\boldsymbol{V} \cdot \nabla p) = \nabla \cdot \frac{K}{C_p} \nabla H - \nabla \cdot \boldsymbol{q_R} + \Phi + S_h \qquad Ec.\ 2\text{-}6 \ [9]$$

Variation rate of enthalpy in the control volume

Enthalpy difference in the incoming and outgoing flow in the control volume

Work produced by the pressure change and pressure gradient

Conductive heat loss

Radiative heat loss

Viscous dissipation term

Ohmic heating input in the CV

Being Φ the viscous dissipation factor (usually neglected), expressed as:

$$\Phi = \sum \left[\mu \left(\frac{\partial v_i}{\partial x_j} + \frac{\partial v_j}{\partial x_i} \right) - \frac{2}{3} \mu \frac{\partial v_k}{\partial x_k} \delta_{ij} \right] \frac{\partial v_i}{\partial x_j} \qquad Ec.\ 2\text{-}7 \quad [9]$$

Where:

ρ:	gas density
V:	gas velocity
t:	time
p:	pressure
μ:	viscosity
g:	gravity acceleration
H:	gas enthalpy
K:	thermal conductivity
C_p:	specific heat at constant pressure
T:	temperature

The source term in the fluid momentum equation is the Lorentz force given by:

$$\boldsymbol{F} = \boldsymbol{J} x \boldsymbol{B} \qquad Ec.\ 2\text{-}8$$

where the magnetic field is $\boldsymbol{B} = \nabla X \boldsymbol{A}$
The source term, S_h, includes the Joule heating rate given by:

$$S_h = Q = \frac{J^2}{\sigma} = \boldsymbol{J} \cdot \boldsymbol{E} \quad Ec.\ 2\text{-}9$$

2.9.2 ANSYS-Maxwell.

ANSYS Maxwell is the industry-leading electromagnetic field simulation software for the design and analysis of electric motors, actuators, sensors, transformers and other electromagnetic and electromechani-cal devices. Maxwell uses the accurate finite element method to solve static, frequency-domain and time-varying electromagnetic and electric fields [38].

In this thesis, Maxwell must calculate the electromagnetic fields from the multi-physical fields in a fault arc. This can be reached by the coupling of Maxwell and ANSYS-Fluent, so that, Fluent makes a mapping of the electric conductivity of the fluid and export this to

Maxwell to calculate the magnetic flux density **B**. Electromagnetic fields are described by Maxwell's equations:

Magnetic field Gauss´ law $\boldsymbol{\nabla \cdot B = 0}$ *Ec. 2-10*

Faraday´s law $\nabla x \boldsymbol{E} = -\frac{\partial \boldsymbol{B}}{\partial \mathrm{t}}$ *Ec. 2-11*

Gauss´ law $\nabla \cdot \boldsymbol{D} = \mathrm{q}$ *Ec. 2-12*

Ampere´s generalized law $\nabla x \boldsymbol{H} = \boldsymbol{J} + \frac{\partial \boldsymbol{D}}{\partial \mathrm{t}}$ *Ec. 2-13*

Where:

$\boldsymbol{J}$:	current density
$\boldsymbol{B}$:	magnetic flux density
E:	electric field
D:	electric field density
H:	magnetic induction field
q:	electric charge density

$\boldsymbol{B}$ (Tesla) and $\boldsymbol{E}$ (V/m) are the magnetic and electric fields, respectively, and $\boldsymbol{H}$ and $\boldsymbol{D}$ are the induction fields for the magnetic and electric fields, respectively. q (C/m^3) is the electric charge density, and $\boldsymbol{J}$ (A/m^2) is the electric current density vector.

With the last equations it is proceeding to reduce some terms, and adding other like the Lorentz forces and the Joule heating, and to facilitate understanding the energy conservation equation is changed to temperature terms, remaining as shown below.

Mass conservation equation.

$$\frac{\partial \rho}{\partial t} + \nabla \cdot (\rho \boldsymbol{V}) = 0 \qquad \textit{Ec. 2-14}$$

Momentum conservation equation.

$$\rho \frac{\partial (\boldsymbol{V})}{\partial t} + \rho (\boldsymbol{V} \cdot \nabla) \boldsymbol{V} = -\nabla p + \frac{4}{3} \nabla \mu (\nabla \cdot \boldsymbol{V}) - \nabla x \mu (\nabla x \boldsymbol{V}) + \boldsymbol{J} x \boldsymbol{B} \qquad \textit{Ec. 2-15}$$

Energy conservation equation.

$$\rho C_p \left(\frac{\partial T}{\partial t}\right) + \rho C_p (\boldsymbol{V} \cdot \nabla) T = \nabla \cdot (k \nabla T) + \frac{\partial p}{\partial t} + (\boldsymbol{V} \cdot \nabla p) - \nabla \cdot \boldsymbol{q_R} + \boldsymbol{J} \cdot \boldsymbol{E} \qquad \textit{Ec. 2-16}$$

2.9.3 Altair-Flux

Flux is the leading software for electromagnetic. This software uses the Finite Element Method techniques to solve the electromagnetic equations in the model. Flux has a module where it can simulate transient magnetic and steady-state AC phenomena, in its user's guide documents [39].

The equations used for the solving are:

- Maxwell's equations (for a magnetic system)
- The constitutive equations of the matter, (relation between two physical quantities (especially kinetic quantities as related to kinematic quantities) that is specific to a material or substance, and approximates the response of that material to external stimuli, usually as applied fields or forces.

Regardless of the software tool used for the simulation of the electric arc, the methodology will always be the same, a transient simulation, involving the Maxwell and Fluid mechanics equations.

This way, when applying Navier-stokes modified equations to arc plasma, specifically in momentum equation (Ec. 2-4) and energy equation (Ec. 2-5), electromagnetic terms must be specified representing ohmic heating and Lorentz force interaction with fluid dynamics. Figure 2-15 shows the physical processes, fluid dynamics and electromagnetism interaction that takes place in the electric arc.

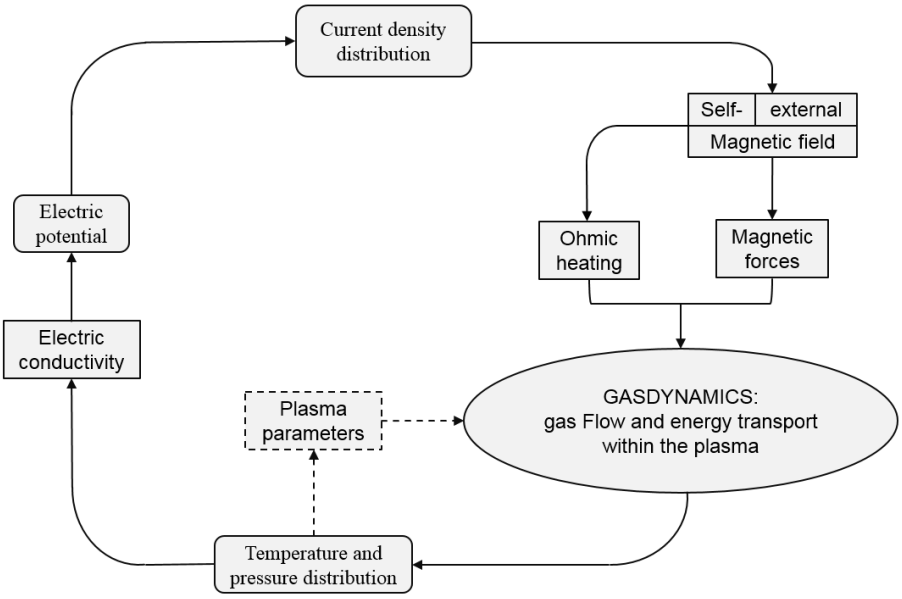

Figure 2-15 Interaction of physical processes in the arc column [9].

The process is as follows: a potential is established in one of the terminals of the CB (or a current), this tends to be distributed and moved through the electric arc. Subsequently the current flowing through the arc generates a magnetic field (or an external field can be imposed), and this generates a magnetic force. Another consequence of the current is that it tends to increase the temperature produced by the Joule effect. These two terms (joule heat and magnetic force) are considered in the momentum and energy equations which are solved by the CFD software. Next, the software shows the new values of temperature and pressures that change the properties of the plasma that will be used for the next iteration, these new values of temperature and pressure also modify the electrical conductivity that is finally used to calculate the new potential and the process start again

Chapter III

To validate the methodology described here, the results obtained in this thesis research are compared with the simulation reported by [9]. The methodology used is the same, with two variations, the movement of the arc is simulated with the product Fluent letting calculate the magnetic field density (**B**) with the product Maxwell at the same time, allowing the two products running simultaneously. Also, the calculation of **B** is obtained with the software Flux, running different configurations.

3.1. Methodology for simulation

The software ANSYS Workbench include several simulation tools. With these tools it is possible to run several structural, thermal, fluid, and electromagnetic analyses. Users can also simulate different physics coupled, for example, determine the volumetric expansion of component as a function of temperature change, coupling ANSYS Fluent + ANSYS Mechanical. For the present project, the MHD module for Fluent is used. The methodology to initialize the software is explained in [36], and described as follows.

- **Start ANSYS Workbench:** Click on Fluid Flow (Fluent), the tool will load in the graphic user interface (GUI). Once Fluid Flow Fluent load, an analysis system is created as shown in Figure 3-1.

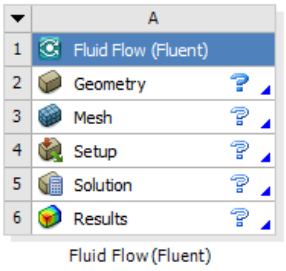

Figure 3-1 Toolbox of Fluent.

- **Create a Geometry:** The ANSYS DesignModeler may be used as a geometry editor for existing CAD models. In this tool it is possible to navigate within the graphical user interface, create, modify and/or cleanup their geometry in preparation for their analyses, generate 2-D sketches and convert them into 2-D or 3-D models, modify 2-D and 3-D geometry, to name a few characteristics. This tool features two basic operating modes: DesignModeler 2D sketching and DesignModeler 3D Modeling.
- **Create a Computational Mesh:** ANSYS ICEM CFD is a meshing tool within the ANSYS Workbench. ANSYS ICEM CFD can parametrically create meshes from a geometry and simplifies the mesh generation process.
- **Write User-Defined Functions**: User-defined functions (UDFs) allow the user to customize ANSYS Fluent. A UDF can enhance the standard code features. Users can use a UDF to define their own boundary conditions, material properties, and source terms for the flow; initialize a solution; or enhance post-processing. UDFs are written in the C programming language, and the source code is saved with a `.c` extension.

- **Set up the multi-physical field simulation in ANSYS Fluent**. Users may use the ANSYS Fluent fluid flow systems to set up and solve a 3D multi-physical field problem. This software contains the broad physical modeling capabilities needed to model flow, turbulence, heat transfer, and reactions for industrial applications ranging from air flow over an aircraft wing to combustion in a furnace, from bubble columns to oil platforms, from blood flow to semiconductor manufacturing, and from clean room design to wastewater treatment plants.
- **Set up MHD module:** The MHD module is provided as an addon-module with the standard FLUENT licensed software. The MHD module consists of a UDF library and a pre-compiled scheme library, which needs to be loaded and activated before calculations can be performed. The MHD module is loaded into FLUENT through the text user interface (TUI). The module can only be loaded when a valid FLUENT case file has been set or read. The description of this module is in Annex B.
- **Coupling MAXWELL-FLUENT.** The coupling between Maxwell-Fluent is achieved through a UDF provided by Schneider Electric, which for reasons of copyright cannot be shown, however, the logic is as follows:

    1. Prepare the model with the same geometry in Maxwell and Fluent, in addition to the same parameters for current.
    2. In Maxwell, a magnetostatics analysis is carried out and it is specified that the electrical conductivity of the air will be a function of the temperature.
    3. The UDF in fluent performs a mapping of the electrical conductivity which is exports to Maxwell.
    4. Maxwell reads these new values and performs calculations for the magnetic flux density in each cell. Subsequently, these data are sent to Fluent.
    5. Fluent takes the magnetic flux density values that it uses to calculate the Lorentz force.
    6. Fluent calculates the new position of the arc and the process is repeated from step 3.

  The coupling can be done in 3D or 2D analysis.

- **Coupling FLUX-FLUENT**. The coupling between Flux-Fluent results a quite complex, since they are from different companies, making direct communication between software impossible. Therefore, understand by Flux-Fluent coupling, the use of these two tools separately. The objective of this analysis will simply serve to know if the B values calculated in Maxwell are within the same order of magnitude.

    1. Prepare the model with different geometry for the position of the arc, in addition, the modification of conductivity in the arc.
    2. In Flux a magnetostatics analysis is carried out.
    3. Run the calculation and get the values of B at different paths.
    4. Measure the values of interest.

3.2. Description model

In this thesis, the simulation product Fluent, with the MHD module is used, making a coupling with Maxwell. Another round of simulations are done with Fluent-MHD and the **B** is obtained from Flux. For all the cases a simplified geometry is used.

3.2.1 Geometry model

The model used for the simulations have been the same used in [9]. The geometry of the model is shown in Figure 3-2. It constitutes a simplification of the LVCB geometry while being composed of the main elements of these devices: anode, cathode and splitter plate.

- Height: 40mm
- Width: 11mm
- Depth: 2.5mm
- Dimensions of the anode and the cathode: 40x1.5x2.5 (h, w, d) mm
- Splitter plate dimensions: 20x2x2.5 (h, w, d) mm and 20x2x0.1 (h, w, d) mm
- Arc Diameter 2.5 mm.

Which the parts are:

- Anode (A)
- Cathode (B)
- Splitter (C)
- Arc (D)

The rest of the geometry corresponds to the air.

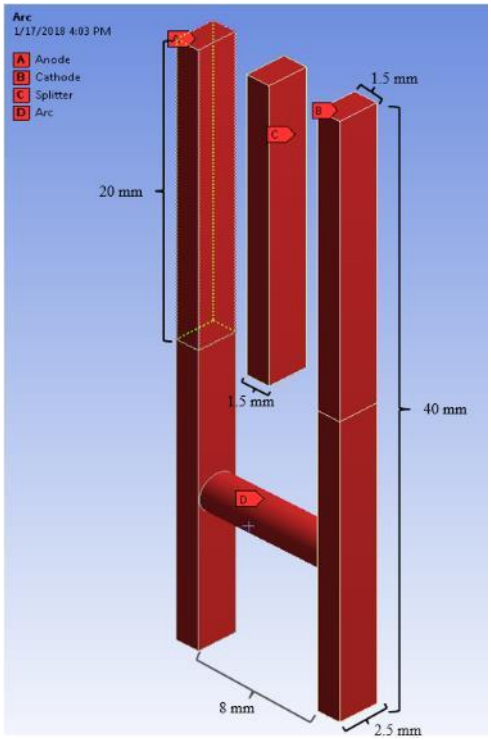

Figure 3-2 Geometry with dimensions.

3.2.2 Mesh

The partial differential equations that govern fluid flow and heat transfer are not usually amenable to analytical solutions, except for very simple cases. Therefore, in order to analyze fluid flows, flow domains are split into smaller subdomains (made up of geometric primitives like hexahedra and tetrahedra in 3D and quadrilaterals and triangles in 2D). The governing equations are then discretized and solved inside each of these subdomains.

Typically, one of three methods is used to solve the approximate version of the system of equations: finite volumes, finite elements, or finite differences. Care must be taken to ensure proper continuity of solution across the common interfaces between two subdomains so that the approximate solutions inside various portions can be put together to give a complete picture of fluid flow in the entire domain. The subdomains are often called elements or cells, and the collection of all elements or cells is called a mesh or grid [40].

A structural hexahedral mesh has been adopted, defining a finer mesh at interfaces and edges, where the change of the parameters value could make the system unstable and divergent. The mesh selected is defined by the following characteristics (Table 3-1 and Table 3-2):

Table 3-1 Description of the $3D_F$ mesh

Edge length (mm)	Number of nodes	Skewness average	Orthogonal quality average	Ratio	Total number of elements	Total number of nodes
20	200	0.0164	0.99838	1.2	1095000	1185470
3	30					
2.5	25					
2	20					
1.5	15					
1	10					

Table 3-2 Description of the $3D_S$ mesh.

Edge length (mm)	Number of nodes	Skewness average	Orthogonal quality average	Ratio	Total number of elements	Total number of nodes
20	200	0.00574	0.99972	1.2	70000	143126
3	30					
0.1	1					
2	20					
1.5	15					
1	10					

- **Edge length:** length of the edge that is divided into nodes.
- **Number of nodes per edge:** number of nodes by which the edge is divided. In this case, after analyzing multiple cases for this geometry, a constant value of 10 times the edge length has been chosen for the number of nodes in each length. Thus, a homogeneous fine mesh has been obtained.
- **Skewness average:** Skewness is one of the primary quality measures for a mesh. Skewness determines how close to ideal (i.e., equilateral or equiangular) a face or cell is. According to the definition of skewness, a value of 0 indicates an equilateral cell (best) and a value of 1 indicates a completely degenerate cell (worst).
- **Orthogonal quality average:** The orthogonal quality for cells is computed using the face normal vector, the vector from the cell centroid to the centroid of each of the adjacent cells, and the vector from the cell centroid to each of the faces. The range of orthogonal quality is 0-1, where a value of 0 is worst and a value of 1 is best.
- **Ratio:** factor by which the spacing is increased in the following nodes. Spacing and Ratio design the finer mesh that is applied at interfaces and complicated edges intersection.
- **Total number of elements:** total number of elements in the whole mesh.
- **Total number of nodes:** total number of nodes in the whole mesh.

Also, the software tool chosen for meshing the model is an important decision; precision, flexibility, and user-friendliness are important characteristics in order to choose the most appropriate. The mesh developed for this model has been designed with the ICEM CFD commercial software, belonging to ANSYS. The characteristics defining the hexahedral mesh created are shown in Figure 3-3-Figure 3-7 and Table 3-1-Table 3-2.

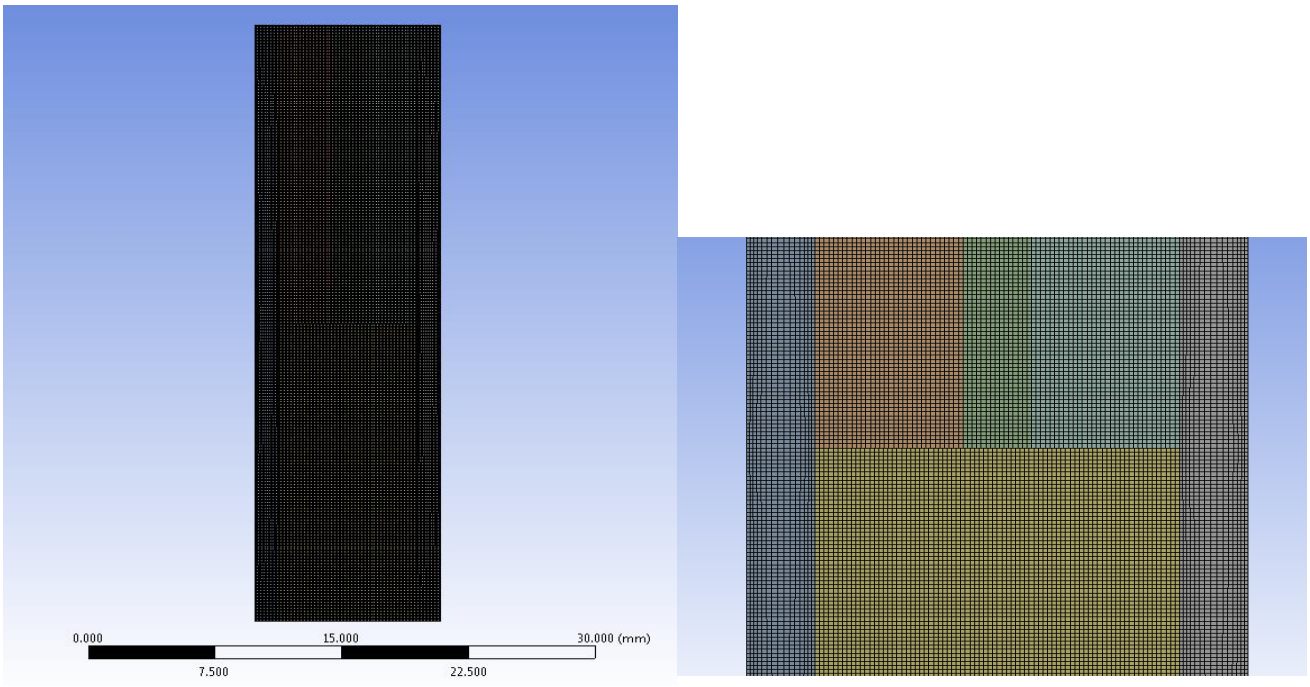

(a) (b)

Figure 3-3 Overview of the full mesh (a), detailed (b).

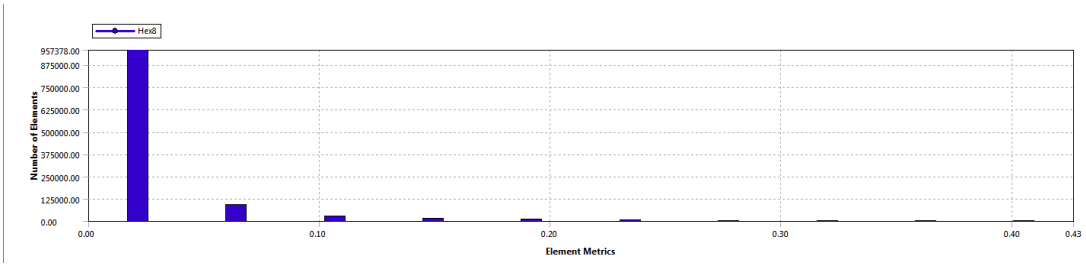

Figure 3-4 Skewness of $3D_F$ mesh.

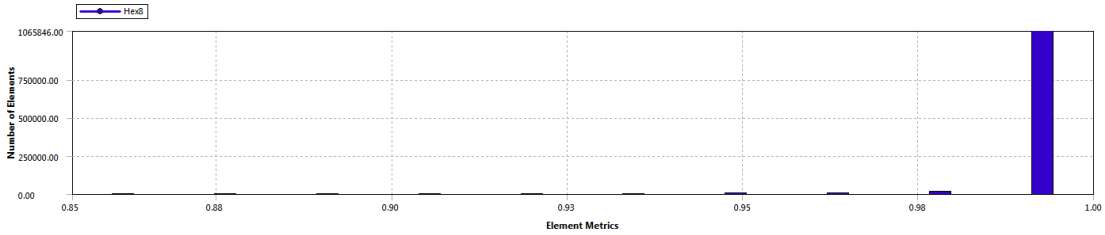

Figure 3-5 Orthogonal quality of $3D_F$ mesh.

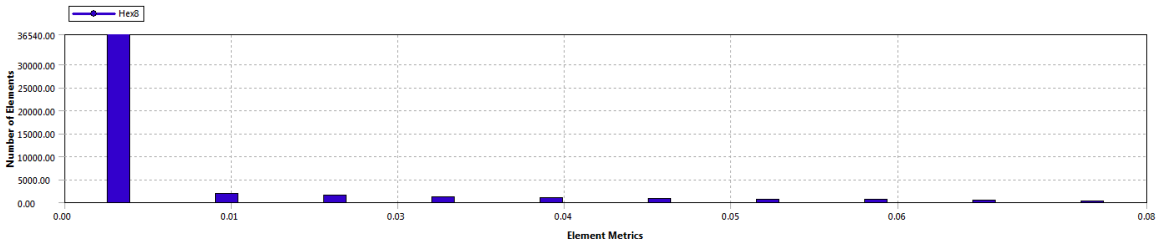

Figure 3-6 Skewness of $3D_S$ mesh.

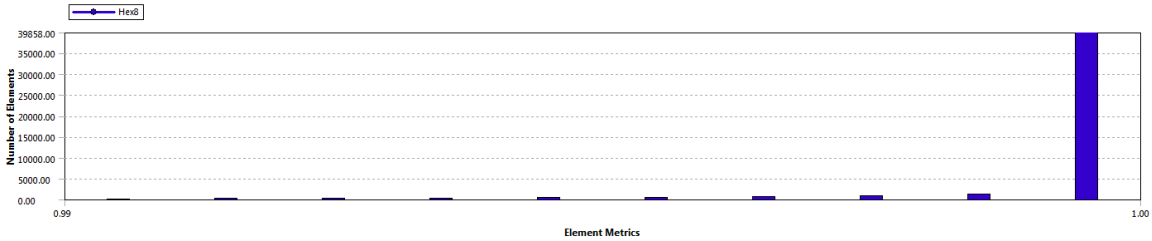

Figure 3-7 Orthogonal quality of $3D_S$ mesh.

3.2.3 Plasma properties as UDF

A user defined function, or UDF, is a function that can be programed and can be dynamically loaded with the FLUENT solver to enhance the standard features of the code. UDFs are written in the C programming language.

UDFs are executed as either interpreted or compiled functions in FLUENT. Values that are passed to the solver by a UDF or returned by the solver to a UDF must be specified in SI units [41].

A UDF allows customizing of own boundary conditions, material property definitions, surface and volume reaction rates, source terms in FLUENT transport equations, source terms in user-defined scalar (UDS) transport equations, diffusivity functions, etc. UDFs are defined using Fluent-supplied function declarations. These function declarations are implemented in the code as macros, and are referred to in this document as DEFINE (all capitals) macros, for example:

The general format of a DEFINE macro is DEFINE_MACRONAME (udf_name, passed-in variables). The full description of UDFs is in Annex C.

In the model used in this thesis the domains have been defined as follow:

- fluid volume or air,
- splitter plate,
- cathode and anode

The material used in solid domains (cathode, anode and splitter) is copper, with constant physical properties and no dependency with T or P. The material used in the fluid volume has been specified as a User Defined Function. The air properties have been obtained from reference [42], which are described below (Figure 2-8-Figure 2-12):

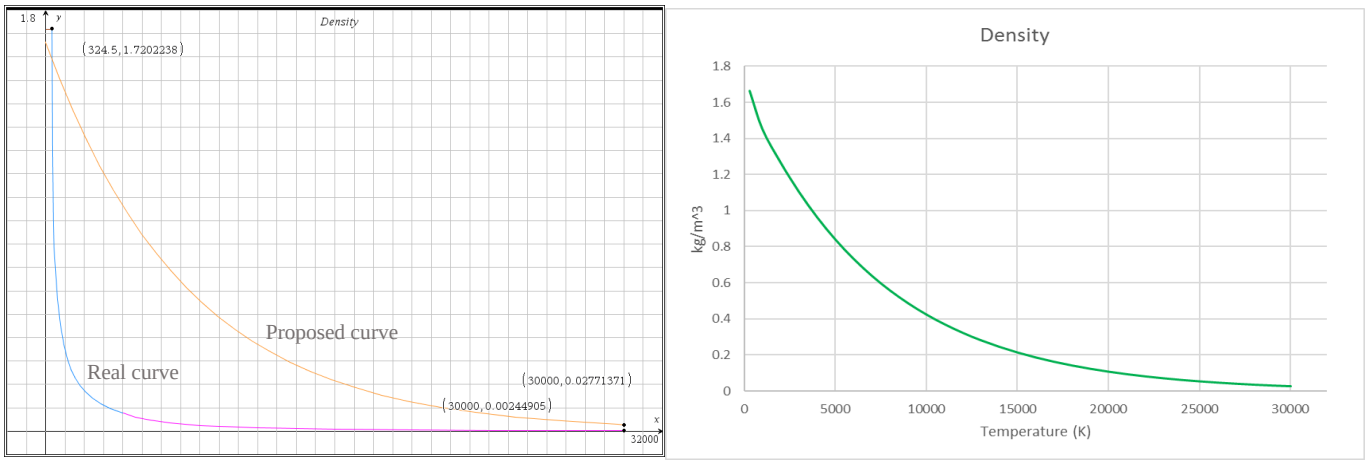

a) b)

Figure 3-8 Density for high temperature air [42], a) plot in TI-Nspire CX CAS software, b) plot in Excel.

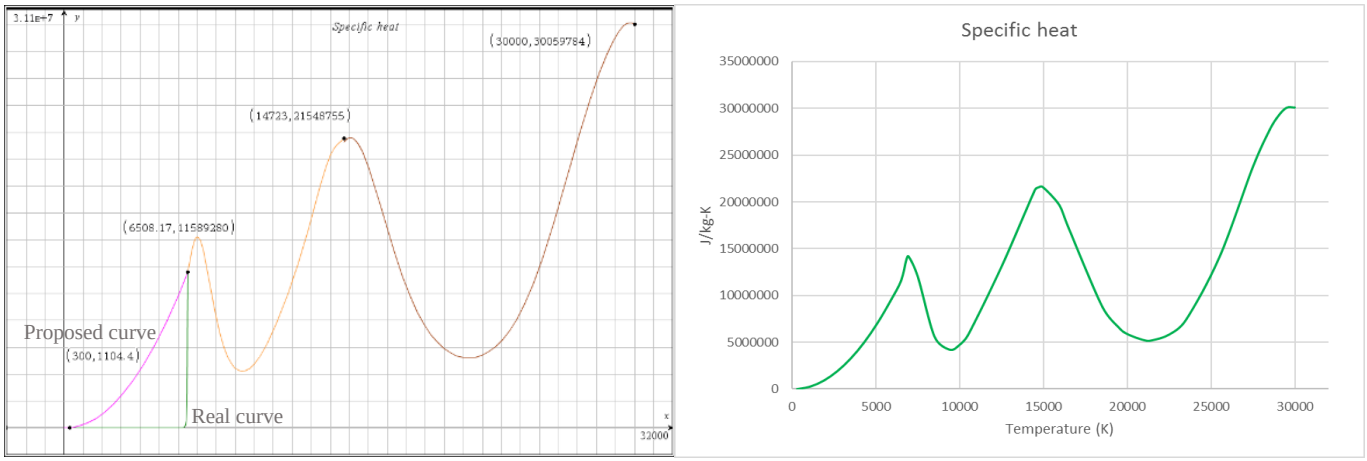

a) b)

Figure 3-9 Specific Heat for high temperature air [42], a) plot in TI Nspire CX CAS software, b) plot in Excel.

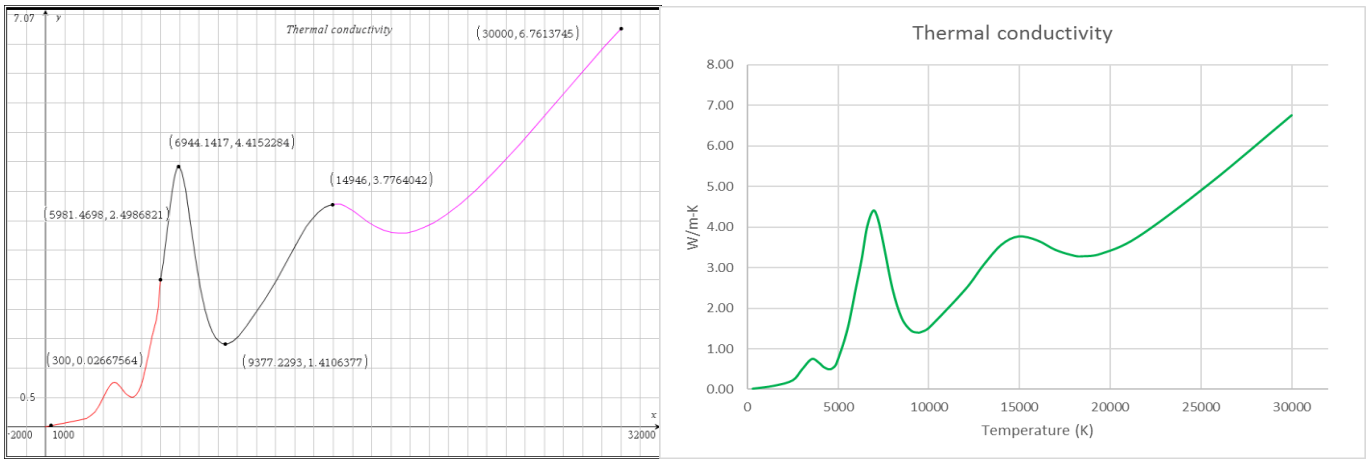

a) b)

Figure 3-10 Thermal Conductivity for high temperature air [42], a) plot in TI-Nspire CX CAS software, b) plot in Excel.

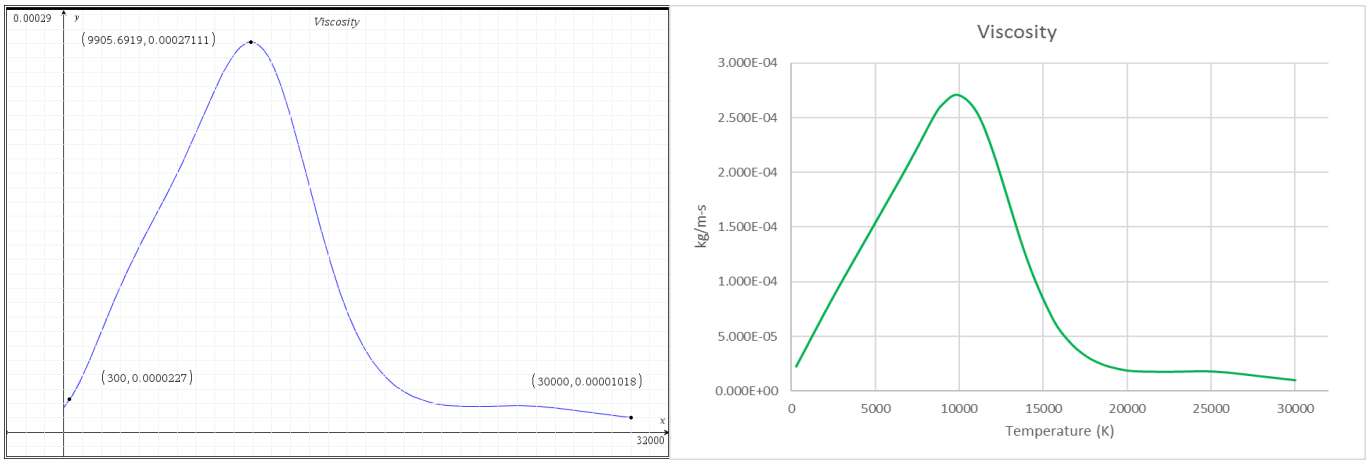

a) b)

Figure 3-11 Viscosity for high temperature air [42], a) plot in TI-Nspire CX CAS software, b) plot in Excel.

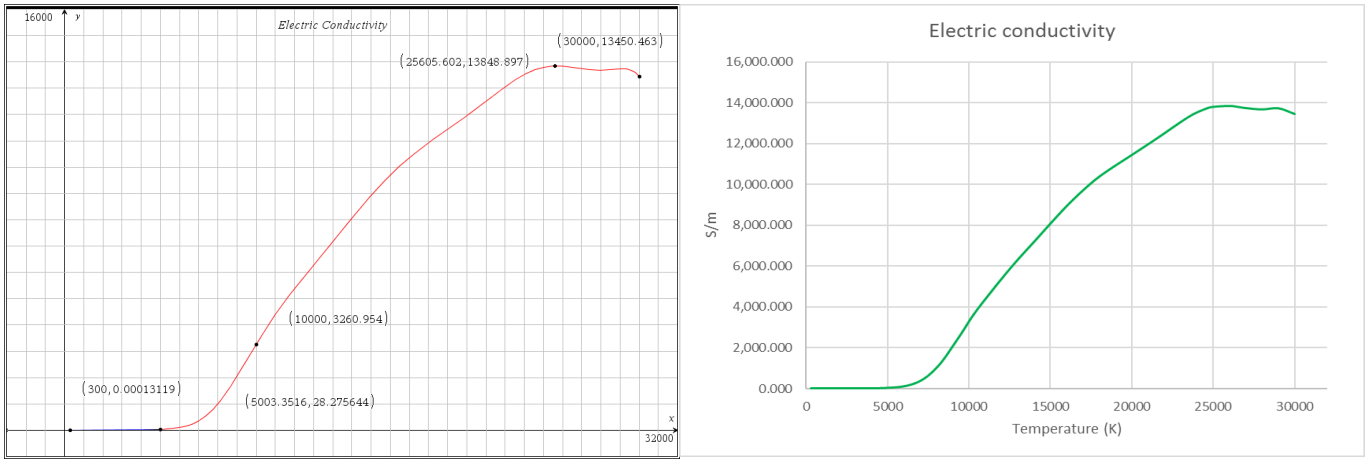

a) b)

Figure 3-12 Electric Conductivity for high temperature air [42], a) plot in TI-Nspire CX CAS software, b) plot in Excel.

As can be seen, physical properties of the air vary in a wide range of temperature. It must be reminded that inside the chamber the air temperature varies from ambient temperature, around 300K, up to around 25000K when plasma state is achieved. Thus, it is important to consider the variation of the air properties with temperature, as the accuracy of the model is directly affected by the correct definition of these values.

Also, in order to obtain convergence in the simulation process some change have been done: for example in the plasma density (Figure 3-8), a smoother curve has been proposed to avoid very large gradients due to the abrupt changes of this property to avoid divergence during the calculation, also the same has been done for the specific heat (Figure 3-9).

3.2.4 Interfaces and boundary conditions

To define a problem that results in a unique solution, it is necessary to specify information on the dependent (flow) variables at the domain boundaries, [43]:

- Specify fluxes of mass, momentum, energy, etc. into the domain. Defining boundary conditions involve:
    - Identifying the location of the boundaries (e.g., inlets, walls, symmetry)
    - Supplying information at the boundaries
- The data required at a boundary depends upon the boundary condition type and the physical models employed.
- User must be aware of the information that is required for the boundary condition and locate the boundaries where the information on the flow variables are known or can be reasonably approximated.
- Poorly defined boundary conditions can have a significant impact on the solution.

As was said before, the following domains have been defined: fluid volume or air, splitter plate, cathode, and anode. The material used in solid domains (cathode, anode and splitter plates) is copper, with constant physical properties and no dependency with T or P. The material used in the fluid volume has been specified as a UDF, with the properties of plasma, (Figure 3-8-Figure 3-12).

Once the domains have been defined, the behavior of interfaces and outside boundaries of the model have to be also defined. The interfaces are the common surfaces between different domains, air, and solid parts. The boundary conditions applied to these common surfaces of the model are described in Table 3-3 and Figure 3-13.

Table 3-3 Boundary conditions applied in the model

Boundary	**Temperature (K)**	**Pressure (Pa)**	**Electric Field**	**Magnetic Field**	**Type of boundary**
Front and back walls of air, splitter plate, and electrodes. Air_Wall_Down	Adiabatic	-	Zero flux	Import magnetic field	No slip wall
Interfaces	Heat exchanger	-	Coupled boundary	Coupled boundary	No slip wall
Openings	300	0	Zero flux	Zero flux	Opening
Anode_Down	500	-	50 A	Zero flux	Wall
Cathode_Down	500	-	0 V	Zero flux	Wall

All the boundaries of the model have been taken from [9], but with some modifications. At the boundaries between the model and the surroundings, at the front and back walls of the air, splitter plate and electrodes, plus the down part of the air (named as Air_Wall_Down in Figure 3-13), no external interaction has been defined, considering the temperature exchange as adiabatic. Neither exists an interaction of the electric and magnetic field with the outside. In order to avoid the reverse-flow, an extra volume of air is added over the splitter, thus the quantity of these flows is reduced, and with this does not affect the simulation, and only the quantity of elements in the mesh is increased in part.

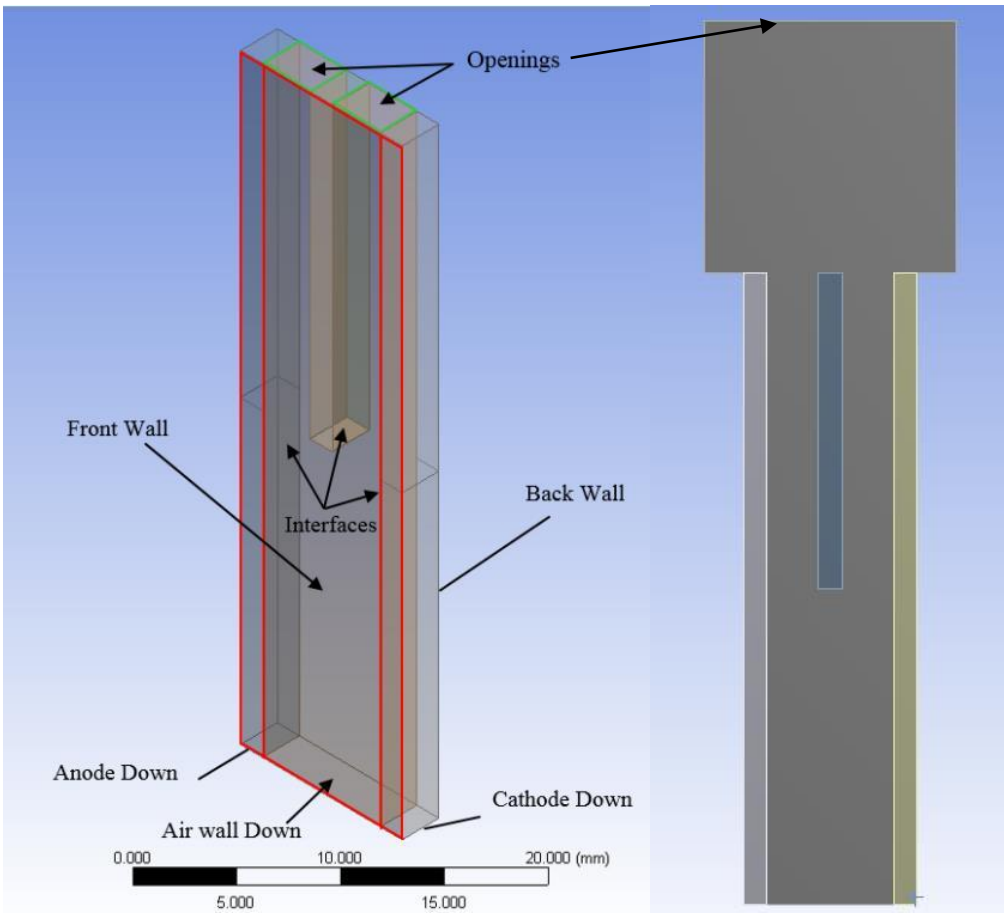

Figure 3-13 Boundary conditions on the model.

- The solid walls have been defined with non-slippery condition, which means that the fluid velocity is zero at the walls in contact with the fluid.
- At the interfaces air-electrodes and air-splitter plate, the temperature exchange has been defined as heat exchanger, just to try to optimize the model proposed by [9]. Regarding electric and magnetic field, a coupled boundary is applied at the interfaces. It implies that the variables will flow between both sides of the interface. Once again, the wall is defined non- slippery.
- At the top face, the opening of the air volume (see Figure 3-13) is at atmospheric conditions, thus the temperature is set to be 300K and the pressure is equal to 0 Pa. No interaction is defined for the electric field. The magnetic field density is exported from Maxwell or Flux.
- The temperature of the lower face of anode and cathode are 500K, in order to improve the stability and avoid divergence errors due to the high difference of temperatures imposed in the initialization stage on the solid part and air volume.
- Finally, in the down face of the anode, an incoming current of 50A has been imposed, and in the down face of the cathode 0V or grounding has been considered, to define the direction of the arc between electrodes.

3.2.5 Parametrization

After geometry, mesh, domains and boundary conditions have been defined, parameterization of the rest physical conditions is necessary:

- **Magnetic fields:** regarding to **B**, Maxwell equations are solved simultaneously with the Maxwell product. Also, the same case with the use of Flux product.
- **Radiation**: The radiation P1 model is used in this case. Radiation takes into account the thermal exchange due to the elevated temperatures appearing in the electric arc. Thus, it is an important term in the energy conservation equation.
- **Arc roots**: In this thesis, the voltage-current density curve characteristics for modeling arc roots is not considered, only need to know the pressure values, current density, and temperature during the arc.
- **Arc initialization**: The ignition of the arc has been modeled initializing a hot cylindrical channel of 10,000K between the rails, which has been initiated at 10 mm from the lower face (Air_wall_down).
- **Solver data**: Finally, the simulation has been set-up to 1ms, with a time-step of $2.5x10^{-6}$s.

3.3. Software Set-up

To reduce the complexity of the simulation, a few assumptions and simplifications are adopted as follows.

- Plasma in the chamber is in a state of local thermodynamic equilibrium (LTE).
- Arc ignition and contact-opening process are not included in the simulation. The calculation begins with a stationary temperature distribution between two electrodes.
- Vapors from electrodes, splitter plates, and wall material are not considered in the model.
- The eddy current in arc and metal part is not included in this model.

3.3.1 Set up in MHD module

As was explained before, in this thesis the MHD module integrated to Fluent, with a coupling between Maxwell and Flux is proposed in a simplified geometry.

The first step is to load the MHD Module**.** The MHD module is loaded into Fluent through the text user interface (TUI). The module can only be loaded when a valid Fluent case file has been set or read. The text command to load the module is:

define → *models* →*addon-module*

A list of FLUENT add-on modules is displayed (Figure 3-14):

```
Done.
define

/define> models

/define/models> addon-module
Fluent Addon Modules:
     0. None
     1. MHD Model
     2. Fiber Model
     3. Fuel Cell and Electrolysis Model
     4. SOFC Model with Unresolved Electrolyte
     5. Population Balance Model
     6. Adjoint Solver
     7. Single-Potential Battery Model
     8. Dual-Potential MSMD Battery Model
     9. PEM Fuel Cell Model
     10. Macroscopic Particle Model
Enter Module Number: [0]
```

Figure 3-14 Modules of ANSYS Fluent.

- Select the MHD model by entering the module number 1. During the loading process a scheme library containing the graphical and text user interface, and a UDF library containing a set of user defined functions are loaded into FLUENT. A message Addon Module: mhd2.1...loaded! is displayed at the end of the loading process.
- Once the MHD module is loaded some configurations are necessary in order to get convergence during calculation and well approximation to reality during the simulation process.
- In Fluent, in the Models task page, select the MHD model, after this choose the electrical potential method (Figure 3-15). This is for the solution problem, also this allows us to define the current density in the boundaries and potentials.

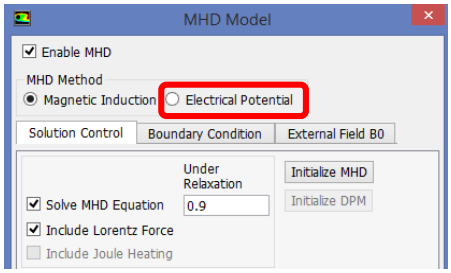

Figure 3-15 Set-up MHD module.

The considerations to start the analysis are:

- Select a transient simulation in the General task page (Figure 3-16 a)
- Choose P1 Radiation model and a Turbulent k-ε or laminar Analysis (Figure 3-16 b)
- Compile plasma UDFs (Figure 3-17), load in the Materials task page (Figure 3-18),
- Define the cell zone condition for each zone of the model (Figure 3-19),

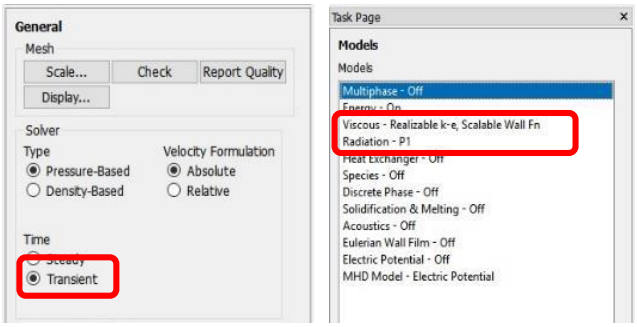

a) b)

Figure 3-16 Set-up of transient simulation, P1 radiation model and turbulent analysis.

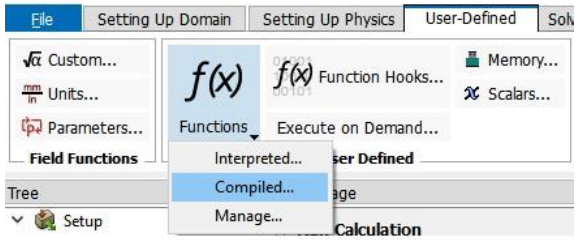

Figure 3-17 Compilation of plasma properties.

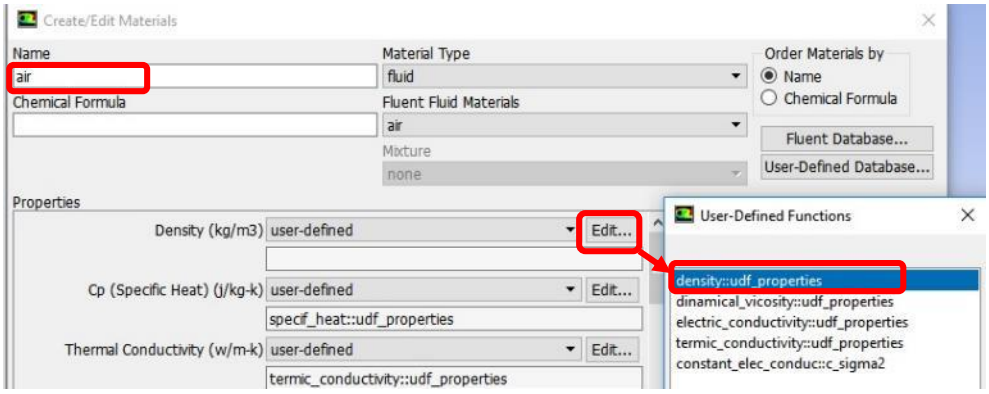

Figure 3-18 Loading material properties.

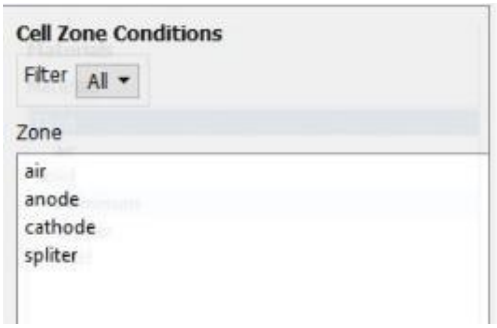

Figure 3-19 Set-up cell zone condition.

- In the solving tap, modify the limits for the simulation and the solution controls (Figure 3-20-Figure 3-21). These modifications depend on the characteristics of the problem, type of simulation and complexity of geometry.

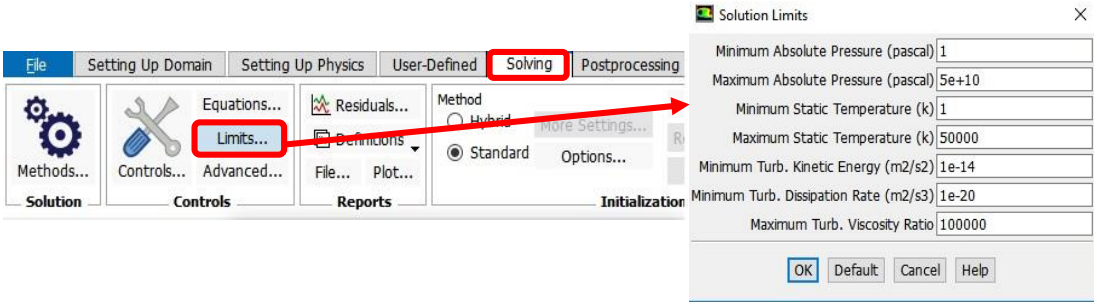

Figure 3-20 Configuration of limits of the simulation.

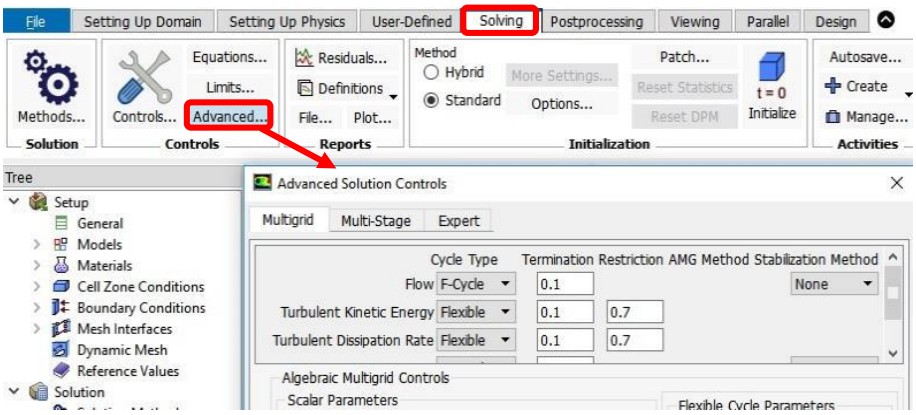

Figure 3-21 Advance configurations for the solution controls.

- In the Solution Methods task page, select the Coupled scheme, with the second order spatial discretization for all the equations, except for the turbulent term and electric potential, keep these last ones in first order (Figure 3-22). Also, modify the relaxation factors as shown in Figure 3-23 to get a quick convergence of the equations.

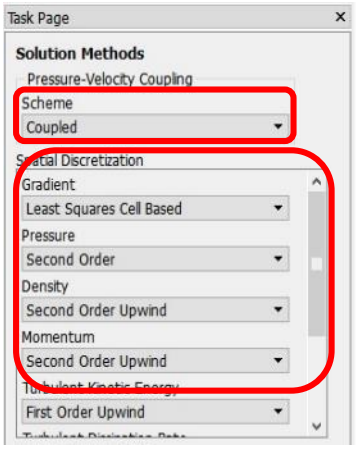

Figure 3-22 Solution Methods Set-up Fluent.

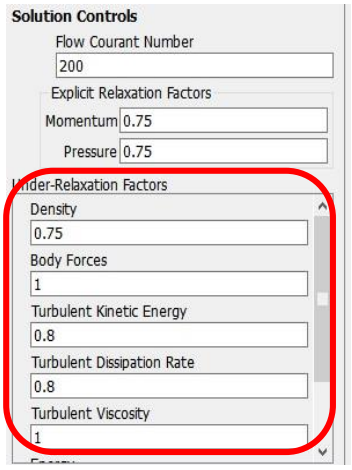

Figure 3-23 Solution Controls Set-up Fluent.

- With all the last preparations for the model, now the simulation can start with a time step of $2.5x10^{-6}$s (or $1x10^{-6}$s), and 30 of maximum iterations for each one (Figure 3-24).

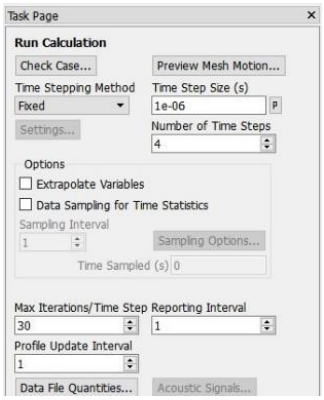

Figure 3-24 Set-up of Run Calculation.

3.3.2 Set up in Maxwell

The steps to start Maxwell are very simple, and the simulation set-up too. First start Ansys-Maxwell in the direction folder where is installed, or open it from Ansys-Workbench (Figure 3-25).

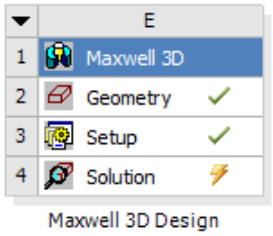

Figure 3-25 Toolbox of Maxwell.

- Since the geometry will be the same as the one used in Fluent, export it from the direction folder where is stored, as, Modeler → Import.
- Consequently, assign the material properties for each zone in the model, and create a vacuum region, which means that in this mart just the magnetic field density will appear, (Figure 3-26-Figure 3-28).

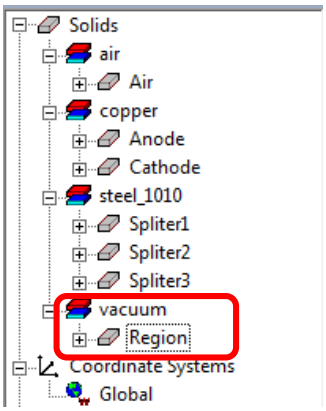

Figure 3-26 Assignation of each zone in the geometry

- Then define the type of analysis to do, in this case, a Magnetostatic is chosen. After that assign the direction and the magnitude of the current at the lower part of the anode and cathode (Figure 3-27). Also, define the characteristics of the mesh, in this case, a mesh with a maximum length of 1 mm is chosen (Figure 3-28).

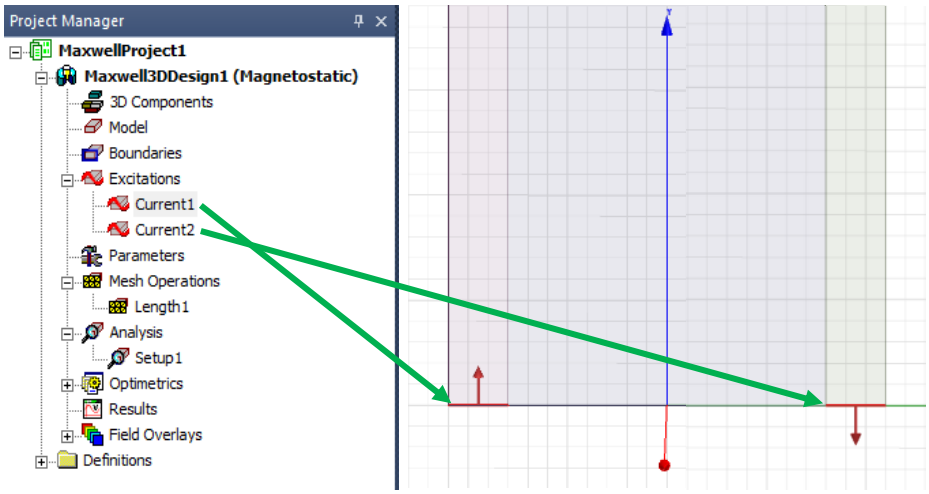

Figure 3-27 Set-up of Magnetostatic simulation and assign of direction current in Maxwell.

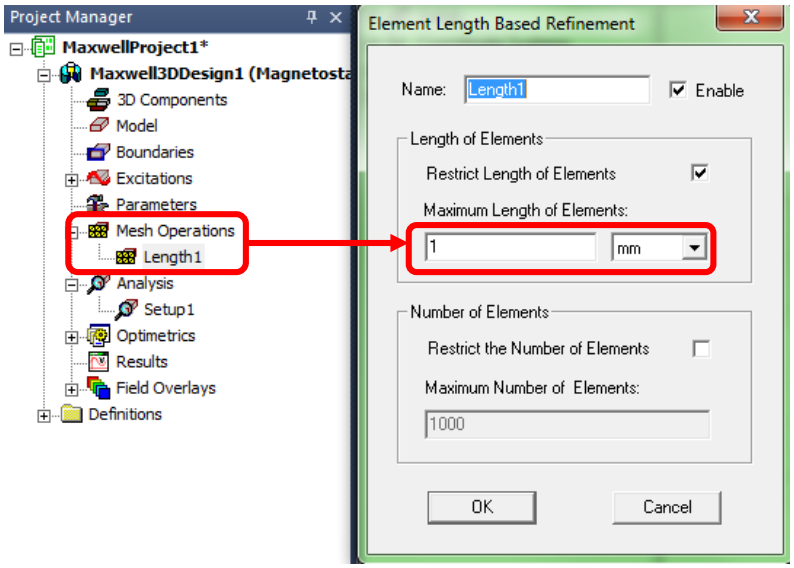

Figure 3-28 Set-up Mesh length in Maxwell.

- After that, right click on Setup1, and select Configure Fluent Conductivity Coupling, then paste the direction folder where the information from Maxwell will be stored, in this way, the UDF for the coupling will access to this folder (Figure 3-29).

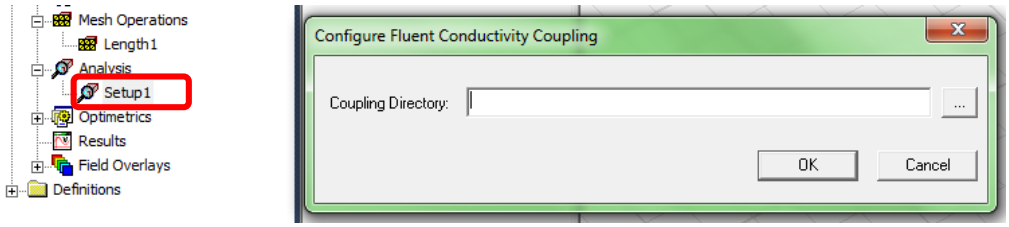

Figure 3-29 Configuration of Fluent conductivity coupling.

- Finally, it is a good practice to check all the set-up with the Validation option from Maxwell, in this way the program checks all the simulations parameters (Figure 3-30).

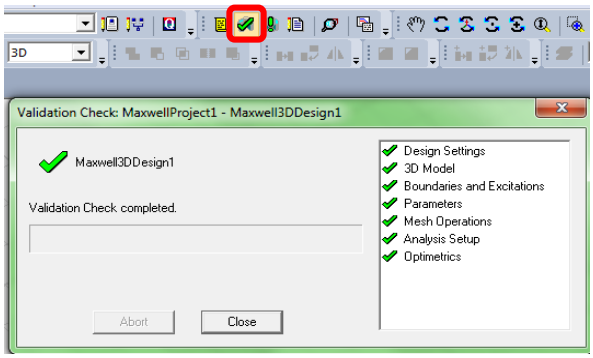

Figure 3-30 Validation check of the set-up.

Set up in Flux

The steps to start the simulation in Flux is similar to Maxwell. The general way to start is as follows:

- The first step to develop a simulation in the software is to import a geometry in the Modeler context section of Altair Flux (Figure 3-31), the models of the qualitative study of the CB were created in a solid modeling computer-aided design (CAD) software. The other cases were built using the geometry section of Flux.

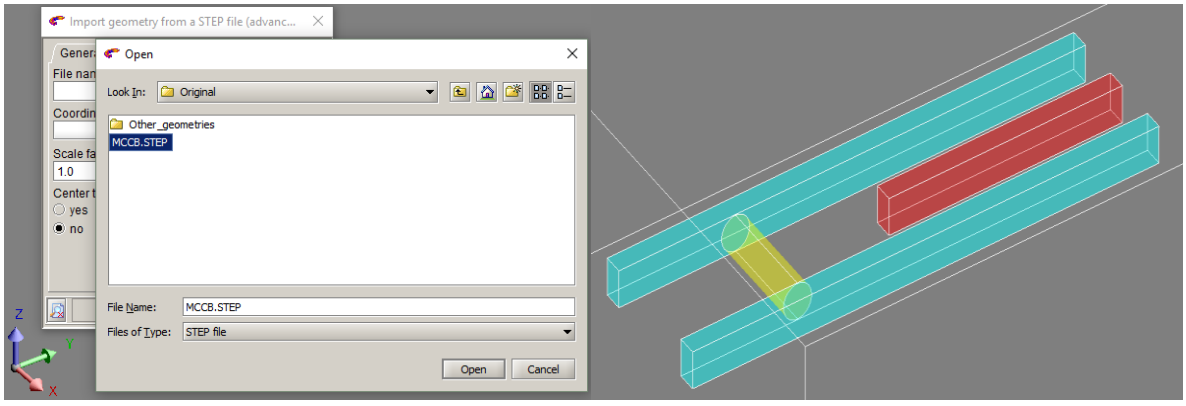

Figure 3-31 Geometry imported from the modeler context.

- The next step is to create the mesh of the model, to do these mesh points are created with the tool of mesh in the Mesh context (Figure 3-32). Once the meshing process is done, the physical context needs to be configured. Now select the application that will help to solve correctly the problem studied, in this case, the application selected is Transient Magnetic (Figure 3-33).

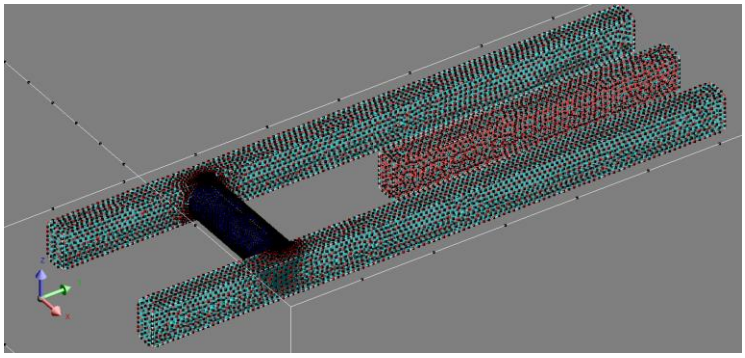

Figure 3-32 Mesh model of the CB.

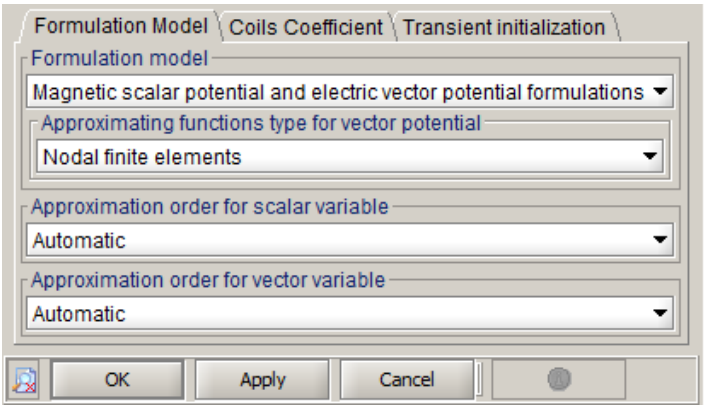

Figure 3-33 Configuration of the formulation model in Transient Magnetic 3D application.

- After that, the next step in the Physics mode, now create the equivalent circuit in the circuit dedicated context (Figure 3-34).

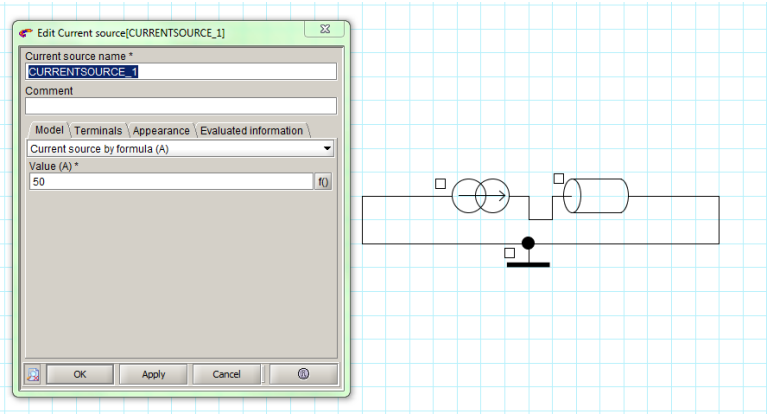

Figure 3-34 Current applied to the model in the circuit dedicated context.

- Consequently, is chosen the materials database that will give the properties of the materials used in the construction of the CB. The database of Flux is opened by selecting the materials option and clicking the option import from material manager (Figure 3-35).

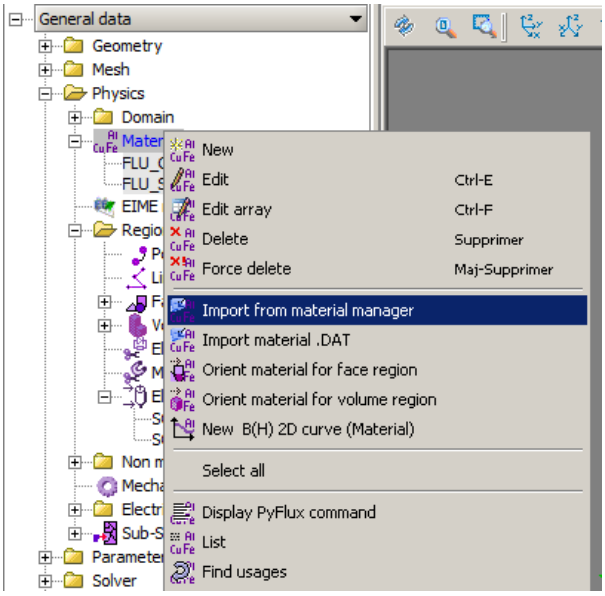

Figure 3-35 Importing material from material manager.

- The following step after this assignation is to create the volume regions, in this option, are designed the properties of the materials for each volume of the geometry. In this case, a region for each component is created. All the material selected were copper.
- After, the assignation of each volume, the next step is to assign the terminals to solid conductors. A face of the geometry is chosen to define the input current and other is assigned to establish the face where the current will get out (Figure 3-36).

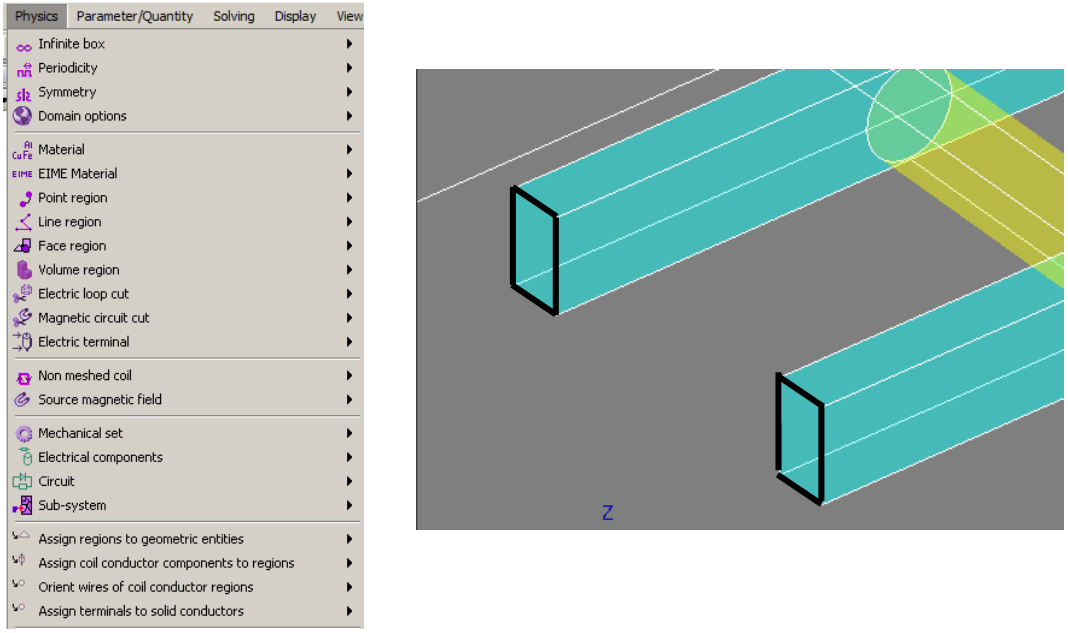

Figure 3-36 Assignment terminals to solid conductors.

- The last step in the physics context is to add and activate the macros needed to avoid the effect of the eddy currents in the DC model. This is done going to Extensions click in Loads and selecting the Macros_Flux3D_Physics/SolidConductorNoEddyCurrent/ SolidConductorNoEddyCurrentCreate.PFM. This step is done for all the macros saved in the folder "SolidConductorNoEddyCurrent".
- Finally, click on the first icon: and select the volume regions that are solid conductors, in this case select all, excluding the air region. The last step before running the simulation is to create a scenario. This is done in the Scenario section and selecting a New scenario (Figure 3-37).

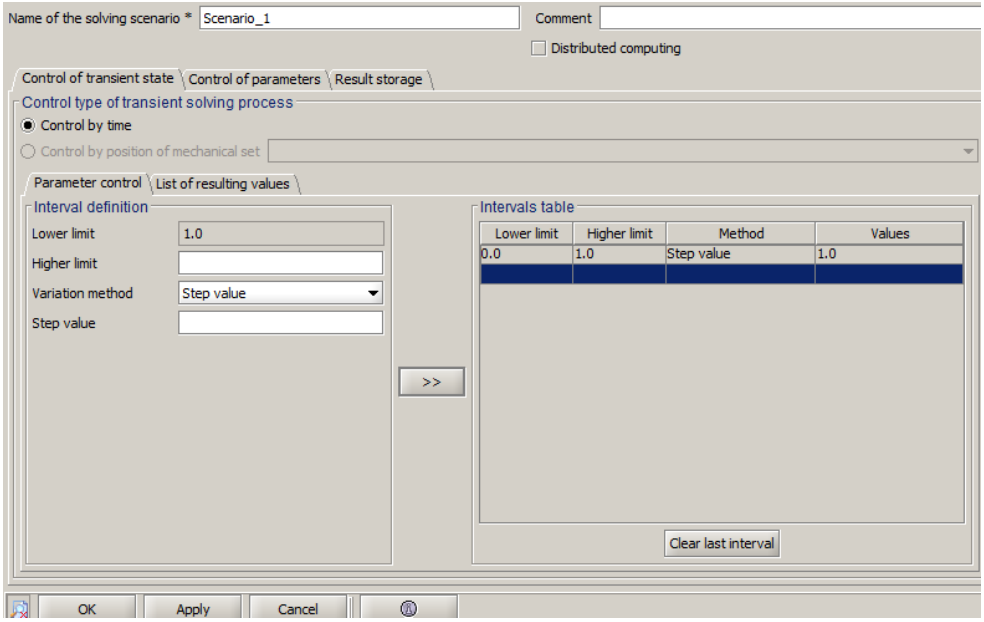

Figure 3-37 Scenario to solve the MCCB extinction module model.

- Now, the model is ready to solve, then, click to solve button. The post-processing analysis depends on the objectives and what want to analyze.

Chapter IV

4.1. Simulations cases

This research project is aimed to obtain the best practical simulation in order to obtain the behavior of the electric arc formed in a CB, using the parameters of the cases described in [9]. In this process, several simulation alternatives were explored, for example: $3D_S$ vs $3D_F$ analysis, laminar vs turbulent flow. In this section, the different cases are explained, and in Table 4-1, the final cases are listed with the most important brief comments. Finally, in chapter 5, the results are discussed.

Table 4-1 Cases analyzed

Case	Type of analysis	Tests		Description
A	Justification analysis	A1	Case simplified 3D	A 3D simplified ($3D_S$) analysis is developed to corroborate that the results are not so far from a 3D Full one.
		A2	Case Full 3D	A Full 3D ($3D_F$) analysis is performed to compare with case A1.
B	Base model	B1	Case base with radiation and laminar model	A $3D_S$ simulation with and radiation, to know the values of current density, temperature, and pressure. Compare the results with [9].
		B2	Case base with radiation and turbulent model	A $3D_S$ simulation with and radiation, to know the values of current density, temperature, and pressure. Compare the results with [9].
C	Coupling Maxwell-Fluent	C1	Case to get **B** and use in case E	A $3D_S$ coupling between Maxwell-Fluent is performed to get a value of **B** more accurate.
D	Coupling Flux-Fluent	D1	Case to get **B** and use in case E	A $3D_S$ coupling between Flux-Fluent is performed to get a value of **B** more accurate.
E	Comparative analysis	E1	Case with **B** from Maxwell	A final $3D_S$ simulation is performed with the values of **B** from the best result (C-D).

In group A are the simulations for the use of a $3D_S$ model instead of a $3D_F$ one. In this case, the magnetic field has been imposed in the negative Z direction with a constant value of 0.2T. The radiation model has been set as P1-radiation model, turbulent model is k-epsilon. During this simulation just the values of temperature and shape of the arc are shown.

For the group B, the models consider the effect of radiation and turbulent/laminar regimen. In this case, the magnetic field has been imposed in the negative Z direction with a constant value of 0.1T. The radiation model has been set as P1-radiation model, turbulent model is k-epsilon and laminar regimen in $3D_S$ geometry to reduce the simulation time, updated data for air and fine mesh. The arc roots, have not been included. This case is the base for the next simulations. Some of the considerations made in [9] have been not taken into account because of the software Ansys-Fluent was not able to perform since it required a more extensive coding. However, all these considerations are mentioned in section 7 to leave them as a future work.

In case C, the coupling between Maxwell-Fluent is performed. This coupling is made in order to obtain the magnetic flux density **B** during the movement of the arc. Similarly, to the case A, the P1-radiation model has been set, $3D_S$ geometry, updated data for air and a fine mesh are used. The results of this analysis will be used to obtain a value of **B** closer to reality, which will be used in case E.

In case D, the same arc simulation is done, with the goal of obtaining the magnetic flux density **B**, with the use of the Flux product. The magnetic flux results are compared with the ones obtained in the case C. The objective of this simulation is to have an alternative calculation that allows comparing the values of **B** calculated in Maxwell during the electric arc phenomenon.

Finally, in case E, the values of **B** obtained from Case C and D are used in case base B. This is done in order to obtain an arc behavior more similar to reality. In this case, the P1-radiation model has been set, $3D_S$ geometry, updated data for air and a fine mesh are used. A comparative with [9] and case B is done but, taking into account that the results are somewhat different because they are not considering the arc roots, neither the calculation of **B** in the same software.

In each simulation case, the results of temperature, pressure and current density are presented. The temperature is presented in rainbow scale and current density in color vectors. In the case of pressure is presented in plots showing the evolution during the time. The image contours have been extracted from the middle plane of z-axis at different time steps. Besides, graphics for the evolution of maximum current density in the air and in the splitter plate and temperature of the fluid flow are shown.

All the simulations models have been run in parallel in a computer with eight cores, of 3.5 GHz each and 32 GB of RAM, in a Windows 10 operating system. For the case B the simulation was done in serial with one core. The simulation model of 1ms took around one day to be solved and in some cases three days.

4.2. Case A: Justification analysis

In case A, a simulation in $3D_F$ and another in $3D_S$ are performed. In this case, only the maximum temperature values are measured throughout the simulation at different timesteps. The main objective of these simulations is to justify the use of a $3D_S$ model instead of a $3D_F$ one. With $3D_S$ models, the computational times are considerably reduced. However, the

temperature values, as well as the duration of the electric arc, are expected not to be exactly the same. The simplification of $3D_F$ to $3D_S$ should mainly be understood as a measure to quickly obtain the shape and characteristics of an electric arc, however, this approach is not the most appropriate, and only for reasons of this thesis is used. In Chapter 7 the modeling of the $3D_F$ phenomenon is placed as future work.

4.3. Case B: Base Model

In case B, a simulation based on reference [9] is performed in order to have a comparative for the next simulations. This way has been taken the same dimensions for the whole geometry, a 40x11mm chamber, with the anode, cathode, splitter plate and air, has been designed, including a full geometry without symmetry and with $3D_S$ and UDF data for air. The initialization of the arc has been defined by a hot channel of 10,000 K at 10mm from the lower face of the air and 50 A is injected from anode to cathode. The radiation P1 model has been used, the turbulent model is k-epsilon and a constant magnetic field of 0.1 T has been imposed in the negative Z direction.

This base model does not consider the arc root birth because of the software Ansys-Fluent was not able to perform it since it requires a more extensive coding. In this case, the coupling between Fluid flow and Maxwell equations is performed by the MHD module of Fluent. The main objective for this is the verification of the parameters and be sure that are right between the two-physics involved.

4.4. Case C: Coupling Maxwell-Fluent

In this case, the coupling between Maxwell-Fluent is presented. The base model C, previously presented, with 50A of input current in the anode, one splitter plate in the chamber and the rest of the characteristics explained are the same. The difference in this second case is a coupling between Maxwell and Fluent to obtain the magnetic flux density **B** during the movement of the electric arc. Similarly, to the case B the P1-radiation model has been set, $3D_S$ geometry, UDF data for air and a fine mesh are used, the initialization of the arc has been defined by a hot channel of 10,000 K at 10 mm from the lower face of the air.

The main concern in this thesis is the value of **B** which is imposed in all the cases. For example, in case B, a constant value is assigned but in the real life this value can change in function of current density, the permittivity of the medium, the surrounding and it varies with time. For these reasons a coupling between two tools is chosen, to obtain an appropriate value of **B** during the arc movement.

A $3D_S$ simulation is done, since, this particular coupling takes a long time to finish, to have an idea, in a mesh of 200,000 elements the simulation time for each time step is around 10 minutes, and given that the mesh used in $3D_F$ has more than 1 million elements the computational time grows, making almost impossible the study of more complex cases with the same computing facilities.

4.5. Case D: Coupling Flux-Fluent

In case D, similar to the case B but with a different software, the coupling between Flux-Fluent is presented, with 50A of input current in the anode, one splitter plate in the chamber and the rest of the characteristics explained are the same. $3D_F$ geometry is used, also, like the case C, the initialization of the arc has been defined by a channel at 10 mm from the lower face of the air.

As was explained in the case C, the concern in this thesis is the value of **B** which is imposed in all the cases. Because in real life, this value can change in function of current density, permittivity of the medium, the surrounding, and it varies with time. In this manner, the objective of this simulation is to have an alternative calculation that allows us to compare the values of **B** calculated in Maxwell during the electric arc phenomenon.

The computational time of this coupling is less compared with case C. However, given that the software used is incompatible, the changes to the plasma shape (in Flux) must be performed in a parametric model, changing the diameter, length, and inclination with approximations to reality. This generates a greater error level in comparison to the results of case C, making an analysis of this type not very precise but quick.

4.6. Case E: Comparative analysis

Finally, in case E, a comparative simulation is performed based on the best results between C and D. An input current of 50A is injected to the anode, one splitter plate in the chamber and the rest of the characteristics explained are the same. Also, the P1-radiation model has been set, a $3D_S$ geometry, UDF data for air and a fine mesh are used, also, like the case B, the initialization of the arc has been defined by a hot channel of 10,000 K at 10 mm from the lower face of the air.

The results from this simulation are compared with case B, in which an imposed constant magnetic field of 0.1T was used. The results will show notable differences, because of, case B will be more an approximation and in case E will result more similar to real life. It is important to remember that some considerations imposed in [9] were omitted for the reasons explained in case A and B.

With this last case, the main objective of this thesis is achieved, giving all the main parameters necessary for a suitable simulation during arc phenomena using the MHD module of Ansys-Fluent and the considerations necessary for a plasma in an air atmosphere.

All these are the cases that finally gave better results, others were simulated with different configurations, but without promising results, and of all the 5 cases exposed here, only cases B and E showed a better performance compared to the others. In section 5 the results of each one is explained in detail. In Annex D a comparative with the experimental test of [9] is performed.

Chapter V

Throughout this section the main results of the simulations will be described, in each case, the contours of temperature will be exposed at different timesteps, in addition to the graphs as a function of time for temperature, pressure, current density and radiation. The results obtained correspond to the cases described in chapter IV, using the same order. At the end of each case, a summary with the most important results is presented.

5.1. Case A1. Justification analysis ($3D_S$ model)

As discussed in chapter IV, the cases A1 and A2 were prepared with the idea of justifying the use of $3D_S$ models instead of a $3D_F$. This approach is very important because the use of $3D_S$ models reduce considerably the computational time. After reviewing the results obtained, the use of $3D_S$ models can be justified. Furthermore, the behavior of the electric arc is the same, except at the starting process.

As always happen, the use of 3D models gives more precise results since it is a closer representation of what happen in the real world. Nevertheless, for the electric arc behavior, a $3D_S$ simulation gives good results. As an example: the electric arc temperature, the behavior of the electric shape and the movement are very close to the $3D_F$ results.

In this section, the results of temperature distribution in the electric arc are presented at different timesteps (Figure 5-1). In this case, a $3D_S$ analysis is performed. The initialization of the arc has been done with a high electrical conductivity, at a height of 15mm from the bottom wall. A current of 50A is entered at the anode and finally, a magnetic flux density of 0.2T is imposed in the negative Z direction (when the temperature reach 10,000K). The initialization is done in this way in order to obtain a quick result. The total simulation time is 0.2ms.

In these results, initially, the electric arc starts at a temperature around 300K and acquires a uniform circular shape. After this, the temperature begins to expand. At 0.07ms the arc reaches the bottom of the splitter and begins to bend, acquiring a "u" shape. After this 0.09-0.16ms the arc continues to deform until it reaches the splitter in 0.17ms. Finally, the arc continues moving vertically, ending in 0.2m. It is observed that in this time the arc still does not leave the area of the splitter.

The graph of temperatures is presented in Figure 5-2, where a tendency to rise is observed, the temperature reaches a peak of 14,838K in 0.02ms. After this, the temperature tends to fall at a value of 9,890K in 0.057ms and then drops to 6,875K 0.081ms.

Finally, from 0.1ms until the end of the simulation (0.2ms), the temperature stabilizes in 6,000K, without observing a very noticeable variation. Next, in case A2, a $3D_F$ analysis is used and the results are compared with case A1.

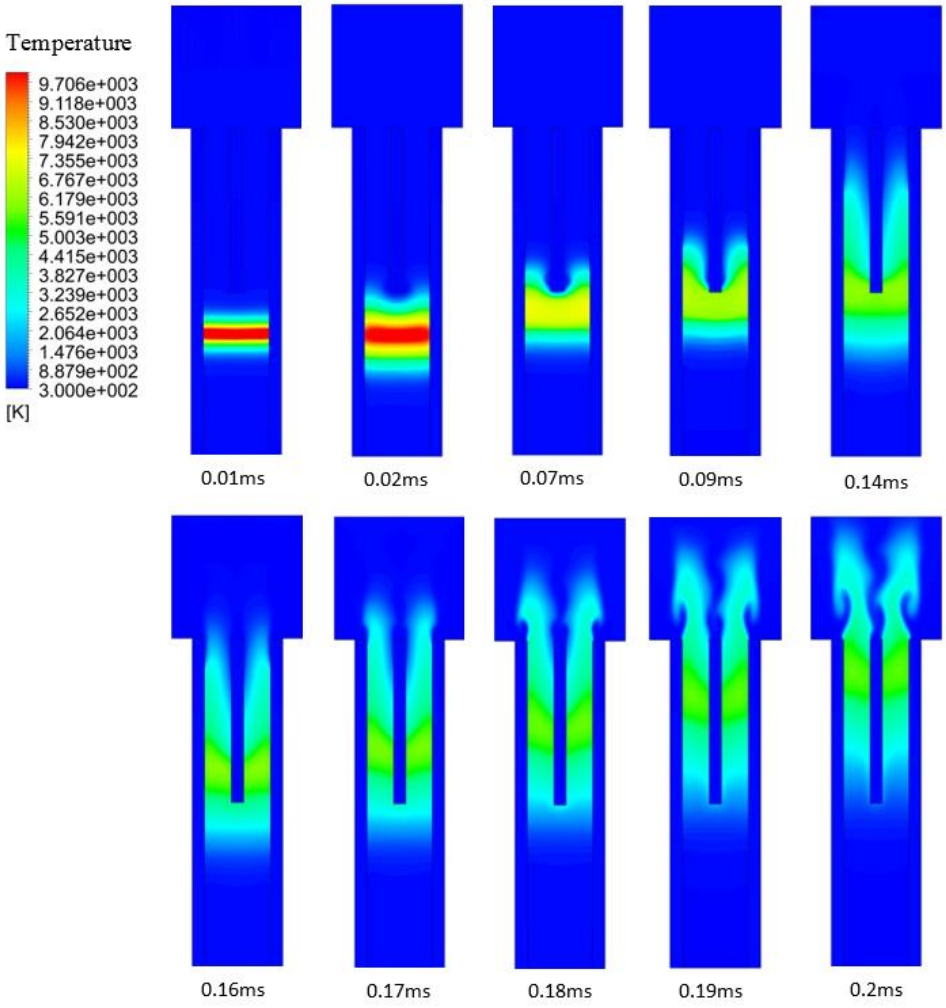

Figure 5-1 Arc movement, expressed by temperature for case A1.

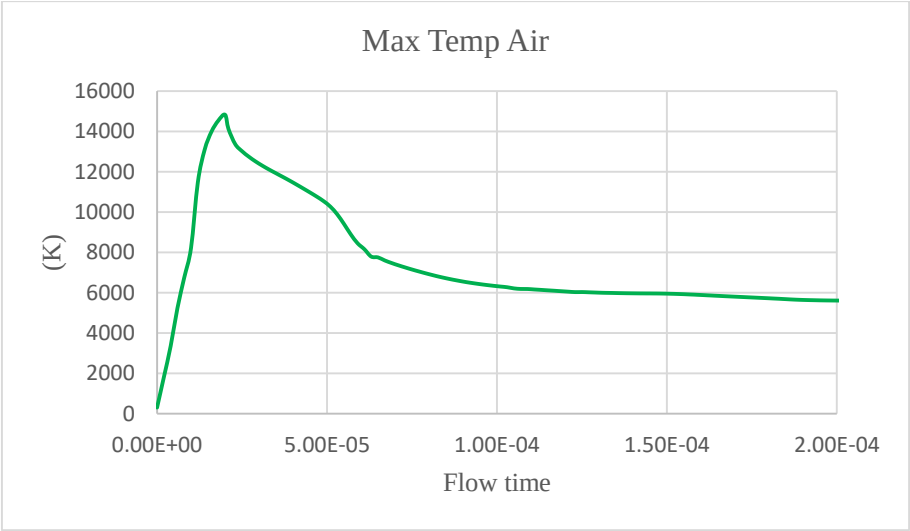

Figure 5-2 Maximum temperature in air for case A1.

5.2. Case A2. Justification analysis ($3D_F$ model)

First, the results of temperature distribution in the electric arc are presented at different timesteps (Figure 5-3). The initialization is the same as the one proposed for case A1. The total simulation time is 0.2ms.

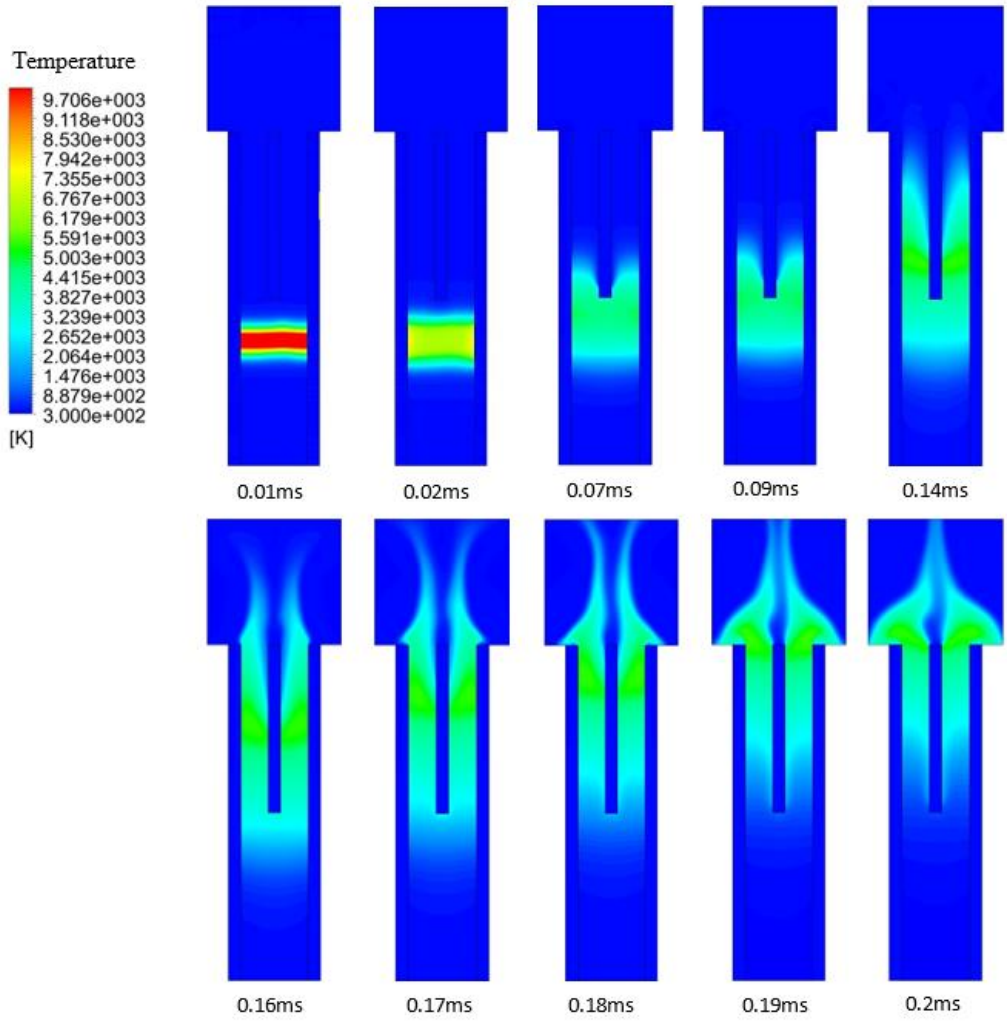

Figure 5-3 Arc movement, expressed by temperature for case A2.

In these results, it can be seen that initially the electric arc starts at a temperature around 300K and acquires a uniform circular shape. After this, the temperature begins to expand (0.2ms), even faster than the case A1. At 0.07ms the arc reaches the bottom of the splitter and begins to bend, acquiring a "u" shape. After this, from 0.09-0.16ms the arc continues to deform until it reaches the splitter in 0.17ms, (similar to case A1). However, from 0.17ms the arc moves faster, reaching the half of splitter. Finally, the arc almost reaches the outer part of the splitter, advancing a little more than the case A1.

The temperature graph is presented in (Figure 5-4), where a tendency to rise is observed, the temperature reaches a peak of 16,784K in 0.004ms. After this, the temperature tends to fall at a value of 7,580K in 0.012ms and then drops to 4,777K in 0.044ms. After this, the

temperature again begins to increase, reaching a value of 5,495K in 0.1ms. From this time until the end of the simulation (0.2ms) the temperature varies around 6000K, with a tendency to increase.

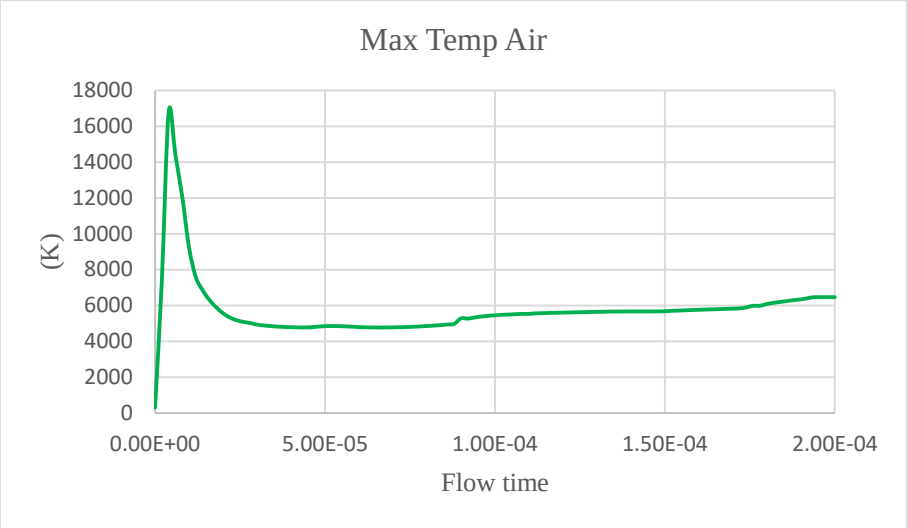

Figure 5-4 Maximum temperature in air for case A2.

Comparison case A1 vs case A2

Now a brief comparison of these two cases is done. First of all, in both cases the total simulation time analyzed was 0.2ms. The temperature distribution remains uniform at time 0, (around 10,000K). In 0.02ms the temperature distribution is slower in case A1 compared with case A2, where it expands faster. Also, a slower behavior from 0.02-0.14ms can be observed in case A1, and in case A2 is a bit faster, besides in 0.14ms the arc is just entering the splitter and in case A2 it is already inside.

From 0.16ms to 0.2ms the arc continues moving in both cases, however, it is still observed a slower behavior in case A1, where a $3D_S$ analysis is developed. At the last time (0.2ms) in case A1 the arc is still inside the splitter, on the other hand, for case A2, the arch has already left it. Concluding from this analysis that in the case of $3D_S$ the simulation times are slightly greater than with respect to a $3D_F$, a possible reason for this may be the symmetry conditions imposed in the $3D_S$, and for the case of $3D_F$ the complete thickness is considered (2.5mm), and an adiabatic condition at the walls. However, at the end of both cases the temperature values stabilize around 6000K, indicating that although they are different at the start, the arc tends to behave similarly for both cases after a while.

It should be noted that always a $3D_F$ analysis is better to understand the phenomenon, because it gives more precise results since it is a closer representation of what happen in the real world. Nevertheless, the computational time is too long, and since the only difference between these two cases is a difference in time and the temperature variation is only at the beginning, it is valid to perform a $3D_S$ analysis to know the general behavior of an electric arc, besides saving considerable time.

5.3. Case B1. Base Model (laminar regimen)

In this section, the results related to case B1 are exposed, in which a laminar analysis is performed. The Figure 5-5 shows the arc movement expressed by temperature (rainbow scale) and current density (vectors) at different times. The timesteps chosen in this case have been the same done by [9], 0, 0.3, 0.5, 0.6, 0.7 and 0.8 in order to compare the results of the arc movement.

In this case, the arc is ignited at 0ms, at 10mm from the lower part of the chamber. After that, a current of 50 A is injected from the anode, and an imposed magnetic field of 0.1T is applied in the negative z-direction.

It should be noted that this case was made in a laminar regime, however, several tests were simulated and the model did not stabilize, achieving only 0.7ms of simulation. That is why it is reported that in the rest of the cases described in chapter IV they are carried out in a turbulent regime. It remains to investigate how to make a stable laminar analysis, and therefore it is left in chapter 7 of future work.

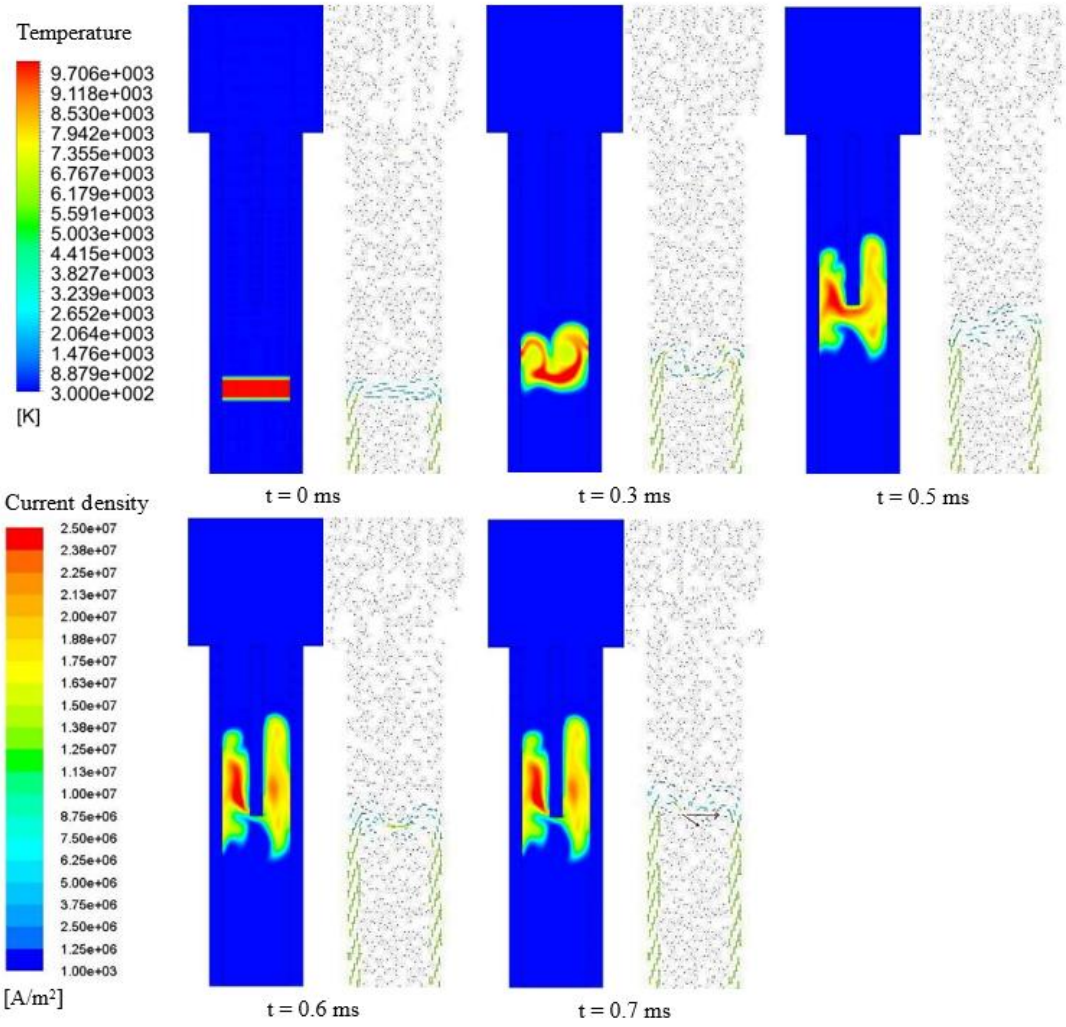

Figure 5-5 Arc movement, expressed by temperature and current density for case B1.

At time 0 (start of the simulation), the arc has the shape of a perfect circular channel, the current flows through this and exits at the bottom of the cathode. It is observed that in 0.3ms the arc still does not reach the splitter zone, besides, it has a very diffuse shape, and it does not seem to behave similar to presented in [9]. The reason can be due to the resolution methods used in [9] are unknown, and be related to a numerical error, however, in this thesis simulations the most robust resolutions methods of Fluent were used.

In 0.5ms the arc is already inside the splitter, and it acquires a "u" shape, but the arc is a bit diffuse. In 0.6ms the arc is now divided in two, due to the interference caused by the splitter. In 0.7ms, which is the last point before the simulation diverged, it is observed that the arc was already divided, however, the displacement with respect to 0.6ms seems null. It is not possible to deduce more in this case. Nevertheless, it is still to be investigated until achieving a stable model in a laminar regime.

Among the similarities between models (case B1 and [9]), the following can be highlighted. The vertical movement of the arch is almost achieved for this case. The temperature values are within the same order of magnitude (10,000K-12,000K). In case B1, the current density magnitudes (J) are almost the same as [9], and a tendency to decrease may be observed, later when the arc continues moving the J tends to decrease, since, the greater the area, the lower the current density is. In both cases the results are in the same order of magnitude ($10^5 – 10^7$ A/m^2).

Among the differences, some are highlighted. First of all, the arc shape for case B1 it is very diffuse, and when it touch the splitter it takes longer to get in, in addition, the arc shape has no symmetry, and in [9] it can been seen that there is symmetrical. Finally, the case B1 could only be simulated for 0.7ms, being impossible to extend this time.

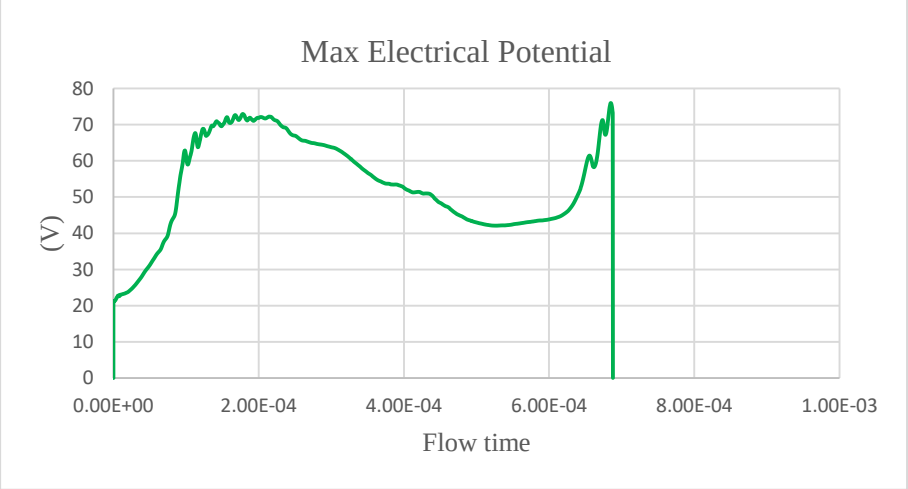

Figure 5-6 Maximum electric potential for case B1.

The voltage values that are measured in this case (Figure 5-6), although the curves for the arc root are not considered, tend to describe a similar behavior to what was is presented in [9]. At the beginning (0ms) it increases until a value of 20V. Then it begins to rise quickly

until it stabilizes at a value between 70-80V (0.01-0.026ms). This voltage behavior is very similar to that observed in Figure 2-5.

Next, from 0.2-0.3ms the voltage begins to decrease and reach a value of 42V in 0.65ms. After this, there is an accelerated increase in voltage reaching values above 70V. Finally, passing 0.7ms is when the simulation diverges and the voltage drops to 0. This divergence is not yet clear, one reason could be due to a numerical error or the resolutions methods chosen in Fluent were incorrect.

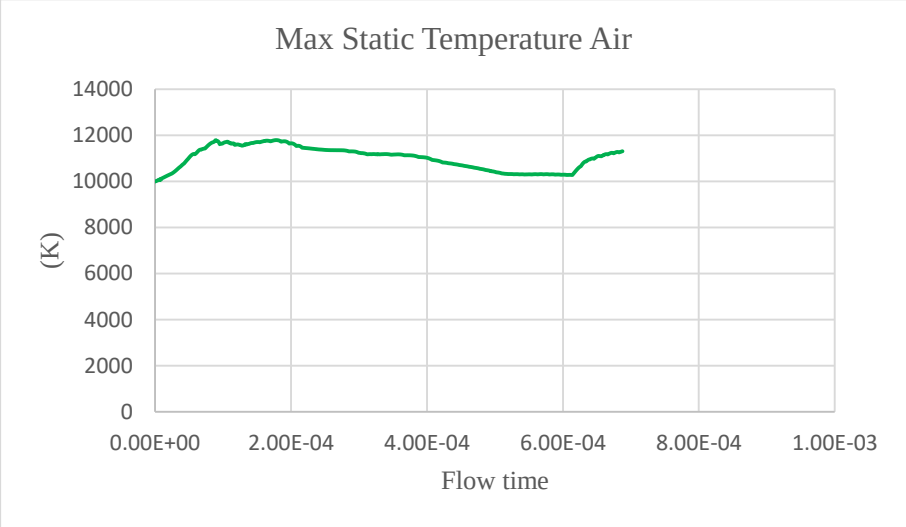

Figure 5-7 Maximum temperature in air for case B1.

In relation to the maximum temperature, the following can be rescued from the graphs. Initially the temperature of the arc starts at 10,000K and then begins to grow until a value of 11,700K at 0.1ms. This increase in temperature is mainly caused by the Joule heating, since during this period the arc shape is uniform, and the cross-section area does not fluctuate very much, making the current density invariable, and causing the increase in energy to be constant.

This temperature value remains almost constant until 0.2ms, when it begins to decrease. Something interesting that can be observed is that, in 0.5ms even though the arc is inside the splitter, the temperature of the arc remains almost constant, this behavior is similar to that is described in [9]. Finally, in 0.6ms the temperature begins to grow again, up to 11,300K, being the last point before diverging.

Analyzing the temperature distribution at the contacts (Figure 5-8) a tendency to increase is observed, until a maximum value of 460K. This is mainly due to the constant 500K temperature imposed in the lower part of each contact, besides, the effects of heat transfer by convection in the walls and the fluid are not considered, since adiabatic walls were assigned, thus generating only an increase by conduction within the metal itself.

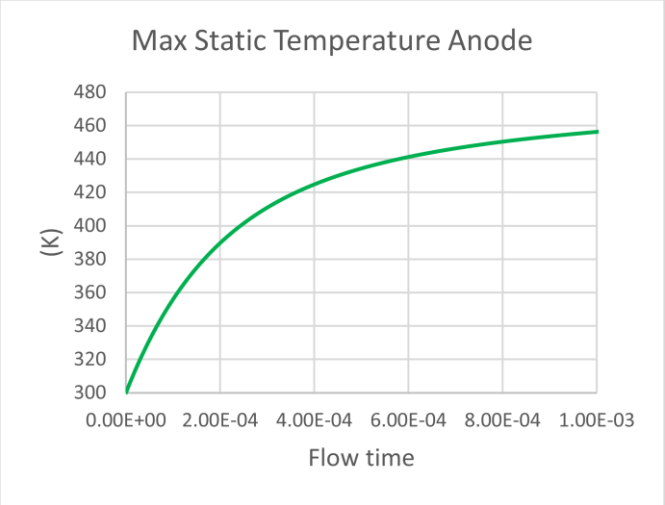

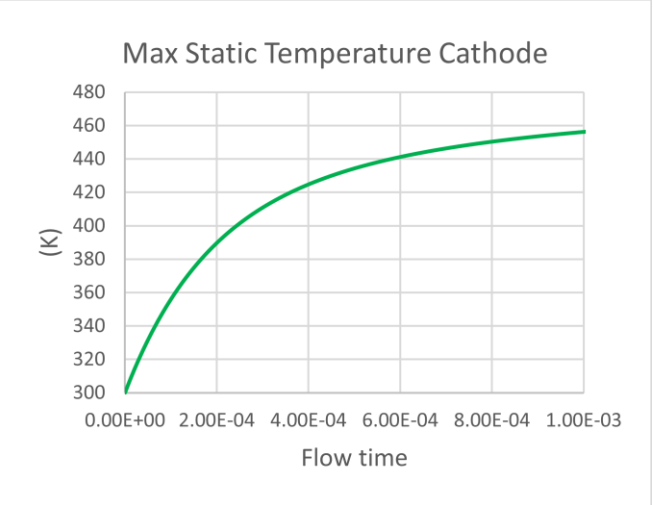

Figure 5-8 Maximum temperature in Anode and Cathode for case B1.

The temperatures measured in the splitter are shown in Figure 5-9, for this case the adiabatic wall condition was not imposed, but rather a coupled wall condition. Since the splitter is in contact with the arc, in addition, to be responsible for cooling and extinguishing it. Therefore, it is important to know the temperature increasing that occurs during this process.

As it is observed, in 0.45ms the temperature begins to grow, and in 0.7ms the maximum value of 358K is reached, this point is when the arc has entered the splitter. With this, it is possible to notice that the internal increase is not very large, being 58K over the initial temperature value.

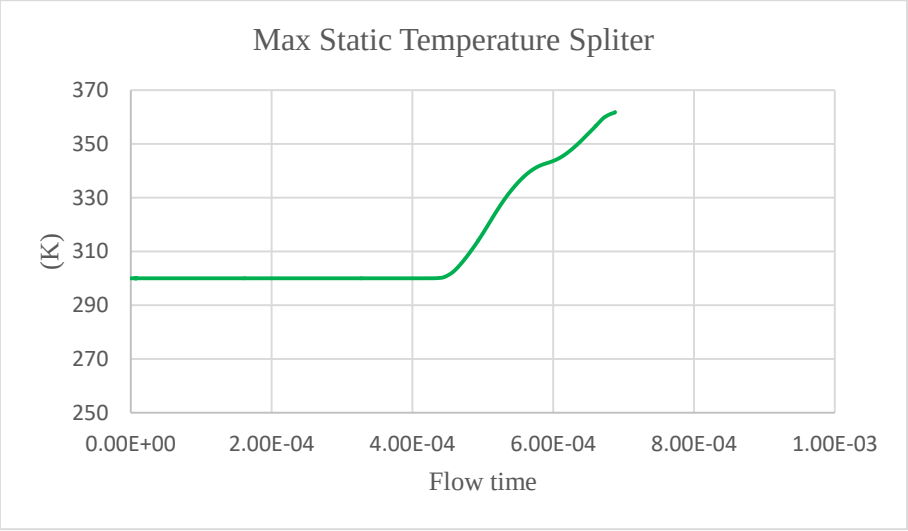

Figure 5-9 Maximum temperature in splitter for case B1.

Another important parameter to measure is the increase of temperature by radiation at the walls, the contacts and the splitter. Knowing the maximum values that are reached during the electric arc will allow to know if the contact material can tolerate such temperatures.

In Figure 5-10 the temperatures in the inner walls of the case B1 are observed, at time 0 the temperature begins to grow to a value above to 2,000K, after this, the temperature gradually begins to decrease to 1,336K in 0.125ms.

Later, in 0.2ms the temperature is above 1,561K, and at this point, it begins to grow steadily, if the simulation had not diverged, it probably could have continued to increase. The last recorded temperature was 2,073K in 0.7ms.

It can be concluded that the material of the contacts would be able to support most of the time this temperature. Furthermore, it must be remembered that the melting point of copper is 1,358K and vaporization is 2,835K, although, it does not discard the possibility that at some points melting or vaporization will be generated.

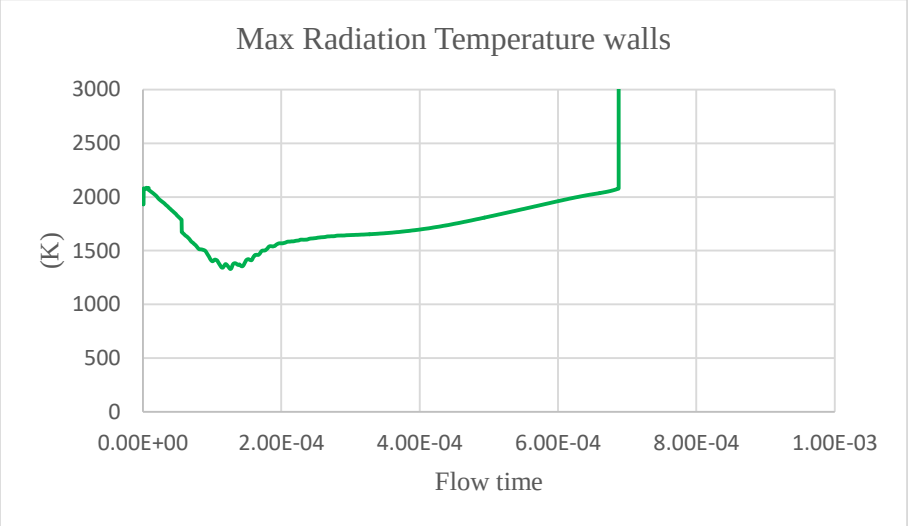

Figure 5-10 Maximum radiation temperature for walls for case B1.

Another important measurement is the maximum distribution of current density in the air, which is shown in Figure 5-11. When the arc starts at time 0, the current density initiates of a zero value, increasing rapidly up to $1.33x10^7$ A/m^2. At this point, the arc is established and a constant magnetic field density of 0.1T is imposed to cause the arc to move. In 0.1ms the current density reaches its maximum value ($7.31x10^7$ A/m^2). After this, the current density begins to increase and decrease periodically (0.1-0.325ms), but with a downward trend. The reason for this is due to the increase and decrease of the transversal cross-section where the current tends to pass.

In 0.325-0.4ms the current stabilizes at $2x10^7$A/m^2, and after, the current continues decreasing. In 0.5ms the current density reaches its lowest value ($8.38x10^7$A/m^2), and, immediately after entering the splitter its increase begins again. Finally, in the last milliseconds of the simulation the current density increases with random min an oscillatory way, increasing and decreasing in each step.

Although the results of these curve are not the same as that reported in [9], a similar behavior can be observed. In addition to having the same order of magnitude (10^6-10^7A/m^2).

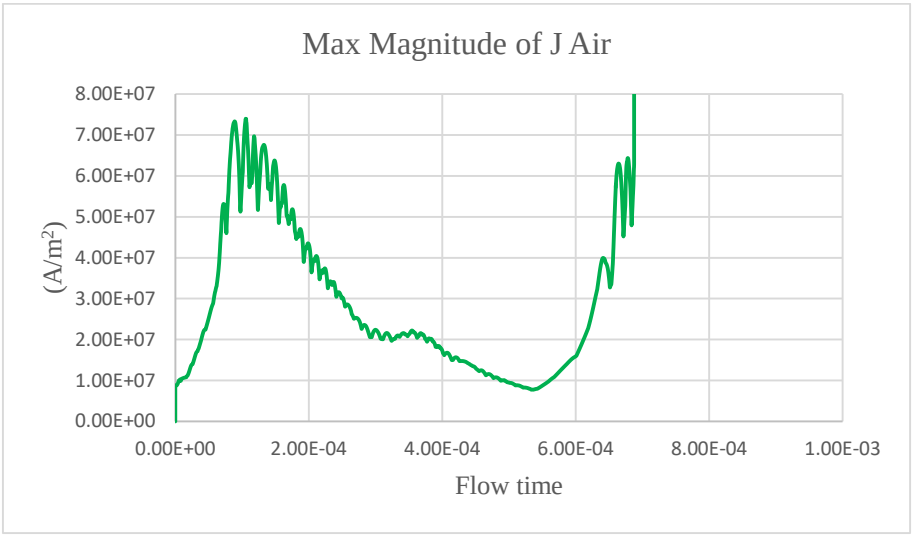

Figure 5-11 Maximum current density in air for case B1.

Now the current density in the splitter is analyzed (Figure 5-12). From 0 to 0.458ms the current density is practically 0, being this a fair value, since during this period the arc has not reached the lower part of the splitter and therefore the current has not started to flow yet.

After this, in approximately 0.5ms, the current begins to flow in the splitter, growing a little, but in 0.6ms the current grows quickly, reaching a value of $5.07x10^6 A/m^2$, after this, in 0.7ms current density is triggered to very large values, and in this point the simulation diverges.

It is not possible to know the behavior of the current density in the splitter beyond 0.7ms, but the observed in Figure 5-12 tend to describe a similar behavior to what was presented in [9]. However, the orders of magnitude are not the same anymore, because in [9] values between 10^4-$10^5 A/m^2$ are reported, and in case B1 the values are between 10^6-$10^7 A/m^2$.

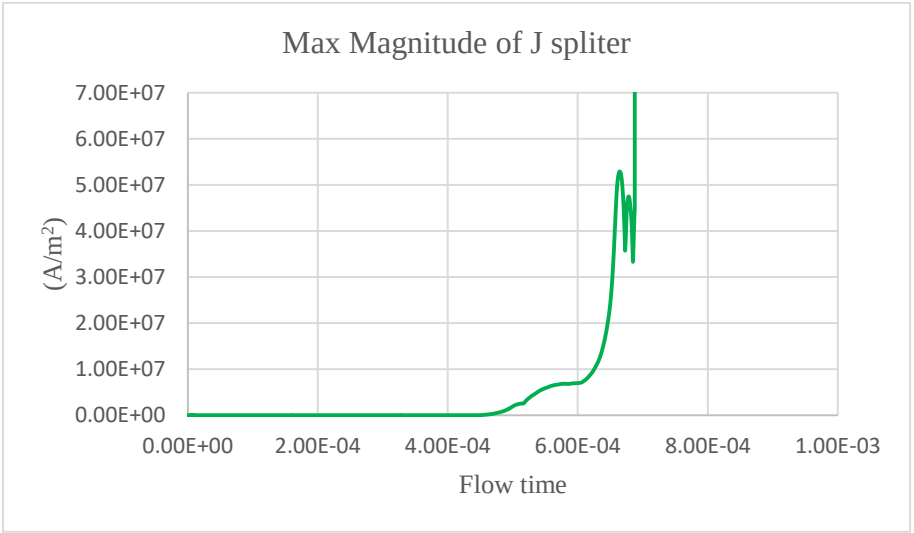

Figure 5-12 Maximum current density at the splitter for case B1.

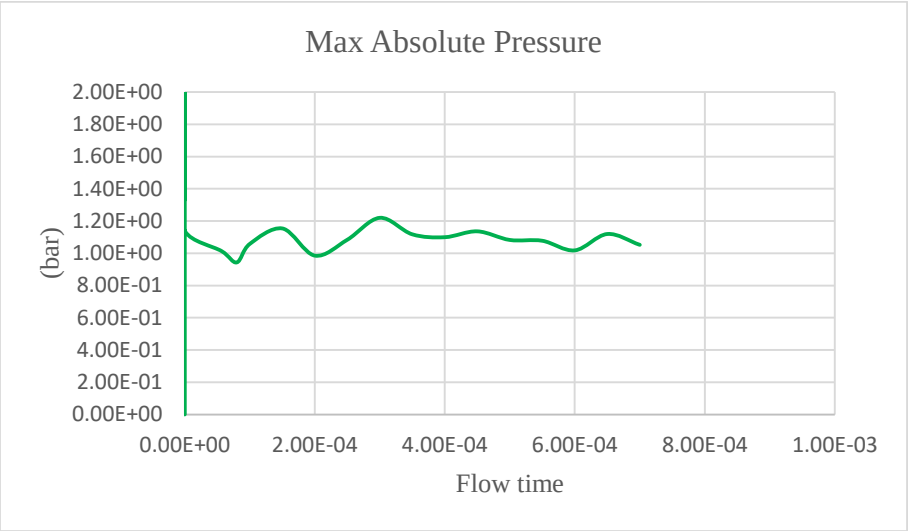

Figure 5-13 Maximum absolute pressure for case B1.

Finally, in this section the results of pressure in the air are discussed (Figure 5-13). First, a very large value is observed at the beginning of the simulation (0ms), this is attributed mainly to the initialization of 10,000K which causes the pressure to increase abruptly [15], but this is only momentary. After this pressure peak, an instantaneous decrease is observed, reaching values around 1.1bar. Subsequently, the values begin to rise and fall, but always staying close to 1bar. These oscillating values may be due to the reverse-flow that appeared during the simulations, this tended to generate certain variation levels in the results. One way to avoid it is to extend the corresponding domain of air, however, this involves more mesh elements and more calculation time. Another possible reason for these oscillating values is the arc displacement, since this tends to push the fluid around.

It is concluded from this result that the pressure shown here is very close to what was presented in [9], because the values are kept close to the atmospheric pressure (1bar) in both analyzes. However, in [9] the maximum values recorded are 1.2bar, and for case B1 they are more than 10bar (in 0ms).

Finally, although it was tried to duplicate the model proposed in [9], with the same conditions, (except for the arc roots), it was not possible to do it. One possible cause of not achieve a good result for this case is that the solution methods selected in Fluent were not adequate for the laminar regime, and this generated a numerical error when solving the equations. However, it should not be forget that the electric arc phenomenon is very fast, the particles movement has at a high speed, as is explained in [44]. For this reason, the turbulent model should be the most suitable for this phenomenon. However, it remains to investigate how to achieve the correct stabilization in this case.

5.4. Case B2. Base Model (turbulent regimen)

In this section, the results related to the case B2 are exposed, in which a turbulent analysis is performed. The Figure 5-14 shows the arc movement expressed by temperature (rainbow scale) and current density (vectors) at different times. The timesteps chosen in this case have been the same of case B1, 0, 0.3, 0.5, 0.6, 0.7 and 0.8 in order to compare the results of the arc movement with this case.

In this case, the arc is ignited at 0ms, at 10mm from the lower part of the chamber. After that, a current of 50 A is injected from the anode, and an imposed magnetic field of 0.1T is applied in the negative z-direction.

At time 0 (start of the simulation), the arc has the shape of a perfect circular channel, the current flows through this and exits at the bottom of the cathode. It is observed that in 0.04ms the arc begins to move vertically through the contacts, the shape is not perfectly circular, although it retains a similar shape as at the beginning. In 0.3ms the arc reaches and enter the splitter, also, it begins to bend acquiring a "u" shape. At 0.5ms the arc is almost inside the splitter and now generating a “u” form more remarkable. In 0.6ms the arc is now completely divided in two, due to the interference caused by the splitter. At time 0.7ms, the arc continues its movement through the splitter, however, it is still more than halfway to finish.

Finally, the arc continues to move until 0.8ms, where the arc at the top begins to unite into one, but the arc still does not leave the splitter. Contrary to what was presented in [9], where at this time the arc had already left the splitter zone. This can be attributed that, the analysis done in this case is turbulent, besides, in [44] it is explained that in a turbulent regime the arc tends to last more than in laminar.

Comparing this results with [9], it is observed that the way in which the arc moves and the form it acquires in this process are quite similar, although in this case the arc roots are not taken into account, nor the calculations for the magnetic flux density.

Among the similarities between models (case B2 and [9]), the following can be highlighted. The vertical movement of the arch is fully achieved for this case. The temperature values are within the same order of magnitude (8000K-13000K). Although the current density values are not exactly equal to [9], they are close, also in case B2 a tendency to decrease may be observed, later when the arc continues moving the J tends to decrease, since, the greater the area, the lower the current density is. In both cases the results are in the same order of magnitude (10^6–$10^7 A/m^2$).

Among the differences, some are highlighted. The electric arc over time begins to acquire a diffuse shape, although it is using a mesh very similar as proposed in [9], this can be attributed to the solution methods in Fluent respect to CFX are different. Besides, a turbulence model is being used for this case and in [9], a laminar model is used. Also, it should be remembered that, magnetic flux density (**B**) is not calculated within the simulation, instead, a constant magnetic field density of 0.1T is imposed to cause the arc to move. Nevertheless, in the real world this field could be different and vary over time.

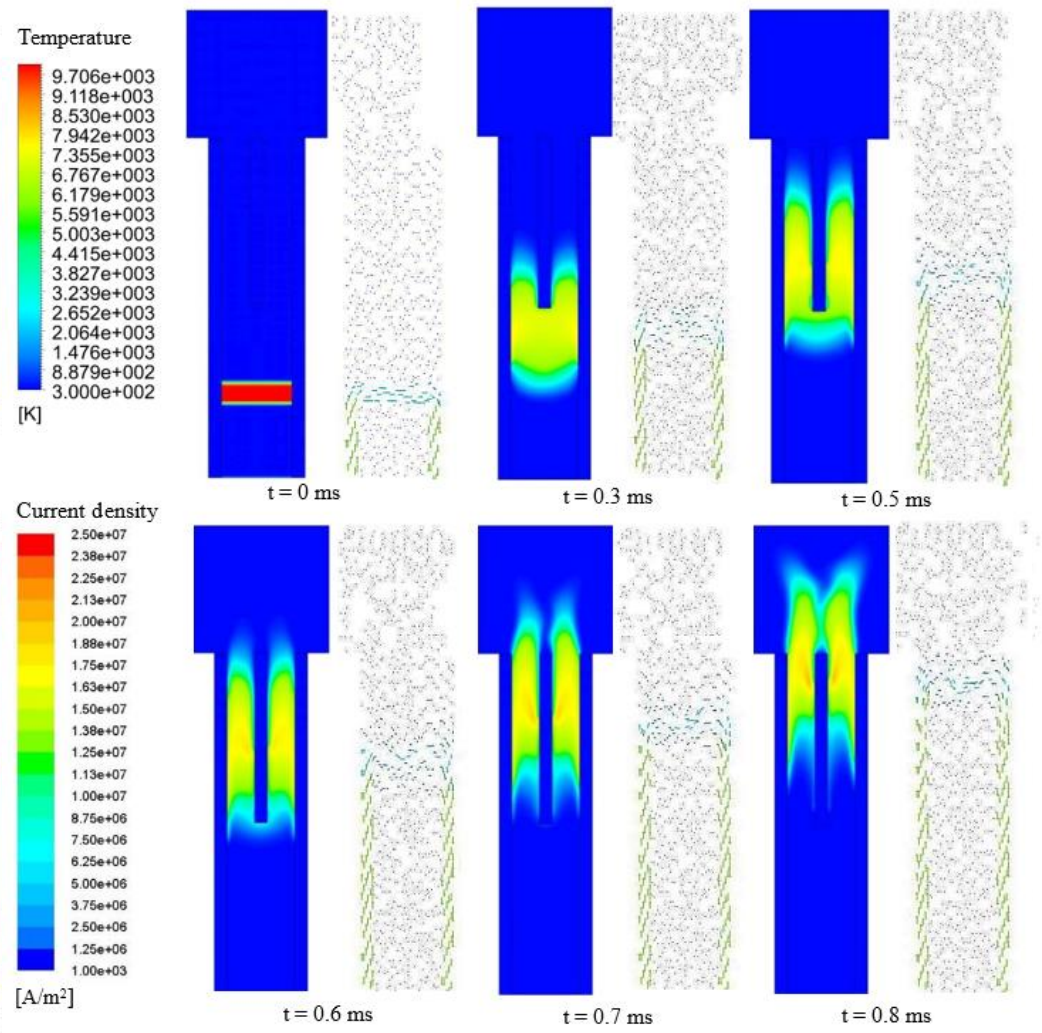

Figure 5-14 Arc movement, expressed by temperature and current density for case B2.

The voltage values that are measured in this case (Figure 5-15), although the curves for the arc root are not considered, tend to describe a similar behavior to what ~~was~~ is presented in [9]. At the beginning (0ms) the voltage increases until a value of 121V at 0.05ms. Then it begins to decrease until it stabilizes at a value between 70-80V (0.4-0.8ms), instant when the arc begins to surround the splitter. At this point, the voltage is almost constant. Finally, in 1ms the value of the voltage rises to 175V reaching the final part of the simulation when the arc almost has left the splitter.

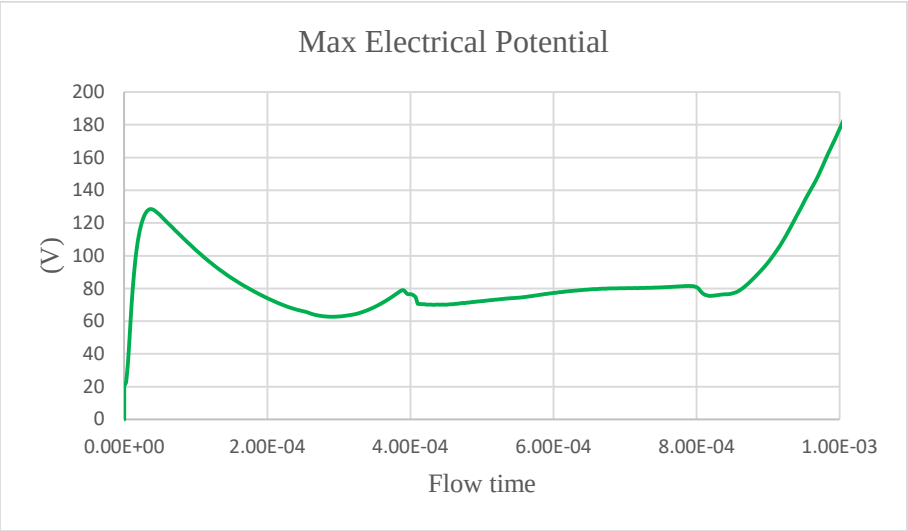

Figure 5-15 Maximum electric potential for case B2.

In relation to the maximum temperature, the following can be rescued from the graphs (Figure 5-16). Initially the temperature of the arc starts at 10,000K and then begins to grow until a value of 10,127K at 0.0152ms. This increase in temperature is mainly caused by the Joule heating, since during this period the arc shape is uniform, and the cross-section area does not fluctuate very much, making the current density invariable, and causing the increase in energy to be constant. Then, in 0.2-0.6ms the temperature decreases to a value around 8,000K, instant when the arc shape begins to vary, at this point the cross-sectional area of the arc becomes larger causing the current density to tend to fall and therefore the heat produced by the Joule effect is less.

Next, in 0.6ms the arc is already inside the splitter, the temperature again tends to grow to a value of 8,570K, since, when the arc gets in the splitter, the cross-section area of the arc it is reduced, and the current density trends to increase, producing more heat by Joule effect. Finally, from 0.865ms to 1ms the temperature begins to grow again until reach a final value of 12,000K. This last value is contrary to what is presented in [9], where at the end of the simulation the temperature drops to 8,000K. However, since the temperature of 12,000K in case B2 only occurs at the end of the simulation, this case can be considered as a fairly close approximation to what is presented in [9], at least before the arc leaves the splitter.

Analyzing the temperature distribution at the contacts (Figure 5-17) a tendency to increase is observed, until a maximum value of 460K. This is mainly due to the constant 500K temperature imposed in the lower part of each contact, besides, the effects of heat transfer by convection in the walls and the fluid are not considered, since adiabatic walls were assigned, thus generating only an increase by conduction within the metal itself.

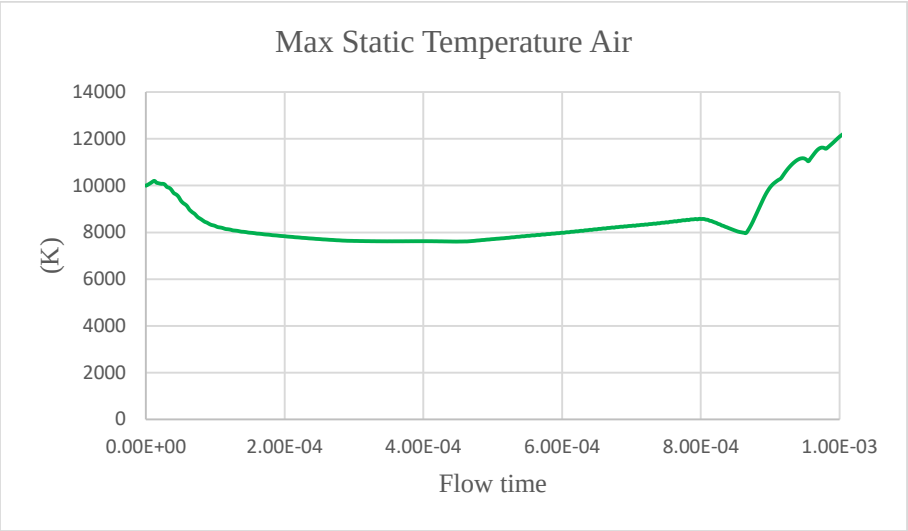

Figure 5-16 Maximum temperature in air for case B2.

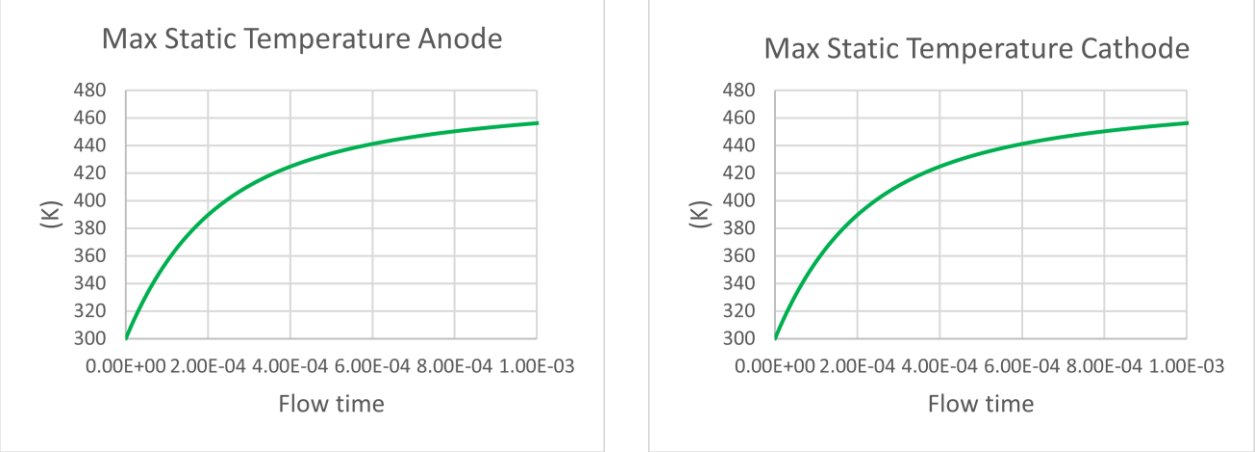

Figure 5-17 Maximum temperature in Anode and Cathode for case B2.

The temperatures measured in the splitter are shown in Figure 5-18, for this case the adiabatic wall condition was not imposed, but rather a coupled wall condition. Since the splitter is in contact with the arc, in addition, to be responsible for cooling and extinguishing it. Therefore, it is important to know the temperature increasing that occurs during this process. As it is observed, in 0.2ms the temperature begins to grow, and in 0.524ms the maximum value of 360K is reached, this point is when the arc has entered the splitter. After this, the temperature tends to fall steadily, reaching a final value of 344K. With this, it is possible to notice that the internal increase is not very large, being 60K over the initial temperature value, confirming, once again, that this is an insignificant increase. Therefore, this analysis can be omitted for the next simulations.

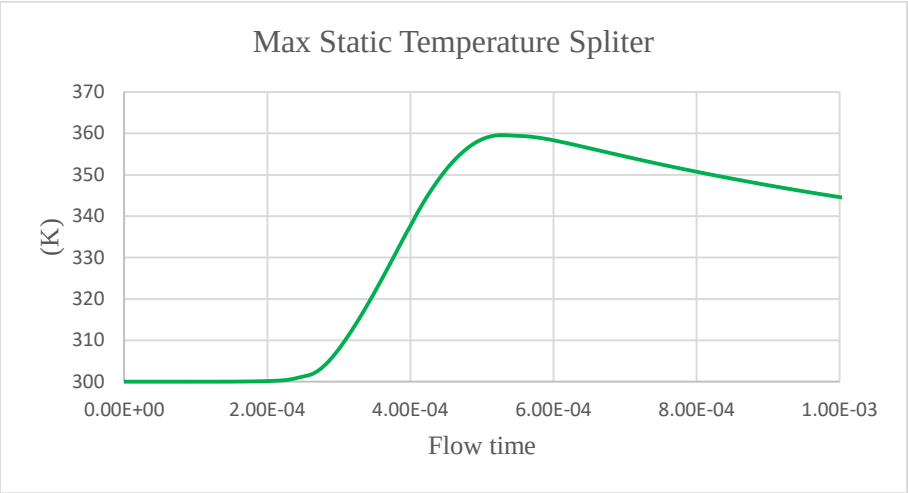

Figure 5-18 Maximum temperature in splitter for case B2.

Another important parameter to measure is the increase of temperature by radiation at the walls, the contacts and the splitter. As was explained for the case B1, knowing the maximum values that are reached during the electric arc will allow to know if the contact material can tolerate such temperatures. In Figure 5-19 the temperatures in the inner walls of the case B1 are observed, at time 0 the temperature begins to grow to a value above to 2,000K, after this the temperature gradually begins to decrease to 1,690K in 0.0627ms. Which is also when the arc temperature is decreasing. Later, from 0.2-0.9ms, the temperature varies from 1,800-2,200K. Finally, in 0.9ms the temperature rises suddenly to 3,000K, coinciding with the moment when the arc temperature grows, (Figure 5-16). Since vaporization it is not considered, this radiation temperature can be used as a reference to know if a material is vaporized or not. It can be concluded that the material of the contacts would be able to support most of the time this temperature. Furthermore, it must be remembered that the melting point of copper is 1,358K and vaporization is 2,835K, although, it does not discard the possibility that at some points melting or vaporization will be generated.

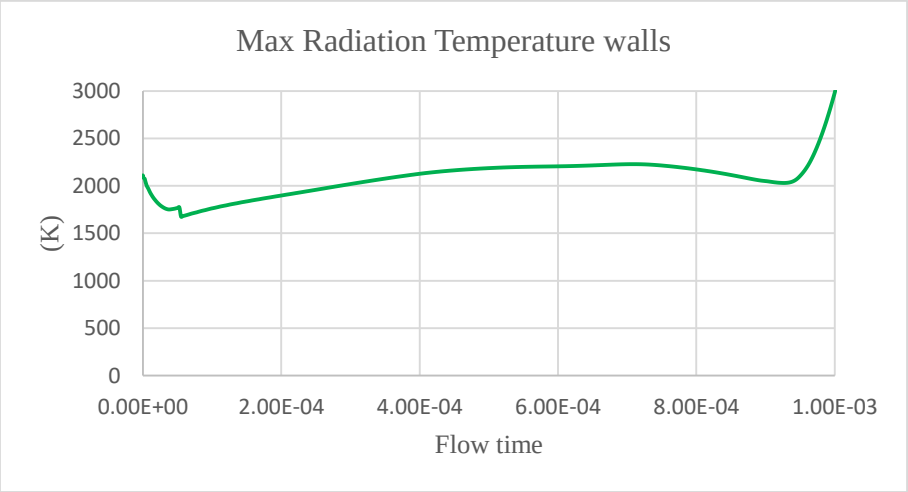

Figure 5-19 Maximum radiation temperature for walls for case B2.

Other important measurement is the maximum distribution of current density in the air, which is shown in Figure 5-20. When the arc starts at time 0, the current density initiates of a zero value, increasing rapidly up to $1.21x10^7$ A/m^2. At this point, the arc is established and like the case B1 a constant magnetic field density of 0.1T is imposed to cause the arc to move. In 0.2ms the current density drops to a value of $3.86x10^6$ A/m^2 which is maintained until 0.285ms, when the arc reaches the splitter.

Next, in 0.4ms the current density increases to value of $1.15x10^7$ A/m^2. Later, from 0.4-0.443ms when the arc enters the splitter, the current density tends to decrease. After that, from 0.443-0.8ms the current density remains almost constant, increasing to a maximum of $1.25x10^7$ A/m^2 at 0.8ms. Finally, passing this time the arc is close to leaving the splitter, and the current density grows to a value of $5.49x10^7$ A/m^2. Contrary to what was presented in [9], where at this time there is a value close to zero.

For case B2, the large value of current density that is observed means that the extinction of the electric arc is later than 0.8ms. Although the results of these case are not the same as that reported in [9], a similar behavior can be observed. In addition to having the same order of magnitude (10^6-10^7A/m^2).

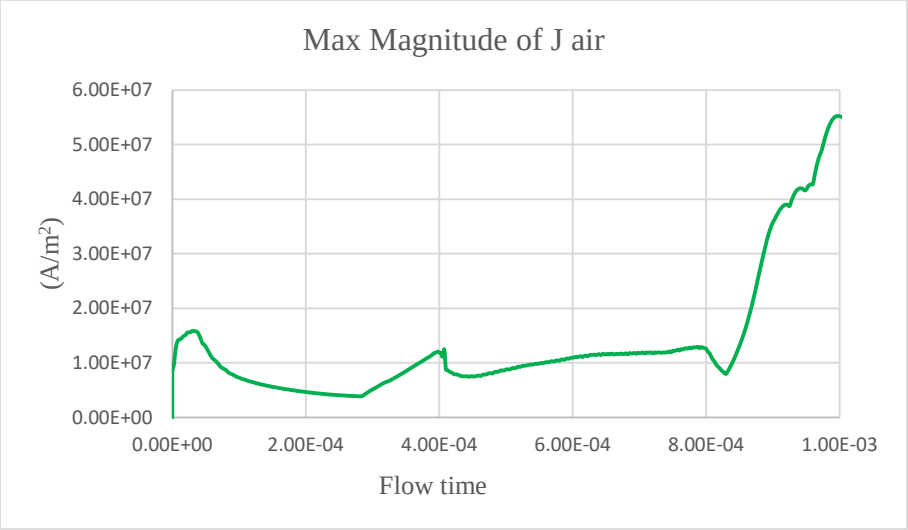

Figure 5-20 Maximum current density in the air for case B2.

Now the current density in the splitter is analyzed (Figure 5-21). From 0 to 0.243ms the current density is practically 0 being this a fair value, since during this period the arc has not reached the lower part of the splitter and therefore the current has not started to flow yet. After this, from 0.243-0.4ms, the current begins to flow in the splitter, reaching a value of $1.40\ x10^7$ A/m^2, which is two orders of magnitude higher as that reported in [9]. Later, from 0.4-0.8ms the current density varies little, but there is a tendency to increase. Finally, from 0.8-1ms the current density begins to fall to 0, indicating that the arc has already left splitter zone. The results shown for the **J** in the splitter show a behavior quite similar as that reported in [9], however, for the case B2 there are two orders of magnitude higher. But even with this difference, the results are quite close to that presented in [9].

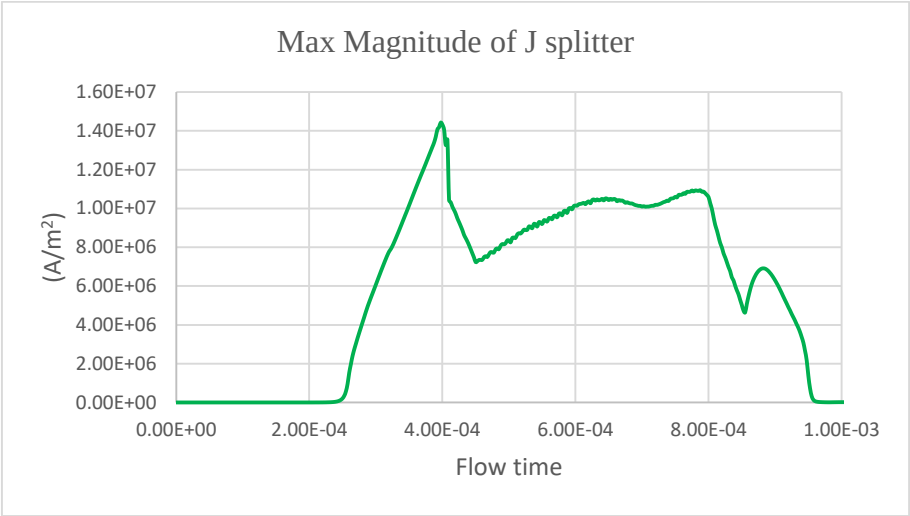

Figure 5-21 Maximum current density at the splitter for case B2.

Finally, in this section the results of pressure in the air are discussed (Figure 5-22). First, a very large value is observed at the beginning of the simulation (0ms), this is attributed mainly to the initialization of 10,000K which causes the pressure to increase abruptly [15], but this is only momentary. After this pressure peak, a decrease is observed in 0.05ms, reaching values around 1bar. Subsequently, the pressure stabilizes at 1bar, without noticeable variation during the rest of the simulation.

It is concluded from this result that the pressure shown here is very close to what is presented in [9], because the values are exactly to the atmospheric pressure (1bar). However, only at the beginning of the simulation there is a very large peak of pressure, and it stabilizes earlier than the model described in [9].

As a final point, in case B2 was possible to duplicate the model proposed in [9], with the same conditions, (except for the arc roots). But, in this case a turbulent regimen was chosen. Although, there are still some discrepancies in some results, but these differences are small.

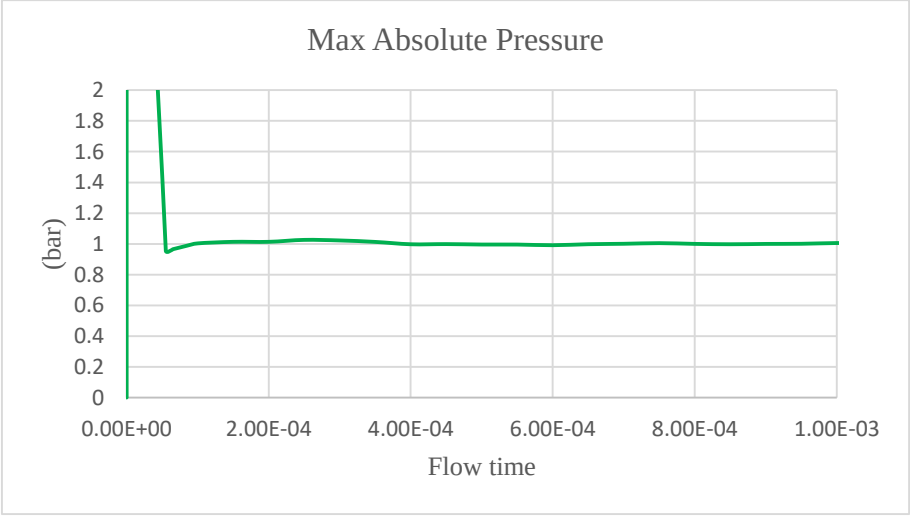

Figure 5-22 Maximum absolute pressure for case B2.

Comparison case B1 vs case B2

For the case B1 and B2 the same conditions of case A1 were imposed, with the difference that case B1 is in laminar regime and case B2 in turbulent regime. First, it is observed that both simulations differ in the arc shape, since in case B1 the shape is very diffuse, and only reach the lower part of the splitter. For the case B2 all the simulation can be completed, the arc reaches the top of the splitter at 0.8ms, and the shape is less diffuse.

The electric potential for both cases is within the same order of magnitude, although in case B2 there are values close to twice the magnitude of what is exposed in B1. On the other hand, the temperature in the air are very similar, for the case B1, it stabilizes above 10000K and for case B2 below this temperature. The temperatures in the contacts are practically the same in both cases, and the temperature in the splitter seems to have the same behavior, and the temperature reached is almost the same. The radiation temperature in both cases shows a similar trend, since in the beginning it stabilizes in 2000K, and later it grows above this temperature.

Now, the current densities in the air are distant, but within the same order of magnitude, having maximums of $7x10^7 A/m^2$ and minimums of $1x10^7 A/m^2$. In the case of the splitter, the current density is practically 0 (initially) in both cases, and when the arc touches the lower part of the splitter the current begins to flow and the current density begins to grow.

Related to pressures levels, in both cases the behavior is almost the same, since is very close to what is presented in [9]. However, only at the beginning of the simulation there is a very large peak of pressure, (for both cases), this is attributed mainly to the initialization of 10,000K which causes the pressure to increase abruptly.

Finally, since only the analysis in a turbulent regime was stabilized, it is the one that is chosen to be used in the following cases. It remains to stabilize the simulation in laminar regime, which is left for the future work section. The reason can be related to a numerical error, however, in this thesis the most robust resolutions methods of Fluent were used.

In conclusion, based on these two analyzes, the one that gives better results is the B2, since, in this model all the arc movement, the temperature values, and the current density are very close to what is presented in [9]. The only condition is that it must be performed in a turbulent regime. The case B1 unfortunately was not able to model the arc beyond 0.7ms, and therefore, this case is discarded.

5.5. Case C1. Coupling Maxwell-Fluent

In this section, the results related to the case C1 are exposed, where the main purpose is to obtain the values of the magnetic flux density **B** during the arc movement, by a coupling of the Maxwell-Fluent software.

Like the case B, the arc is ignited at 0ms, at 10mm from the lower part of the chamber (Figure 5-23). After that, a current of 50 A is injected from the anode and the magnetic flux density is calculated by coupling with Maxwell. At time 0 (start of the simulation), the arc has the shape of a perfect circular channel, the current flows through this and exits at the bottom of the cathode. As is explained in [24], in the case of the magnetic flux density, there will always be one component most important in the electric arc phenomenon, for the case analyzed here, is in the Z direction (positive and negative). Therefore, it is the only component that will be considered for this analysis.

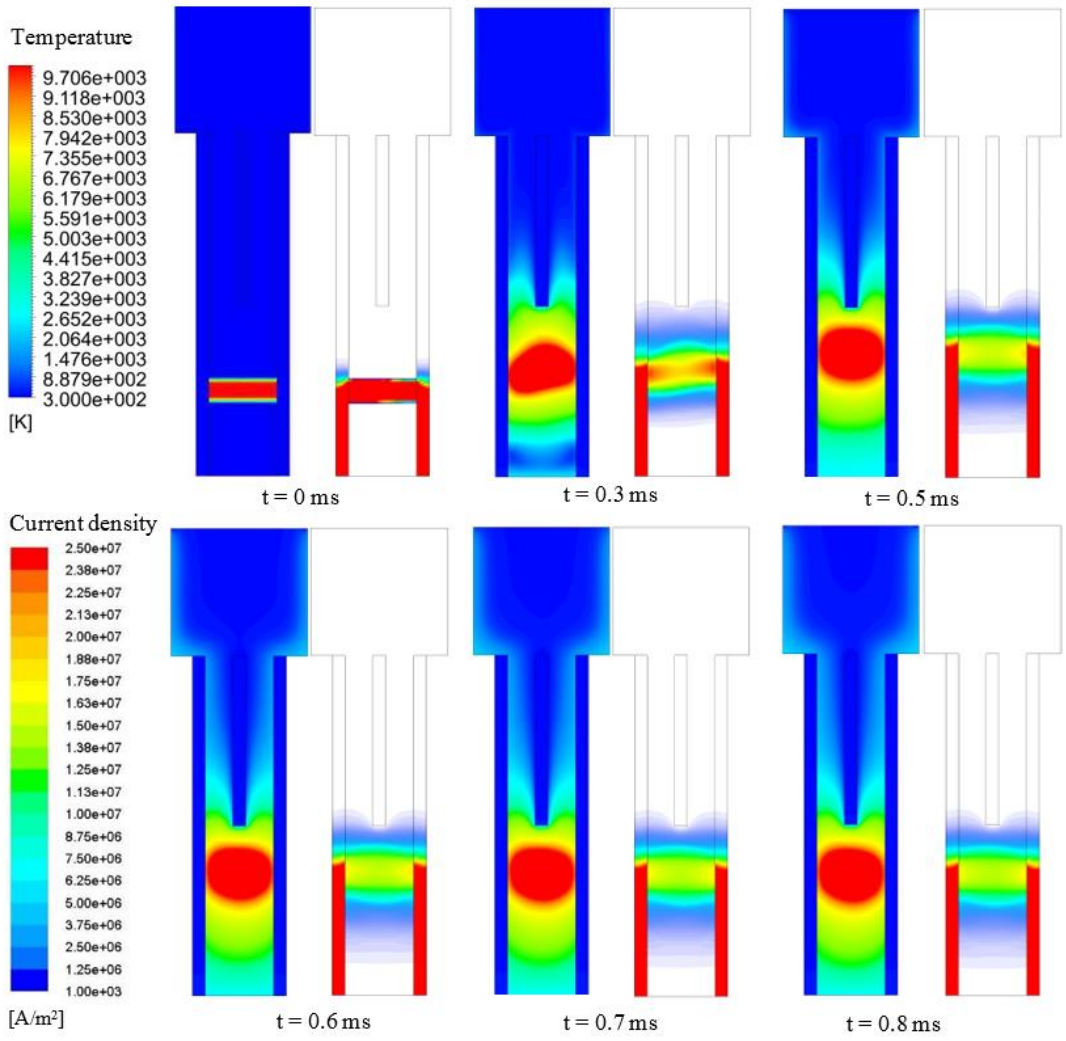

Figure 5-23 Arc movement, expressed by temperature (left) and current density (right) for case C1.

In relation to the maximum temperature, the following can be rescued from the graphs (Figure 5-24). Initially the temperature of the arc starts at 10,000K and then begins to grow until a value of 12,471K at 0.055ms. as was explained during the case A and B, this increase in temperature is mainly caused by the Joule heating. After this, the temperature stabilizes around 12,200K (Figure 5-24), keeping this value the rest of the simulation.

In relation to the arc movement, the following can be rescued from Figure 5-23. At the start of the simulation, the arc has the shape of a perfect circular channel, the current flows through this and exits at the bottom of the cathode. In 0.3ms the arc starts to move, and it retains a circular shape. In 0.5ms the arc continues its movement, getting closer to the splitter, in addition, the shape it acquires is more diffuse, but still maintains a circular shape. In 0.6ms the arc seems not to move; besides the shape it presents is almost the same as the previous timestep. After this, from 0.7-0.8ms the arc still maintains its position, however, it should not be confused with a stagnation, but the arc movement is now much slower. This can be understood by looking at the magnetic flux density graph (Figure 5-24), due to it reaches a point where both the $\mathbf{B}_{z+}$ and $\mathbf{B}_{z-}$ are almost the same, canceling each other.

For this case, all the materials from [9] have been used, although, the author does not specify exactly what permeability value is assigned to them, being this a possible reason that similar results are not obtained. In addition, the effects of Eddy currents are not considered in this case. Besides, the coupling does not allow to analyze the current density vectors, for case C the contours are simply exposed on a rainbow scale and for case D by graphs.

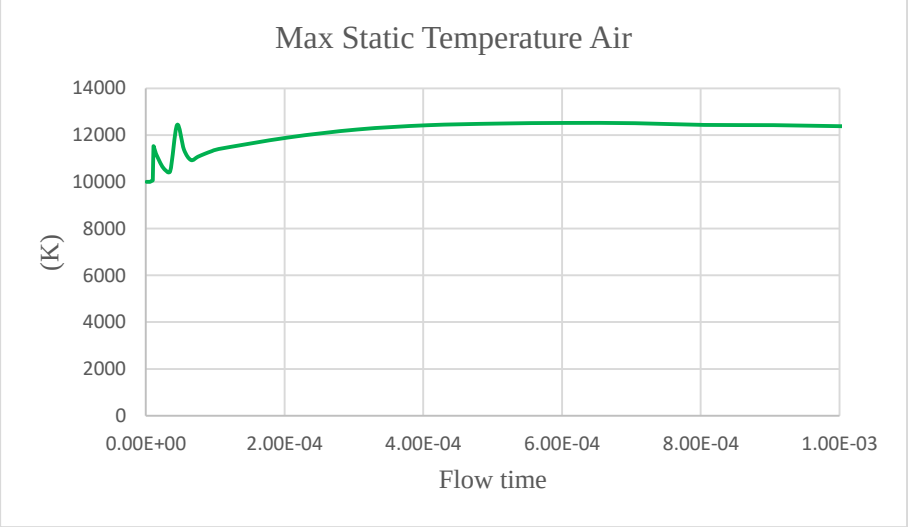

Figure 5-24 Maximum temperature in Air for case C1.

The magnetic flux density (**B**) is of vital interest for this case, since this will be compared with case D and the best results will be used in case E. In this section only the most relevant times are shown (Figure 5-25). It can be observed that the maximum values are around +0.0119T and -0.0177T at time 0. Generated a resulting value of around -0.0058T_z. Therefore, the arc displacement is slow at the beginning, compared to case B1 and B2. After

this time the arc begins to move vertically, however, the closer to the splitter the arc is, the smaller the magnetic flux density is, reaching almost the same values (positive as negative), generating that they cancel each other (Figure 5-26). For this reason, in 1ms the arc is not able to get into the splitter, in order to see this effect, the simulation time must expand beyond.

The measurement of **B** is done using the maximum and minimum values, and these will be used for the case E1, where only the values in the Z direction are the most important, the explanation of this will be presented in [24], since, in this particular case it is the direction where they have more importance for the arc movement.

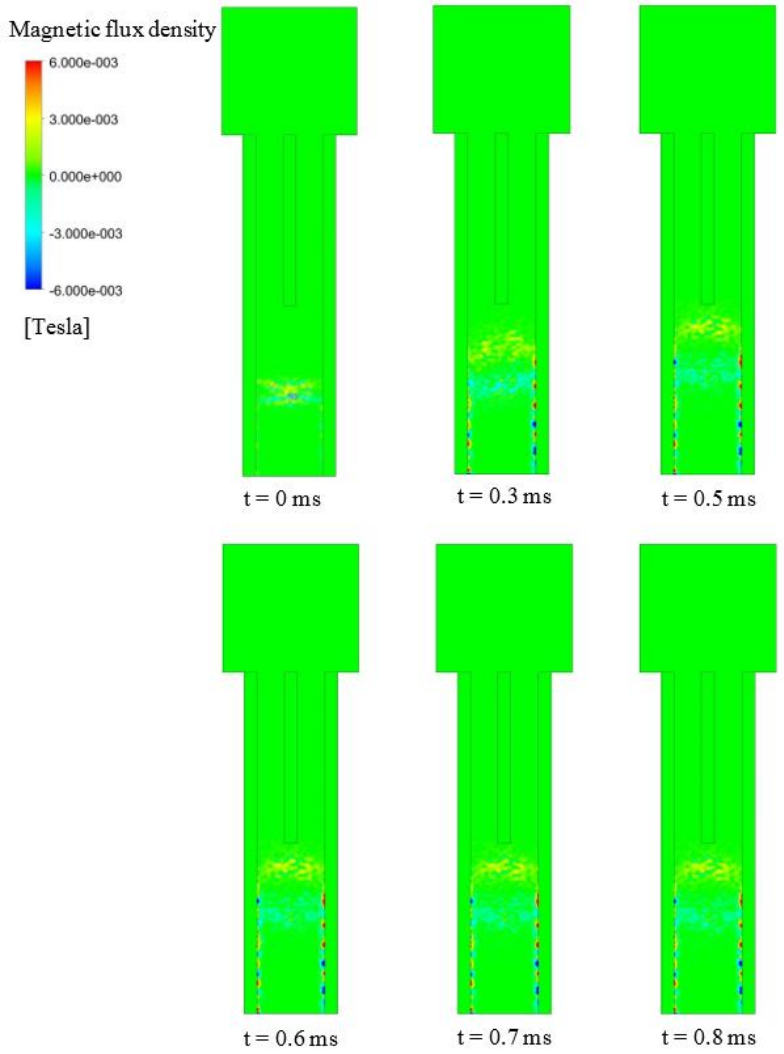

Figure 5-25 Arc movement, expressed by Magnetic Flux Density for case C1.

In Figure 5-25, it is possible to observe where the B values are concentrated, the largest being on the edges of the arc and on the edges of the contacts. There is still a need to improve this analysis since in the Maxwell software, the predefined convergence criteria were used and a 1mm mesh was used for each element.

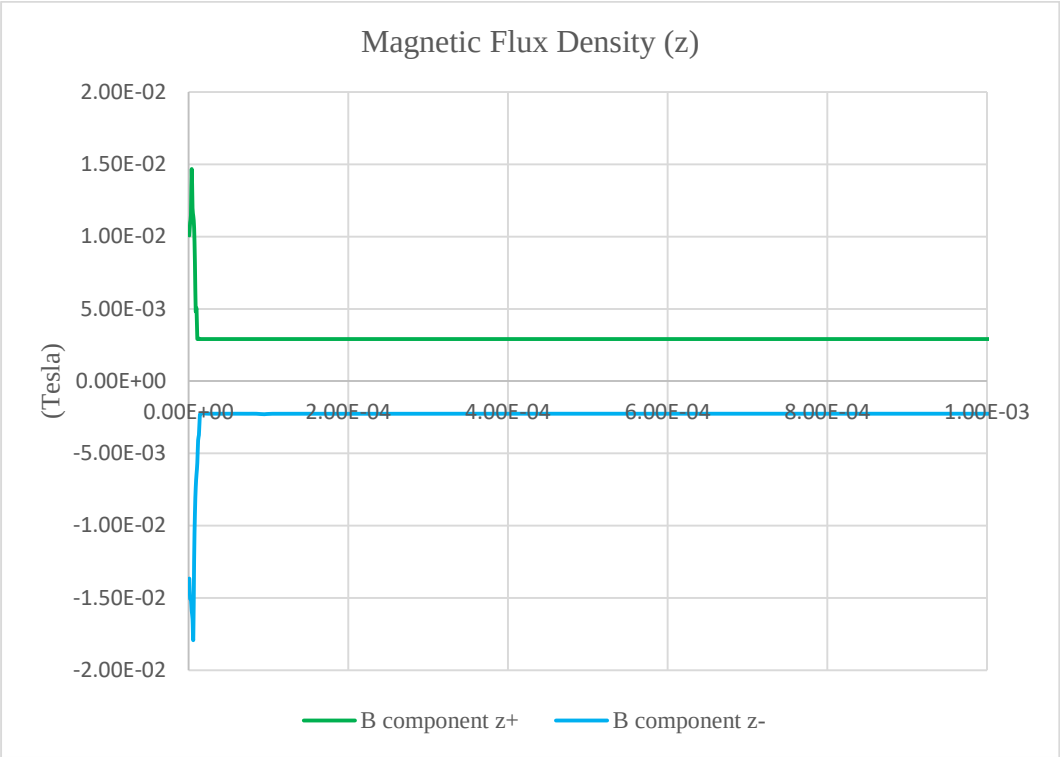

Figure 5-26 Maximum magnetic flux density for case C1.

In Figure 5-26, the values of **B** are showed in a graph. At the beginning of the simulation the values in z- are greater to z+. This higher value that appears in the negative direction causes the product **JxB** to generate a Lorentz force in the vertical direction. And this same force makes the arc move at the beginning. After this, from 0.0014ms onwards the positive values remain constant, at around 0.003T, and for the negative at 0.0022T.

From this point the arc begins to move more slowly, and in some time, would descend, this behavior is not at all expected. However, this is caused by the magnitude and direction of **B**, and this field is affected by the current density distribution and the geometry around the arc. It remains to investigate the reason for this behavior, and achieve the vertical movement during the simulation.

This coupling offers a great advantage, because the **B** is calculated in real time, however, the calculation time is extremely long.

5.6. Case D1. Coupling Flux-Fluent

In this section, the results related to the case D1 are exposed, where the main purpose is to obtain the values of the magnetic flux density **B** during the arc movement, by a coupling of the Flux-Fluent software. To do this, different geometries were used for the electric arc (Figure 5-27), because the movement is not a function of the Lorentz force, but is done parametrically within the Flux software. Even tough, this software is not capable of modeling the equations of fluid mechanics, each position of the arc, have been associated with a time, taking this from previous simulations.

The parametrization is done with an average conductivity for the arc column, also changing its shape and position (assuming the arc moves throughout the model). The magnetic flux density was taken by different paths, on a straight-line. As explained in case C1, for this case only the z component of **B** is used.

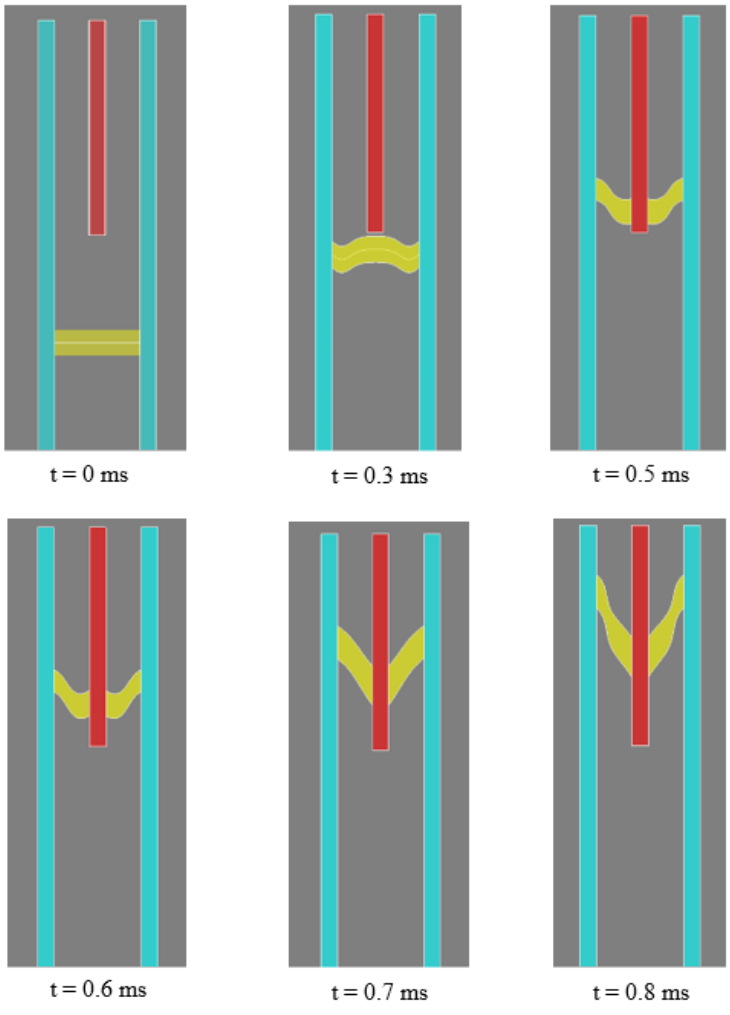

Figure 5-27 Arc movement, expressed by geometry for case D1.

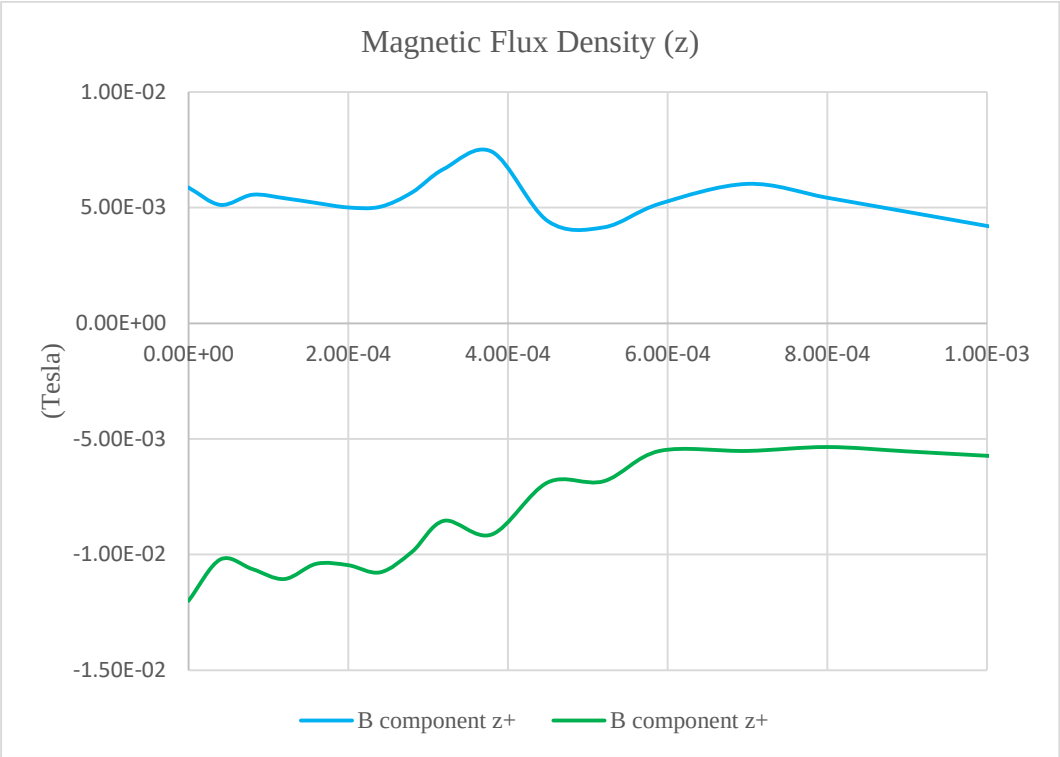

Figure 5-28 Maximum magnetic flux density for case D1.

Analyzing Figure 5-28, it is observed that the **B** is around +0.005T and -0.012T, at the beginning of the simulation, generated a resulting value of around -0.007T_z. While the arc moves, it is observed that the **B** begins to stabilize at a value around +0.005T and -0.005T in 0.6ms. However, at the beginning of the arc the values in the negative direction are higher. This difference of **B** at the beginning generates a Lorentz force that tends to displace the arc in vertical direction, same as described in case C1. Furthermore, the orders of magnitude of this case with respect to C1 are within the same range, corroborating that Maxwell's data is correct and therefore is a good analysis to consider.

Comparison case C1 vs case D2

In these two cases, the most important to analyze was the magnetic flux density. In both cases the orders of magnitude are within the same range (10^{-2}-10^{-3} T) with some small differences during the simulation progress. Between these cases, the best result of **B** is provided by the Maxwell-Fluent coupling (case C1), since the arc is calculated in real time. For the case of the Flux-Fluent coupling (case D1) the arc is calculated with the approximate geometry of an electric arc at different positions.

Although, of both cases it is observed that the **B** is almost the same at the beginning of the simulation. For case C1 the value is -0.0058T and for the case D1 is -0.007T. However, the best result will always be the one obtained from case C1, since this is a real-time value. For this reason, a value of -0.006T will be used for case E.

The simulations made in Flux offer a great advantage, but they are not adequate when it is looking for the dynamic behavior of the electric arc.

5.7. Case E1. Comparative analysis

In this section, the results related to the case E1 are exposed. For this case, a magnetic flux density of 0.006T is imposed in the negative z-direction, based on the conclusion of cases C and D. The results of this case will be compared with case B2 and the reference [9].

In this case, the arc is ignited at 0ms, at 10mm from the lower part of the chamber. After that, a current of 50 A is injected from the anode, and an imposed magnetic field of 0.006T is applied in the negative z-direction (Figure 5-29). At time 0 (start of the simulation), the arc has the shape of a perfect circular channel, the current flows through this and exits at the bottom of the cathode. It is observed that in 0.3ms the arc has begun to reach the lower part of the splitter, at this point the arc moves more slowly, since the magnetic flux density is smaller than the case B2.

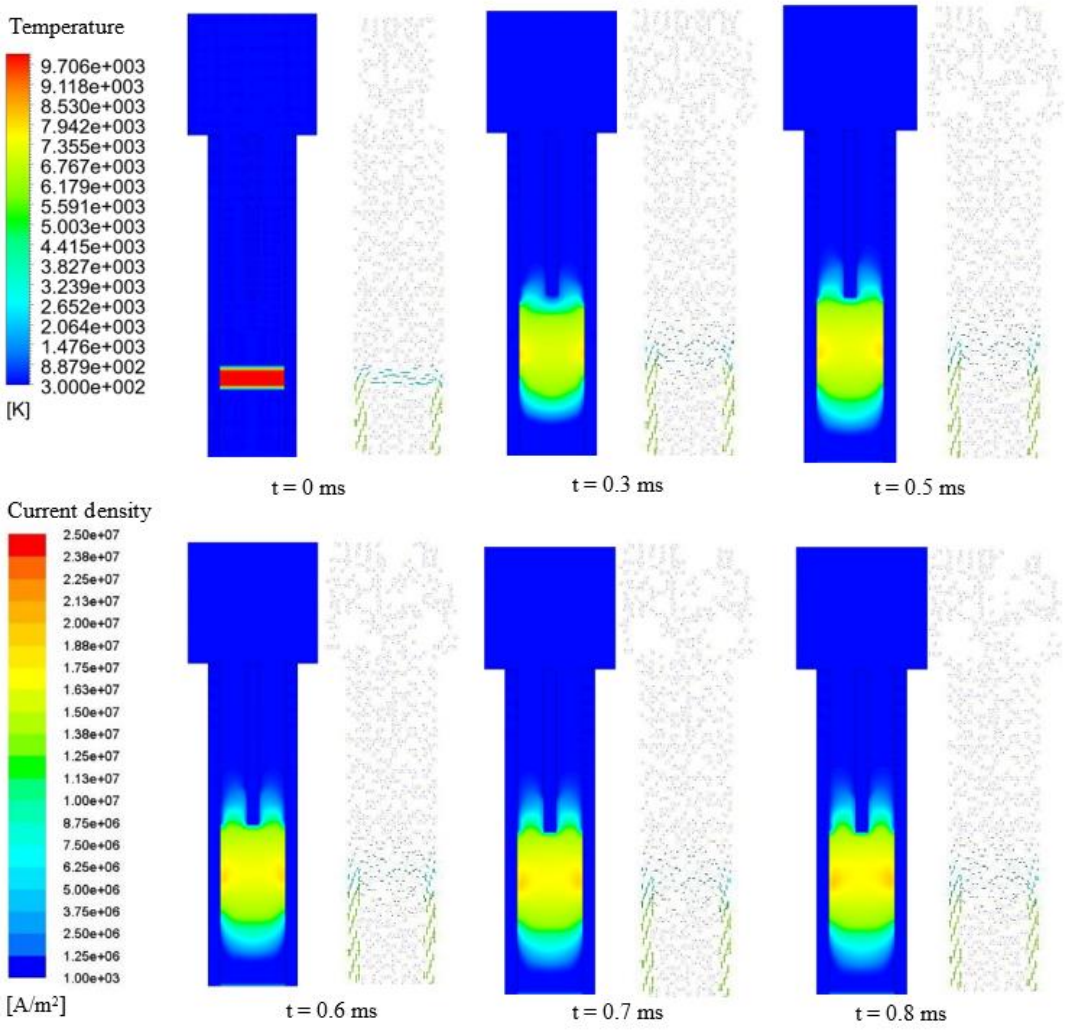

Figure 5-29 Arc movement, expressed by temperature and current density for case E1.

Next, in 0.5ms the arc continues moving vertically, however, it is under the splitter, unable to pass through it. Later, in 0.6ms the displacement continues, although, there is no noticeable change from the previous time. Finally, from 0.7-0.8ms the arc is still in the route to enter

the splitter; however, no significant progress is seen. The reason for this could be due to the magnetic flux density is too small, and the splitter represents an obstacle that delay its speed. However, it remains to investigate and run more simulations and observe the behavior in this zone.

Comparing the results with the case B2, it is notable that the speed of displacement is lower, another behavior that is important to note, is the arc shape since it is bigger in this case, compared with case B2. Among the similarities between cases, the following can be highlighted. The temperature values are within the same order of magnitude (8000K-13000K). Although the current density magnitudes are not the same, they are close, also in case E1 a tendency to decrease may be observed, later when the arc moves, when the arc continues moving the J tends to be constant, because the arc form does not change. Finally, the current density, in both cases, are in the same order of magnitude ($10^6 – 10^7$ A/m^2).

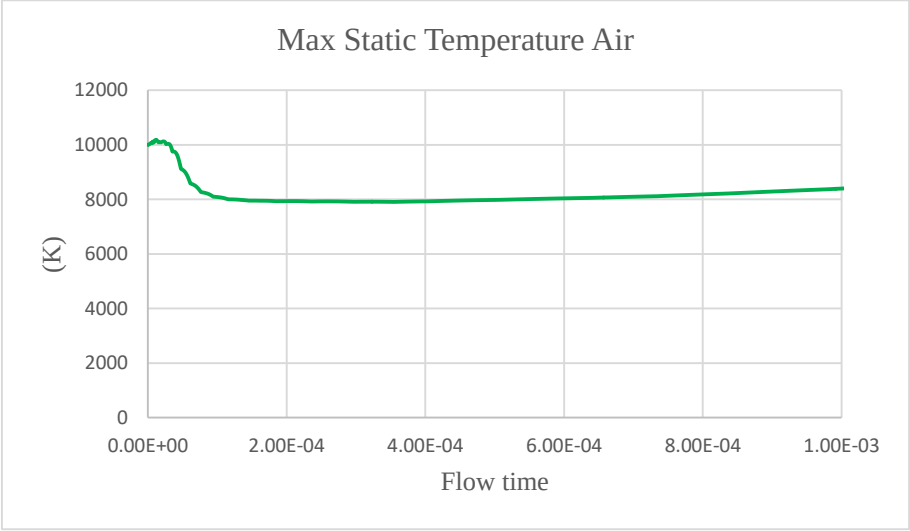

Figure 5-30 Maximum temperature in Air for case E1.

In relation to the maximum temperature, the following can be rescued from the graphs (Figure 5-30). Initially the temperature of the arc starts at 10,000K and then begins to decrease until a value of 8,000K at 0.1ms. This decrease in temperature is mainly caused by the Joule heating and the expansion of the fluid. Then, from 0.2-0.9ms the temperature is constant, in a value of 8,000K, this is maintained almost until the end, when the temperature begins to grow (8,365K) in 0.8ms. This is easy to relate, since the arc almost does not move during this time, maintaining an almost constant shape, and therefore, does not generate disturbances in the temperature distribution.

Analyzing the temperature distribution at the contacts (Figure 5-31) a tendency to increase is observed, only that up to a maximum value of 460K. Which is exactly the same behavior observed in case B2, due to the constant 500K temperature imposed in the lower part of each contact, besides, the effects of heat transfer by convection in the walls and the fluid is not considered.

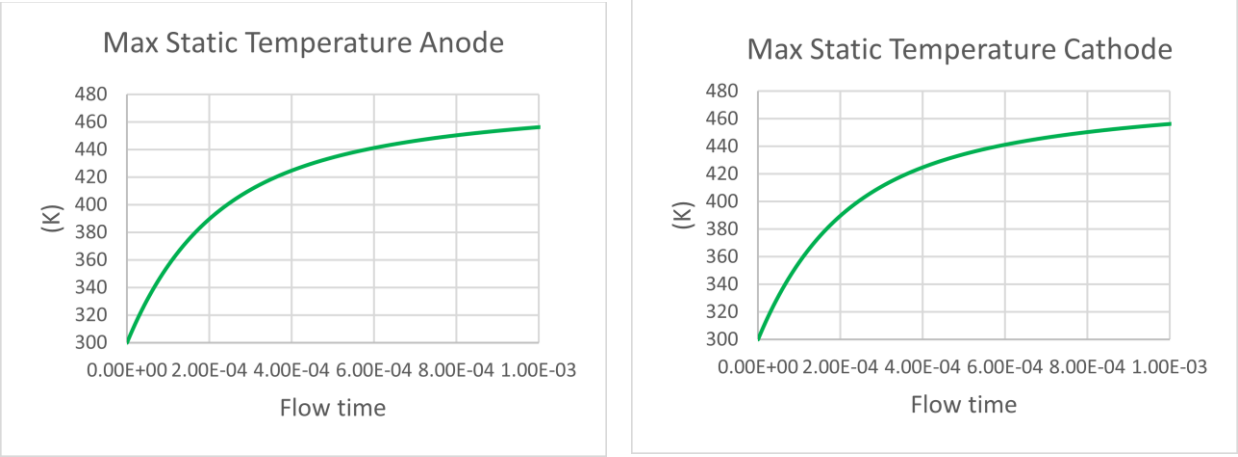

Figure 5-31 Maximum temperature in Anode and Cathode for case E1.

Other important measurement is the maximum distribution of current density in the air, which is shown in Figure 5-32. When the arc starts at time 0, the current initiates of a zero value, increasing rapidly up to $1.3x10^7$ A/m^2. At this point, the arc is established and a constant magnetic field density of 0.006T to cause the arc to move. In 0.2ms the current density drops to a value of $5.68x10^6$ A/m^2.

From 0.4-1.0ms the current density in the arc remains constant, corroborating what was said before. If the transversal area does not change, the J will not change either, and as the arc almost does not move from 0.5-0.8ms the current density does not have to change much. The last registered value observed is $3.6x10^6$ A/m^2.

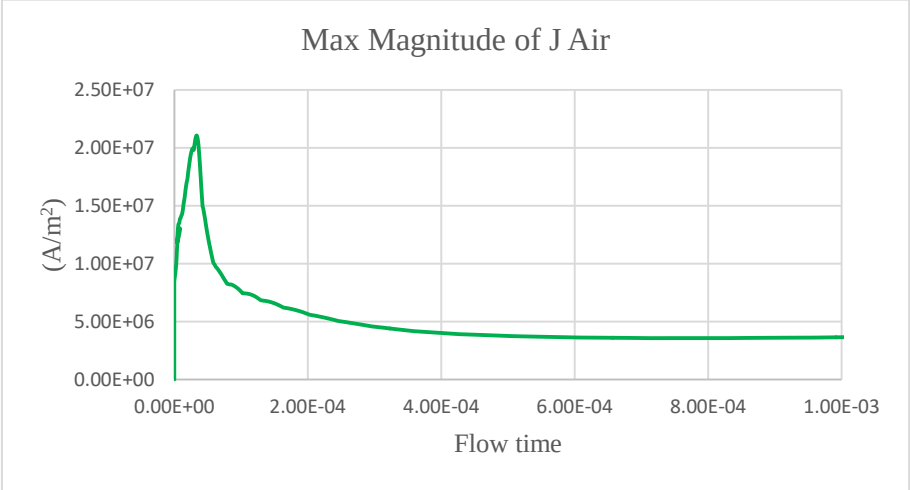

Figure 5-32 Maximum current density in the air for case E1.

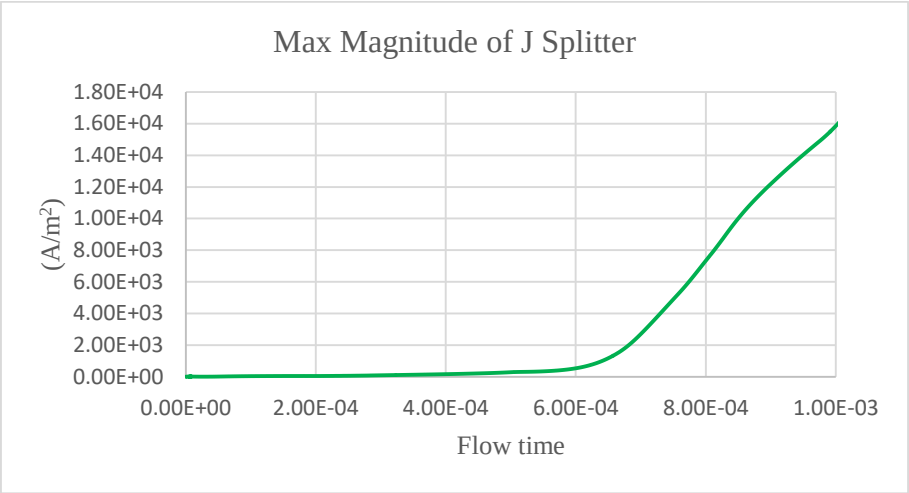

Figure 5-33 Maximum current density at the splitter for case E1.

Now the current density in the splitter is analyzed (Figure 5-33). From 0 to 0.6ms the current density is practically 0 being this a fair value, since during this period the arc has not reached the lower part of the splitter and therefore the current has not started to flow yet. After this, from 0.6-1.0ms, the current begins to grow up to a maximum value of 1.60 x10^4 A/m^2, which is almost in the same order of magnitude, as reported in [9]. Nevertheless, the arc could not move beyond this point, therefore, it is necessary to make a longer simulation until achieving the complete movement of the arc.

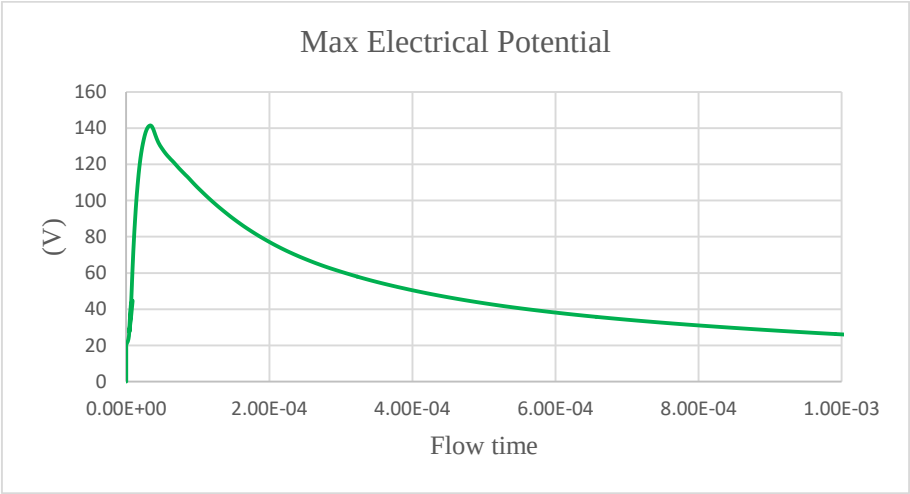

Figure 5-34 Maximum electric potential for case E1.

The voltage values that are measured in this case (Figure 5-34), although the curves for the arc root are not considered, tend to describe a similar behavior to what was is presented in [9]. At the beginning (0ms) it increases until a stop value 143V at 0.03ms. Then it begins to decrease until it stabilizes at a value between 20-30V, instant when the arc begins to surround the splitter. At this point, the voltage is almost constant. Finally, it is not observed that the voltage tends to grow, due to the arc has not entering the splitter, and there is nothing that disturbs its behavior.

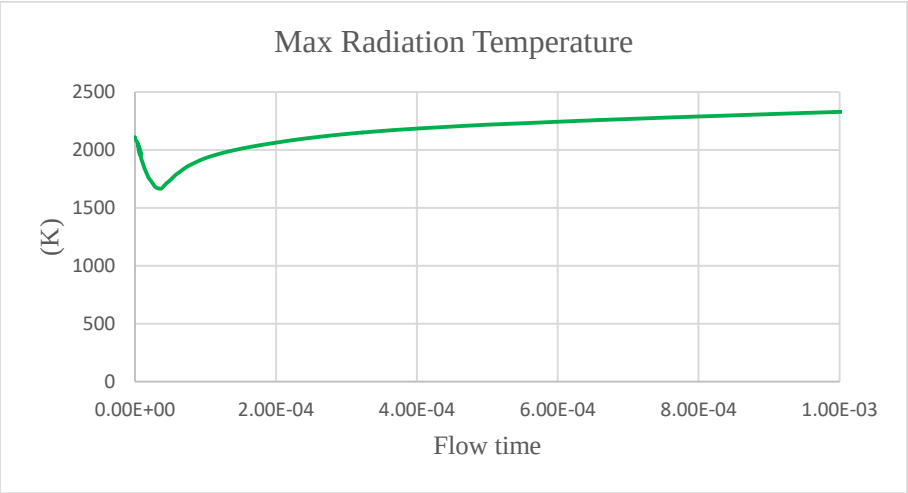

Figure 5-35 Maximum radiation temperature for walls for case E1.

Another important parameter to measure is the increase of temperature by radiation at the walls, the contacts and the splitter. As was explained before, knowing the maximum values that are reached during the electric arc will allow to know if the contact material can tolerate such temperatures. In Figure 5-35 the temperatures in the inner walls of the case B1 are observed, at time 0 the temperature begins to grow to a value above to 2,000K, after this the temperature gradually begins to increase to 2,316K in 0.2-1.0ms. At this point, the temperature does not seem to vary greatly. This behavior is due to, there is no increase in the temperature of the arc, therefore, the amount of energy that it emits by radiation tends to be almost constant. It can be concluded that the material of the contacts would be able to support most of the time this temperature, due to the melting point of copper is 1,358K and vaporization is 2,835K, although, it does not discard the possibility that at some points melting or vaporization will be generated.

Finally, in this section the results of pressure in the air are discussed (Figure 5-36 First, a very large value is observed at the beginning of the simulation (0ms), this is attributed mainly to the initialization of 10,000K which causes the pressure to increase abruptly, but this is only momentary. After this pressure peak, a decrease is observed in 0.05ms, reaching values around 1bar. Subsequently, the pressure stabilizes at this value, without noticeable variation during the rest of the simulation.

It is concluded from this result that the pressure shown here is very close to what is presented in [9], because the values are exactly to the atmospheric pressure (1bar). However, only at the beginning of the simulation there is a very large peak of pressure, and it stabilizes earlier than the model described in [9].

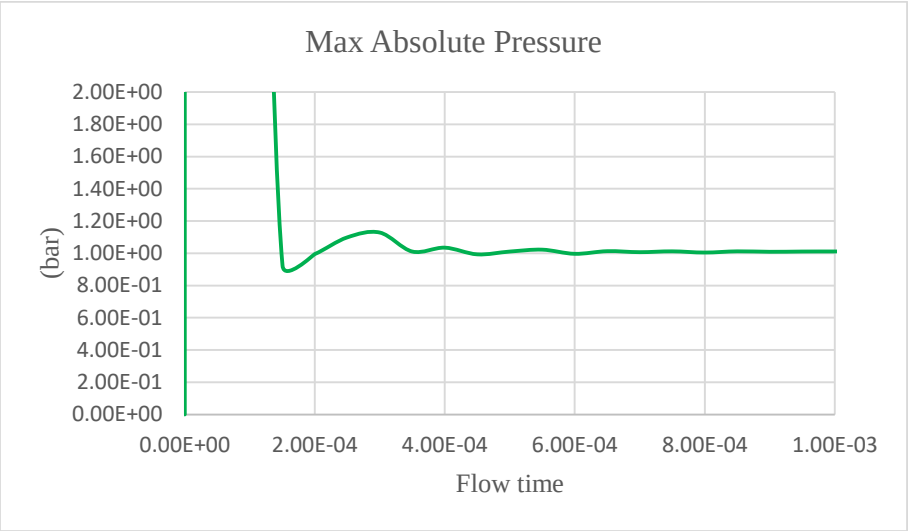

Figure 5-36 Maximum absolute pressure for case E1.

Comparison case B2 vs case E1

Finally, in these two cases a magnetic field were imposed with different magnitudes. For the case B2 a value of 0.1T was used and for the case E1 a value of 0.006T, both in the negative z-direction. First, as expected, for the case E1 the displacement was smaller since the field was about 16 times smaller and this can be corroborated with the results of temperature contours in each case.

Regarding the temperature curves in the air, the results are almost equal, both cases tend to stabilize around 8000K. For the electrical potential, although in both cases reach the same peak values, the behavior over time is different, since for case B2 the voltage stabilizes at around 80V and for the case E1 the voltage tends to fall and stabilize at 20V. It should be noted that the case E1 the total distance traveled by the arc is only up to the splitter, so it does not have the behavior when entering it.

For the current density in both cases, they have the same orders of magnitude, although the values reached vary in each one. But as mentioned before, the case E1 only could model the phenomenon before entering the splitter and, therefore, it is required to make this simulation longer. Finally, in the pressure graph, although in both cases the pressure stabilizes at 1bar, without noticeable variation during the rest of the simulation. It is concluded from this result that the pressure shown here is very close to what is presented in [9], because the values are exactly to the atmospheric pressure (1bar). The comparison between the experimental results of [9] is presented in Annex D

Chapter VI

Conclusions

Nowadays, CBs have become of vital importance to guarantee the integrity of electric equipment and systems, also ensuring the safety of the people who operate them. CBs generally operate at different interruption levels, from high voltage lines to household appliances. In each particular case the way the interrupt the current is a quite different, (electronic CB, vacuum chamber, thermomagnetic, for AC and DC), where the way to reach the interruption varies from one type to another, being for AC easier due to the natural zero crossing, and in the case of DC is a little more complicated due to the absence of this.

However, regardless of the method used or the type of current to be interrupted, the main physical phenomenon that occurs is the formation of an electric arc, with the characteristics of a plasma, which is governed by the Navier-Stokes equations for fluid mechanics, and Maxwell equations for electromagnetic fields. In addition, properties such as viscosity, density, thermal conductivity, specific heat and electrical conductivity are strongly linked to temperature, and varies over a wide range.

Furthermore, in a real short-circuit fall, the electric arc generated inside the CB causes a huge increase in temperature, producing erosion at the contacts and vaporization of metals, mechanical stresses in the walls due to overpressures, values of several tens of KA and large magnetic fields. This is why studying this phenomenon is of vital importance in order to determine an adequate design.

For these reasons, the main objective of this thesis is to provide the methodology to achieve a good characterization of the phenomenon, mainly focused on DC faults, using a simplified CB model. To do this, the Magneto-Hydrodynamic model (MHD) in the Ansys Fluent software is proposed. This model allows the coupling of the Navier-Stokes equations and the Maxwell equations. For this the MHD model is based on some assumptions, such as considering a uniform density for electrons and ions, as well as a uniform density and temperature throughout the fluid, assuming everything is in thermodynamic equilibrium. Unfortunately, the Fluent MHD Module is not capable of calculating the magnetic flux density **B**, to do this, Ansys-Maxwell and Altair-Flux software were used, through a coupling with Fluent.

The model analyzed in this thesis was taken as outlined in [9], but with some modifications. The arc root were not modeled because within the Fluent software this type of boundary condition could not be assigned, also for some simulations a k-ε turbulent regimen is used, a higher volume of air is added in order to avoid reverse-flow in the software, which means that the values of the residuals in the simulation tend not to converge, and finally for the density curves a softened function is used in order to avoid divergence during the simulation, otherwise the simulation diverges (at least for the case B1 in this thesis).

The simulations are divided into several cases (Table 4-1). The size of the model was analyzed in Chapter 3, the dimensions used were 40x11x2.5mm($3D_F$), and

40x11x0.1mm($3D_S$) with four domains (air, splitter, cathode and anode) where the electric arc is ignited at 10mm from the lower face of the chamber by a hot channel of 10,000K. The properties of the plasma were implemented in the model as UDFs, a laminar analysis and a turbulent analysis (k-ε model), and in addition to the effect of the radiation (P1 model). The calculation of the magnetic flux density **B** is carried out using the Maxwell and Flux software.

For cases B, C, and E, the curves analyzed were, current density, temperature and pressure levels, in addition to the radiation temperatures in the walls. In case D, only the magnetic flux density distribution **B** is analyzed.

Case B is the basis for the other analyzes, this is also compared with reference [9], where it is possible to observe a movement and similar shapes. Although the sequence of time do not agree at all, but the ranges of temperatures and current densities are within the same order of magnitude. It is interesting to note that analyzing the arc as a turbulent fluid can greatly influence the time in which it travels, as is mentioned in [44]. Where says that in a turbulent regime the arc is slightly slower than in a laminar one. For cases C and D, the magnetic flux density values are analyzed, which are used as input variables of the last case. For case E, the best values previously calculated in C and D are used, here the results are compared with case B2 since it was the most stable case analyzed. The only data that needs to be considered for futures analysis is the curve of the arc root since Fluent does not allow assigning this boundary condition directly, therefore, it is necessary to write a UDF that facilitates this.

The conclusions of the cases are as follows. For the different analyzed cases, the measurement of temperatures and current densities was done by contours and vectors. Other parameters to be measured were: temperature by radiation, pressure, and voltage.

Related to case A1, the temperature distribution is slower than in case A2, where it expands faster because in 0.14ms the arc is just entering the splitter and in case A2 is already inside. Concluding from this analysis that in the case of $3D_S$ the simulation times are slightly greater than with respect to a $3D_F$, a possible reason for this may be due to the boundary conditions imposed in each case. It should be noted that always a $3D_F$ analysis is better to understand the phenomenon, however, the computational time is too large, and since the only difference between these two simulations is the time and the temperature variation at the beginning of both, it is valid to perform a $3D_S$, thus saving simulation time.

With respect to cases B1 and B2, where a laminar and turbulent analysis is performed respectively, the following conclusions are obtained. The first thing that can be noticed is that they differ in the arc shape, since in the case B1 is very diffuse, reaching only the lower part of the splitter, and for the case B2 the simulation it is completed throughout the arc, reaching almost to the top in 0.8ms.

The electric potential for both cases is within the same order of magnitude, although in case B2 there are values close to double that registered in B1. However, the temperature graphs in the air are very similar, only for the case B1 stabilizes above 10,000K and for case B2 below this temperature. The current densities in the air are observed distant but within the same order of magnitude. In the case of pressures, a very large value is observed at the beginning of the simulation (0ms), this is attributed mainly to the initialization of 10,000K.

After this pressure peak, an instantaneous decrease is observed, reaching values around 1.1bar. Subsequently, the values begin to rise and fall, but always staying close to 1bar. It is concluded from this result that the pressure shown here is very close to the presented in [9], because the values are kept close to the atmospheric pressure.

In case C1 and D1 the most relevant to analyze is the measurement of magnetic flux density **B**. Regarding the orders of magnitude, in both cases they are within the same range (10^{-2}-10^{-3}), with some small differences during the progress of the simulation. From these data, the best results are by Maxwell (Case C1) since it is always calculated with the real shape of the arc. Remains to achieve that Maxwell-Fluent coupling is able to calculate with more precision the magnetic field **B**, or develop a coding that allows calculating **B** within Fluent.

Finally, in case E1 a magnetic flux density more according to real was used, in this case the field is 0.006T, which is about 16 times smaller than case B and this can be corroborated by the results of contours of temperature, since the displacement is much slower, and in 0.8ms the arc only reaches the lower part of the splitter. Regarding the temperature curves in the air, the results are almost equal, both cases (B2 and E1) tend to stabilize around 8000K. The same for the current density, since in both cases they have the same orders of magnitude, although the values reached vary a little. Therefore, if it is wanting to observe the complete movement of the arc, it is necessary to prolong the simulation time more, although this will lead to more calculation time. What remains to be done is to develop a coding that allows calculating **B** within a single software, with this it is expected to reduce the computational time.

As a final conclusion, the MHD methodology is adequate for the modeling of the electric arc phenomenon, assuming that there is only one fluid whose properties are strongly linked to pressure and temperatures. Following all the steps outlined in this thesis it is possible to approach the results of other authors, however, the methods of solving the equations used in each software must be the most robust. With the MHD module of Ansys-Fluent, the coupling of the Navier-Stokes and Maxwell equations is possible, allowing to simulate the behavior of the arc under the influence of an external magnetic field. Among the most important variables to be measured in this type of simulation should be current density, temperature and pressure, other data will be of interest but the main ones should be the mentioned above.

As a final point, and by way of thanks, the work developed in this thesis entitled "*Characterization of Arc Extinction in Direct Current Residential Circuit Breakers*" has been developed at the Tecnológico de Monterrey, at the request of the company Schneider-Electric, which provided the equipment and advice at all times. With the development here, it remains only to say that there is still much work to be done because this is only the beginning of a great project.

Chapter VII

Future work

Regarding the future work there is still a lot of work to do with the developed in this thesis, some proposed ideas are:

- Consider the effect of the Arc-root during the simulations, since in this thesis were omitted due to the software was not able to model them. One way to characterize them would be through UDFs at the contact boundaries. In this way, will be possible to obtain results more similar to the presented in [9].
- Perform a codification that allows the calculation of magnetic flux density **B** within a single software, without the need of performing a coupling, since this generates long simulation times.
- Make a laminar regime simulation, that is stable and compare it with one in a turbulent regime.
- Consider steel-1010 in the splitter, since this is the commercial material with which they are manufactured.
- Carry out the cases C and E considering the $3D_F$ geometry.
- Select other solution methods within the Fluent software, in order to determine which improves the convergence of the results and avoid divergence during simulation.
- Use the real curve for plasma density, since in this thesis a softer one had to be used.
- Analyze the contact opening through a dynamic mesh.
- Simulate a real life short-circuit fault (10KA).
- Use a more realistic CB model with all the materials used, contact movement and vaporization metals.
- Finally, carry out experimental tests in a static model as proposed in [9], this way it will be possible to corroborate if the results are similar to the obtained during simulations.

Bibliography

[1] H. Pugliese and M. VonKannewurff, “Direct current circuit breaker primer,” *Rec. Conf. Pap. - Annu. Pet. Chem. Ind. Conf.*, pp. 1–7, 2010.

[2] G. D. Gregory, “Applying Low-Voltage Circuit Breakers in Direct Current Systems,” *IEEE Trans. Ind. Appl.*, vol. 31, no. 4, pp. 650–657, 1995.

[3] H. Yang *et al.*, “Back-to-back capacitor bank switching performance of vacuum interrupters: Comparison of three contact materials,” *2nd Int. Conf. Electr. Power Equip. - Switch. Technol. ICEPE-ST*, pp. 1–4, 2013.

[4] R. A. Dobre, I. Oleș, C. Negrescu, and D. Stanomir, “Modelling and Simulation of a High-Voltage Direct Current Ballistic Circuit Breaker,” *39th International Spring Seminar on Electronics Technology (ISSE)* pp. 332–335, 2016.

[5] T. Qin, E. Dong, Y. Wang, and J. Zou, “Influence of the Contact Opening Speed on DC Vacuum Arc,” *IEEE Trans. Plasma Sci.*, vol. 43, no. 3, pp. 878–883, 2015.

[6] B. Liu, J. Wu, L. Zhu, and Y. Sun, “Vacuum Arc Characters Research on DC Forcing Interruption,” *1st International Conference on Electric Power Equipment – Switching Technology, China.* pp. 4–7, 2011.

[7] S. Hanashiro, Y. Nikadori, and E. Kaneko, “Investigation on Small DC Vacuum Arc Characteristic under Transverse Magnetic Field,” *3rd International Conference on Electric Power Equipment - Switching Technology (ICEPE-ST), Korea.* pp. 138–141, 2015.

[8] K. A. Corzine, “A new-coupled-inductor circuit breaker for dc applications,” *IEEE Trans. Power Electron.*, vol. 32, no. 2, pp. 1411–1418, 2017.

[9] A. I. Aio, “Modelization and analysis of the electric arc in low voltage,” *Escuela Técnica Superior De Ingeniería De Bilbao,* 2013.

[10] F. Reichert, "Numerische Simulation strömungsmechanischer Vorgänge in SF_6 - Hochspannungsleistungsschaltern". *Universitätsverlag Ilmenau*. 2015

[11] CFX Berlin Software GmbH, “CFX Berlin Software GmbH Simulationskompetenz aus Berlin.” 2015.

[12] Schneider-electric, “QO(B) miniature circuit breakers for QO systems,” 2017. [Online]. Available: http://www.schneider-electric.us/en/product-range/7229-square-d™-qo™-and-qob-miniature-circuit-breakers/. [Accessed: 22-Apr-2017].

[13] R. Gati, J. Ostrowski, M. Schwinne, M. Dhotre, B. Galletti, and Y. Xiangyang, “Switching analysis,” *ABB Rev.*, vol. 3, no. 13, pp. 34–37. 2015.

[14] H. Nordborg, “Simulations of Electrical Arcs: Algorithms, Physical Scales, and Coupling.” *HSR University of Applied Sciences Rapperswill*. 2011

[15] C. Besnard. “Technical Study Internal Arc Guide Theory & Phenomena.” *Schneider-Electric,* ET 487 EN. 2008.

[16] K. Pechrach, "Arc Control in Circuit Breakers Low Contact Velocity". *Saarbrücken, Germany: VDM Publishing House Ltd*., 2009.

[17] J. C. Das, "Arc-flash hazard calculations in LV and MV DC systems - Part I: Short-circuit calculations," *IEEE Trans. Ind. Appl.*, vol. 50, no. 3, pp. 1687–1697, 2014.

[18] A. Nilsson, "Pre-Study of Arc Extinguishing Techniques for a 4-Pole 1500 VDC Contactor," *Department of Applied Physics Chalmers University of Technology*. 2014.

[19] IEEE Industry Applications Society, "Protection and Coordination ofIndustrial and CommercialPower Systems". *IEEE Std 242-2001 BOOK*, 2001.

[20] L. Rendot, "Modélisation magneto-hydrodynamique par la méthode des volumes finis: Application aux plasmas de coupure Loïc Rondot" *Institut polytechnique de Grenoble*, 2010.

[21] E. M. Belbel and M. Lauraire, "Behaviour of Switching Arc in Low Voltage Limiter Circuit Breaker," *IEEE Trans. components, hybrids Manuf. Technol.*, vol. CHMT 8, no. 1, p. 4, 1985.

[22] Q. Wang, X. Li, S. Member, D. Chen, and S. Member, "Analysis of the Interruption Process of Selective Miniature Circuit Breaker With Permanent Magnet Release," *IEEE Trans. Components, Packag. Manuf. Technol.*, vol. 4, no. 7, pp. 1177–1183, 2014.

[23] K. Pechrach, *Arc Control in Circuit Breakers Low Contact Velocity*. VDM Publishing House Ltd., 2009.

[24] D. A. Chávez Campos, "Effect of the electromagnetic fields in the process of arc extinction in molded case circuit breakers," Instituto Tecnológico y de Estudios Superiores de Monterrey, 2018.

[25] S. Rau, S. Member, and W. Lee, "DC Arc Model Based on 3-D DC Arc Simulation," *IEEE Trans. Ind. Appl.*, vol. 52, no. 6, pp. 5255–5261, 2016.

[26] K. Bo, X. Zhou, and G. Zhai, "Investigation on Arc Dwell and Restriking Characteristics in DC High-Power Relay," *IEEE Trans. Plasma Sci.*, vol. 45, no. 6, pp. 1032–1042, 2017.

[27] H. Wu, X. Li, D. Stade, and H. Schau, "Arc Fault Model for Low-Voltage AC Systems," *IEEE Trans. Power Deliv.*, vol. 20, no. 2, pp. 1204–1205, 2005.

[28] R. Morel, "Cahier technique no . 154 LV circuit-breaker breaking techniques," Cahier Technique Schneider Electric no. 154 / p.2, 2000.

[29] M. R. A. Laurens, R. Monrrel, "The low voltage limiting circuit-breaker," *schneider Electr.*, p. 7, 1996.

[30] Study Electrical Engineering Online, "Circuit Breaker - Design and Construction Basics," 2016. [Online]. Available: http://www.studyelectrical.com/2016/01/circuit-breaker-design-and-construction-basics.html. [Accessed: 12-Apr-2017].

[31] S. Electric, "CIRCUIT BREAKERS AND SWITCHES," 2017. [Online]. Available:

http://www.schneider-electric.com/en/product-category/4200-circuit-breakers-and-switches/?filter=business-4-low-voltage-products-and-systems. [Accessed: 12-Apr-2017].

[32] A. Farahat, "CIRCUIT BREAKERS:OIL CIRCUIT BREAKERS," 2015. [Online]. Available: http://machineryequipmentonline.com/electric-equipment/circuit-breakersoil-circuit-breakers/.

[33] J. Shullaw, "DC Power Circuit Breaker Basics," IEEE HVCB Subcommittee Meeting, p. 9, 2011.

[34] C. Gonzalez, "Engineering Essentials: Relays and Contactors," *2014*. [Online]. Available: http://www.machinedesign.com/motion-control/advanced-magnet-design-fine-tunes-motion-down-smallest-nanometer.

[35] skm-eleksys, "SF6 Circuit Breaker Working Principle," 2014. [Online]. Available: http://www.skm-eleksys.com/2012/02/sf6-circuit-breaker-working.html.

[36] X. Li, C. Bao, and H. Wu, "Simulation of Multi-Physical Fields in a Fault Arc," no. 3, pp. 69–73, 2015.

[37] Fluent Inc., "Magnetohydrodynamics (MHD) Module Manual." Lebanon, NH 03766, p. 47, 2006.

[38] ANSYS INC, "ANSYS Maxwell," 2018. [Online]. Available: https://www.ansys.com/products/electronics/ansys-maxwell.

[39] Altair Flux, "Flux Overview," 2018. [Online]. Available: https://altairhyperworks.com/product/flux.

[40] CFD online, "Meshing," 2012. [Online]. Available: https://www.cfd-online.com/Wiki/Meshing.

[41] ANSYS INC, "UDF Manual." 2013. [Online] p. 684. Available: http://users.ugent.be/~mvbelleg/fludf-12-0.pdf

[42] A. Gleizes, Y. Cressault, and P. Teulet, "Mixing rules for thermal plasma properties in mixtures of argon, air and metallic vapours," *Plasma Sources Sci. Technol.*, vol. 19, no. 5, 2010.

[43] ANSYS INC, "Boundary Conditions," 2006. [Online]. Available: http://www.southampton.ac.uk/~nwb/lectures/GoodPracticeCFD/Articles/BCs_Fluent-v6.3.04.pdf.

[44] M. Xi, "a comparative study of k-epsilon turbulence model in DC circuit breaker," no. August 2014, 2016.

[45] A. Piel, *Plasma physics : an introduction to laboratory, space, and fusion plasmas*. Berlin London: Springer, 2010.

[46] A. A. Fridman and A. K. Lawrence, *Plasma physics and engineering*. Boca Raton, FL: CRC Press, 2011.

[47] L. Wang, K. Qin, L. Hu, X. Zhang, and S. Jia, “Numerical Simulation of Vacuum Arc Behavior Considering Action of Adjacent Phases in Vacuum Circuit Breakers,” *IEEE Trans. Plasma Sci.*, vol. 45, no. 5, pp. 859–867, 2017.

[48] S. Shkol’nik, “Anode phenomena in arc discharges :,” *Plasma Sources Sci. Tecnnol.*, vol. 20, no. 13001, 2011.

[49] M. Abbaoui and B. Cheminat, “Determination of the Characteristics of an Electric Arc Plasma Contaminated by Vapors From Insulators jpI,” *IEEE Trans. Plasma Sci.*, vol. 19, no. I, 1991.

Appendix A. The Physics of Electric Arc.

Thermal plasma.

The plasma state is a gaseous mixture of positive ions and electrons [45][46]. Plasmas can be fully ionized, as the plasma in the Sun, or partially ionized, as in fluorescent lamps, which contain a large number of neutral atoms. Here, there are a huge number of charged particles that interact by electric forces. Before going deeper into definitions of the plasma state, it is necessary to recall the characteristic properties of a neutral gas [24].

- Has a number of particles per unit volume, (density n [m^{-3}])
- Motion of particles (in thermodynamic equilibrium) is determined by the temperature T of gas.
- In an ideal gas, the product of number density and temperature gives the pressure, $p = nk_BT$, in which k_B is Boltzmann's constant.
- the plasma state has a mixture of two different gases, light electrons, and heavy ions.
- has individual densities, n_e and n_i in a non-equilibrium state with different temperatures, T_e and T_i of electrons and ions.

Such two-temperature plasmas are typically found in gas discharges. The solar plasma (in the interior and photosphere), on the other hand, is a good example for an isothermal plasma with Te=Ti.

The difference between a neutral gas and a plasma are listed as follow:

- in a neutral gas, particles interact only during a collision,
- when two gas atoms "feel" the short-range van der Waals force, decays with the interparticle distance as r−6.
- the gas atoms fly on a straight path independent of the other atoms. This is quite different in a plasma.
- the Coulomb force that describes the electrostatic interaction decays only slowly as r−2, which makes it a long-range force,
- plasma particle interacts with a large number of other particles, therefore,
- plasmas show a simultaneous response of many particles to an external stimulus.

In this sense, plasmas show collective behavior, which means that the macroscopic result to an external stimulus is the cooperative response of many plasma particles. Mutual shielding of plasma particles or wave processes are examples of collective behavior. The use of an electric discharge is one of the most common ways to create and maintain a plasma [46]. Here, the energy from the electric field is accumulated between collisions by the electron that subsequently transfers a portion of this energy to the heavy neutral particles through collisions. Even with a high collision frequency, the electron temperature and heavy

particle temperature normally will be different. Because the collision frequency is pressure dependent, high pressures will increase this frequency and the electron's mean free path between collisions will decrease.

In a gas discharge (electric arc) with a low degree of ionization, the motion of electrons and ions is governed by the applied electric field and collisions with the atoms [21], [45]–[49] of the background gas. Most of the electron collisions are elastic. Therefore, the ionizing collisions in the calculation of friction forces will be neglected. Because of the equal mass of positive ions and atoms of the parent gas, the momentum exchange between the heavy particles is very efficient. Besides elastic scattering, the process of charge exchange plays an important role, in which a moving ion captures an electron and leaves a slow ion behind. In the momentum balance, this process is equivalent to a head-on collision in a billiards game. The Figure A-1, shows the electron movement in a homogeneous electric field.

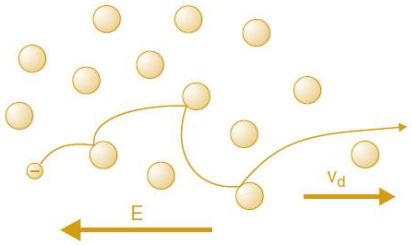

Figure A-1 Electron trajectory in a homogeneous electric field. The trajectory is interrupted by elastic collisions with neutral atoms.[45]

About electromagnetism, there are two types of velocity, the speed of electromagnetic waves and the speed of the electrons, the last is called the drift velocity v_d, which is established when the electric field force is balanced by the friction force. To calculate the value of this velocity is required to know the electron mobility μ_e.

$$v_d = -\mu_e \vec{E}$$

The electron mobility is defined as follows:

$$\mu_e = \frac{e}{v_m}$$

Where v_m is called as the effective collision frequency for momentum transfer. This quantity is inherent to the material. These quantities describe the electric arc discharge, these could be calculated only as a single particle, to be calculated as a set of electrons there exist several fluid models, for example, the MHD.

Appendix B. The MHD module of Ansys-Fluent.

The MHD module of Fluent allows the coupling between the magnetic fields and the behavior of the fluids under the action of these. It is based on two fundamental effects: the induction of electric current due to the movement of conducting material in a magnetic field, and the effect of Lorentz force as the result of electric current and magnetic field interaction. (All the information of this appendix had been taken from reference [37])

Electromagnetic fields are described by Maxwell's equations:

$$\nabla \cdot \boldsymbol{B} = 0 \qquad \textit{Ec. B-1}$$

$$\nabla x \boldsymbol{E} = -\frac{\partial \boldsymbol{B}}{\partial t} \quad \textit{Ec. B-2}$$

$$\nabla \cdot \boldsymbol{D} = q \qquad \textit{Ec. B-3}$$

$$\nabla x \boldsymbol{H} = \boldsymbol{J} + \frac{\partial \boldsymbol{D}}{\partial t} \quad \textit{Ec. B-4}$$

The induction Fields $\boldsymbol{H}$ and $\boldsymbol{D}$ are defined as:

$$\boldsymbol{H} = \frac{1}{\mu}\boldsymbol{B} \qquad \textit{Ec. B-5}$$

$$\boldsymbol{D} = \varepsilon \boldsymbol{E} \qquad \textit{Ec. B-6}$$

In studying the interaction between flow field and electromagnetic field, it is critical to know the current density **J** due to induction. Generally, two approaches may be used to evaluate the current density. One is through the solution of a magnetic induction equation; the other is through solving an electric potential equation.

Magnetic Induction Method

In the first approach, the magnetic induction equation is derived from Ohm's law and Maxwell's equation. The equation provides the coupling between the flow field and the magnetic field.

In general, Ohm's law that defines the current density is given by:

$$\boldsymbol{J} = \sigma \boldsymbol{E} \qquad \textit{Ec. B-7}$$

Where σ is the electrical conductivity of the media. For fluid velocity field **U** in a magnetic field **B**, Ohm's law takes the form:

$$\boldsymbol{J} = \sigma(\boldsymbol{E} + \boldsymbol{U} x \boldsymbol{B}) \qquad \textit{Ec. B-8}$$

From Ohm's law and Maxwell's equation, the induction equation can be derived as:

$$\frac{\partial \boldsymbol{B}}{\partial t} + (\boldsymbol{U} \cdot \nabla)\boldsymbol{B} = \frac{1}{\mu\sigma}\nabla^2 \boldsymbol{B} + (\boldsymbol{B} \cdot \nabla)\boldsymbol{U} \qquad \textit{Ec. B-9}$$

From the solved magnetic field **B**, the current density **J** can be calculated using Ampere's relation as:

$$\boldsymbol{J} = \frac{1}{\mu}\nabla x \boldsymbol{B} \qquad Ec.\ B\text{-}10$$

Generally, the magnetic field **B** in a MHD problem can be decomposed into the externally imposed field $\mathbf{B_0}$ and the induced field **b** due to fluid motion. Only the induced field **b** needs to be solved. From Maxwell's equations, the imposed field $\mathbf{B_0}$ satisfies the following equation:

$$\nabla^2 \boldsymbol{B_0} - \boldsymbol{\mu}\sigma' \frac{\partial \boldsymbol{B_0}}{\partial t} = 0 \quad Ec.\ B\text{-}11$$

Where σ' is the electrical conductivity of the media in which field $\mathbf{B_0}$ is generated.

Electric Potential Method

The second approach for the current density is to solve the electric potential equation and calculate the current density using Ohm's law. In general, the electric field **E** can be expressed as:

$$\boldsymbol{E} = -\nabla\varphi - \frac{\partial \boldsymbol{A}}{\partial t} \qquad \text{Ec. B-12}$$

Where ' and **A** are the scalar potential and the vector potential, respectively. For a static field and assuming $\mathbf{b} << \mathbf{B_0}$, Ohm's law given in Equation B-8 can be written as:

$$\boldsymbol{J} = \boldsymbol{\sigma}(-\nabla\varphi + (\boldsymbol{U}x\boldsymbol{B_0})) \qquad Ec.\ B\text{-}13$$

For sufficiently conducting media, the principle of conservation of electric charge gives:

$$\nabla \cdot \boldsymbol{J} = 0 \qquad Ec.\ B\text{-}14$$

The electric potential equation is thus given by:

$$\nabla^2\varphi = \nabla \cdot (\boldsymbol{U}x\boldsymbol{B_0}) \qquad Ec.\ B\text{-}15$$

The boundary condition for the electric potential φ is given by:

$$\frac{\partial\varphi}{\partial n} = (\boldsymbol{U}x\boldsymbol{B_0})_{boundary} \cdot \boldsymbol{n} \qquad Ec.\ B\text{-}16$$

For an insulating boundary, where *n* is the unit vector normal to the boundary, and

$$\varphi = \varphi_0 \qquad Ec.\ B\text{-}17$$

For a conducting boundary, where φ_0 is the specified potential at the boundary. The current density can then be calculated from Equation B-13.

With the knowledge of the induced electric current, the MHD coupling is achieved by introducing additional source terms to the fluid momentum equation and energy equation. For the fluid momentum equation, the additional source term is the Lorentz force given by:

$$\boldsymbol{F} = \boldsymbol{J}x\boldsymbol{B} \qquad Ec.\ B\text{-}18$$

Loading the MHD Module. The MHD module is loaded into FLUENT through the text user interface (TUI). The module can only be loaded when a valid FLUENT case file has been set or read. The text command to load the module is:

define → *models* →*addon-module*

A list of FLUENT add-on modules is displayed:

```
Done.
define

/define> models

/define/models> addon-module
Fluent Addon Modules:
     0. None
     1. MHD Model
     2. Fiber Model
     3. Fuel Cell and Electrolysis Model
```

Figure B-1 Modules of ANSYS Fluent.

Select the MHD model by entering the module number 1. During the loading process a scheme library containing the graphical and text user interface, and a UDF library containing a set of user defined functions are loaded into FLUENT. A message Addon Module: mhd2.1...loaded! is displayed at the end of the loading process.

Selecting an MHD Method

The method used for MHD calculation can be selected under MHD Method in the MHD Model panel. The two methods, Magnetic Induction and Electrical Potential. For the Magnetic Induction method, 2 or 3 user-defined scalars are allocated for the solution of the induced magnetic field in 2-D or 3-D cases. The scalars are listed as B_x, B_y and B_z representing the Cartesian components of the induced magnetic field vector. The unit for the scalar is Tesla.

For the Electrical Potential method, 1 user-defined scalar is solved for the electric potential field. The scalar is listed as φ and has the unit of Volt. Table B-1 lists the user-defined scalars used by the two methods.

Table B-1 User-Define Scalars in MHD Model

Method	Scalar	Name	Unit	Description
Induction	Scalar-0	B_x	Tesla	X component of induced magnetic field (b_x)
	Scalar-1	B_y	Tesla	Y component of induced magnetic field (b_y)
	Scalar-2 (3-D)	B_z	Tesla	Z component of induced magnetic field (b_z)
Potential	Scalar-0	Phi	Volt	Electric potential (φ)

For the complete explanation and the characteristics of the MHD Module consult reference [37] "*Magnetohydrodynamics (MHD) Module Manual*", where include all the parameters for the set-up, solution controls, setting up boundary conditions, initialization, iterations, post processing, and other parameters.

Appendix C. User Define Functions (UDFs)

A user-defined function, or UDF, is a program function that can be dynamically loaded with the FLUENT solver to enhance the standard features of the code. UDFs are written in the C programming language. (All the information of this appendix had been taken from reference [41]). UDFs are executed as either interpreted or compiled functions in FLUENT. Values that are passed to the solver by a UDF or returned by the solver to a UDF must be specified in SI units. A UDF allows to:

- Customization of boundary conditions,
- material property definitions,
- surface and volume reaction rates,
- source terms in FLUENT transport equations,
- source terms in user-defined scalar (UDS) transport equations,
- diffusivity functions, etc.

UDFs are defined using Fluent-supplied function declarations. These function declarations are implemented in the code as macros and are referred to in this document as DEFINE (all capitals) macros.

The general format of a DEFINE macro is DEFINE_MACRONAME (udf_name, passed-in variables)

For example,

the macro DEFINE_PROFILE(inlet_x_velocity, thread, index)

defines a profile function named inlet x velocity with two variables, thread and index, that are passed into the function from FLUENT. These passed-in variables are the boundary condition zone ID (as a pointer to the thread) and the index identifying the variable that is to be stored. Once the UDF has been compiled, its name (e.g., inlet x velocity) will become visible and selectable in drop-down lists in the appropriate boundary condition panel (e.g., Velocity Inlet panel) in FLUENT.

The udf.h header file contains definitions for DEFINE macros as well as #include compiler directives for C library function header files. It also includes header files for other Fluent supplied macros and functions (e.g., mem.h). The udf.h file must be written at the beginning of every UDF source code file using the #include compiler directive:

```
#include "udf.h"
```

Grid Terminology

A mesh is broken up into control volumes, or cells. Each cell is defined by a set of grid points (or nodes), a cell center, and the faces that bound the cell (Figure C-1). Fluent uses internal data structures to define the domain(s) of the mesh, assign an order to cells, cell faces, and grid points in a mesh, and establish connectivity between adjacent cells. A thread is the internal name of the data structure in Fluent that is used to represent a (boundary or

cell) zone. Cell threads are groupings of cells, and face threads are groupings of faces. A domain is the internal name of the data structure in Fluent that is used to represent a grouping of node, face, and cell threads in a mesh.

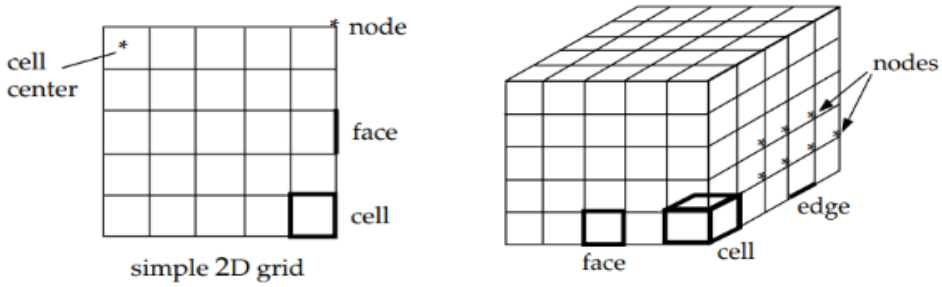

Figure C-1 Grid components [41].

Table C-1 Grid nomenclature.

cell	control volume into which domain is broken up
cell center	location where cell data is stored
face	boundary of a cell (2D or 3D)
edge	boundary of a face (2D or 3D)
node	grid point
cell thread	grouping of cells
face thread	grouping of faces
node thread	grouping of nodes
domain	a group of node, face, and cell threads

Data Types in Fluent

Some of the more commonly-used FLUENT data types are:

cell t
face t
Thread
Domain
Node

- **cell t** is the data type for a cell ID. It is an integer index that identifies a particular cell within a given thread.
- **face t** is the data type for a face ID. It is an integer index that identifies a particular face within a given thread.
- **The Thread data type** is a structure that acts as a container for data that is common to the group of cells or faces that it represents. For multiphase applications, there is a thread structure for each phase, as well as for the mixture. See Section 1.8.1 for details.

- **The Node data type** is a structure that acts as a container for data associated with the corner of a cell or face.
- **The Domain** data type is a structure that acts as a container for data associated with a collection of node, face, and cell threads in a mesh.

In this thesis Is not the main objective explain how to program an UDF, for that reason, for the complete explanation and the programming of the UDFs consult reference [41] "*ANSYS FLUENT 12.0 UDF Manual*", where include all the considerations for the programming and other parameters.

4.2 Example

As was said in chapter 3 some of the parameters to consider are: Dynamic Viscosity (μ), thermic Conductivity (K), Electric Conductivity (σ), Density (ρ), specific Heat (C_p), as a function of temperature for an air-plasma and written as UDFs. An example of how these properties are programmed is like the one shown below.

```
1  /******* UDF that simulates the electric conductivity**************
2  ***************of dry-air plasma at 1 atm ***********************/
3
4  #include <udf.h>
5
6  DEFINE_PROPERTY(electric_conductivity, c,t)
7  {
8  real ele_cond;
9  real temp = C_T(c, t);
10
11     if (temp > 10.0  && temp <=5000.0)     ////10 K && 5000 K
12        ele_cond = 2.0E-05*(temp*temp) + 0.0019*temp - 1.9981;
13
14        else if (temp > 5000. && temp <= 30000.)     ////3000 K && 30000 K
15        ele_cond = 1.0E-17*pow(temp,5) + 1.0E-12*pow(temp,4) - 4E-08*pow(temp,3) + 0.0008*pow(temp,2) - 5.1813*temp + 12266;
16
17        else
18        ele_cond = 13451.6;
19
20
21 return ele_cond;
22 }
```

1
2
3
4

Figure C-2 Example of UDF codification.

In this example, the property for electrical conductivity is coded, in point number 1, the title we want is added, and so that when we access it we can quickly know what the code does. Point 2 indicates the library for the UDF, in this way Fluent can compile it, the DEFINE_PROPERTY text indicates that the UDF will be used to modify a property of the material used, C_T indicates that the temperature value will be taken by all the cells, and this will be used to modify the parameters that are desired. Point 3 is an IF cycle where the intervals are specified for the function that describes the behavior of the electrical conductivity. Finally, point 4 gives a value of electrical conductivity that is assigned to the cell, this is done as a loop until all the cells in the domain have a value assigned as a function of temperature.

The coding is repeated in a similar way for all the other properties of the plasma, thus ensuring that all of them will vary as a function of temperature.

Annex D

Comparative analysis vs experimental test

This section presents a comparison of the cases analyzed in this thesis and the experimental results provided by [9]. In this tests an input current of 50A and one splitter plate have been considered. Unfortunately, was reported that the oscilloscopes did not triggered and so, no voltage, current and pressure data was recorded. But, the arc movement, shown in Figure D-1, was correctly recorded. For this reason, only, the arc movement of the different cases is compared.

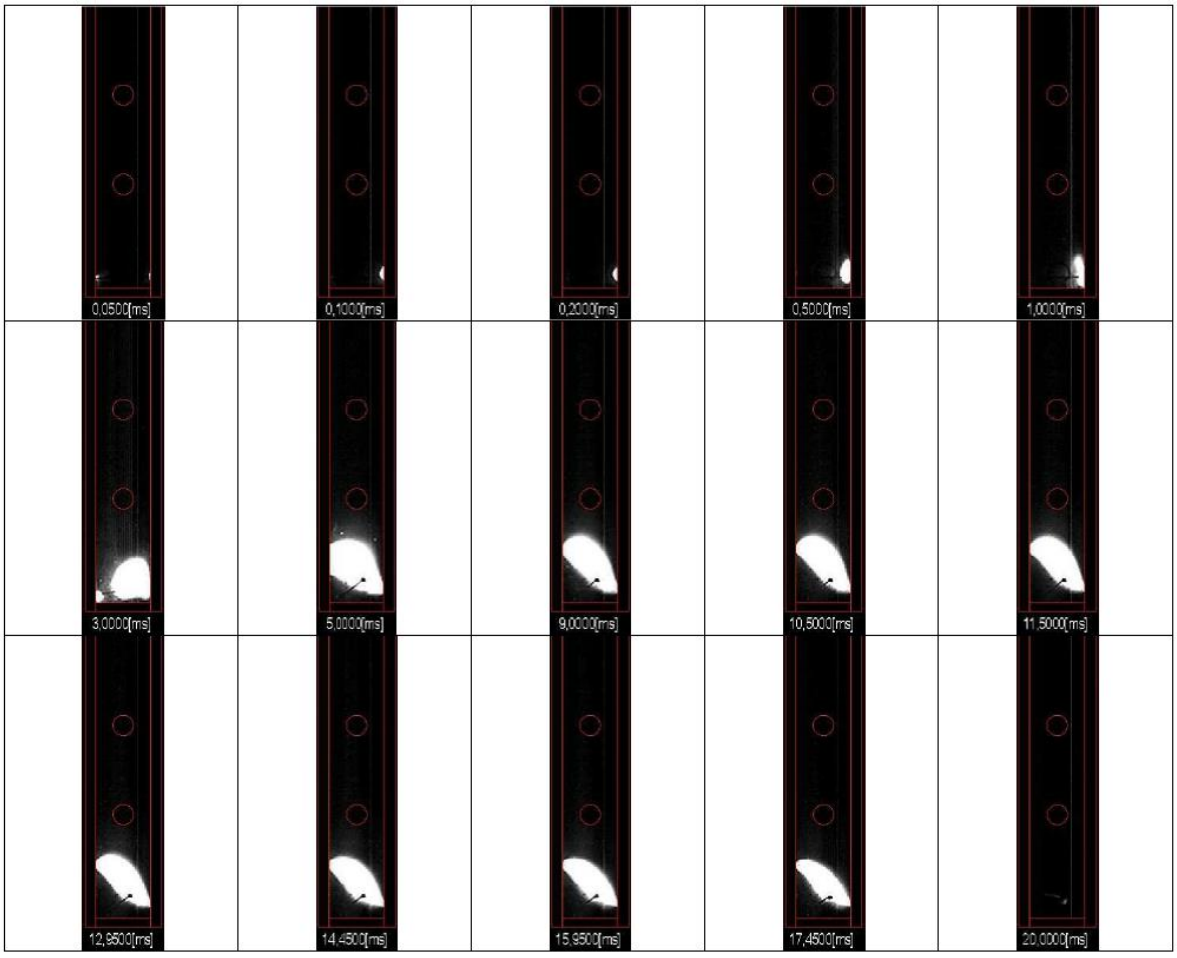

Figure D-1 Arc movement images from reference [9].

As can be observed in Figure D-1 the arc barely moves upward, and before finishing the test (17.45ms) the arc has disappeared. This makes it possible to understand that the arc is extinguished by itself, possibly caused by a cooling of the medium, making it impossible for the current to continue flowing. And as is mentioned in [9], it does not really matter whether the chamber has or not splitter plates, because the arc does not reach that area.

Case B1 vs experimental test

Comparing the results of Figure D-1 it is observed in the first instance that the times do not match, since the experimental tests record times of 20ms, and the simulations time only of 1ms.

However, if only the shapes of the arch are compared, the following can be highlighted. In the laminar case (Figure D-2) the shape of the arc varies greatly with respect to that presented in Figure D-1. For the case laminar the form is completely diffuse, and in Figure D-1 the arc tends to maintain a partially uniform shape. In addition, for case B1 the arc enters the splitter, when for the experimental test it never touches it. Therefore case B1 can be taken as an imprecise result.

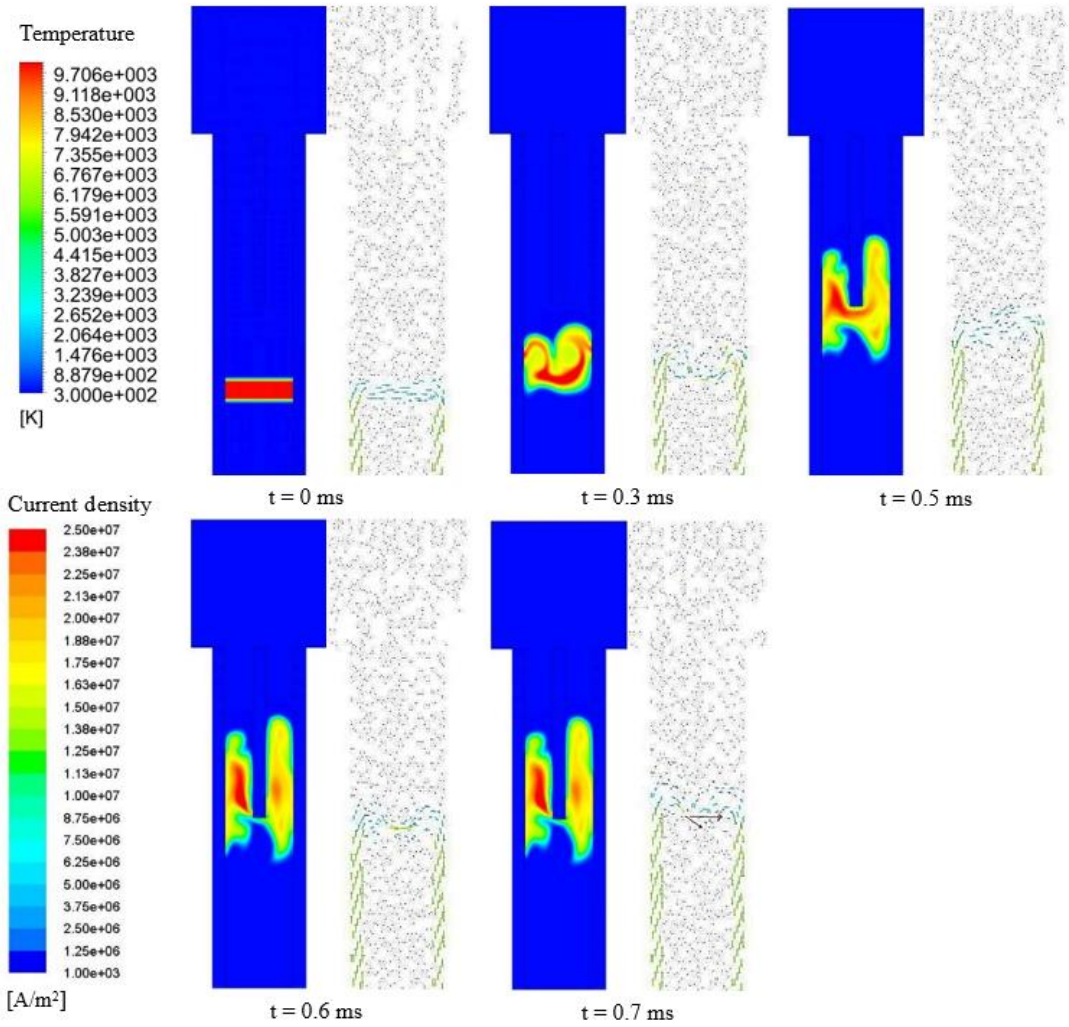

Figure D-2 Arc movement, (temperature and current density) for case B1.

Case B2 vs experimental test

For case B2, the times do not coincide either, so only the arc shape is considered. What can be seen from Figure D-3 is that the arc does reach the splitter, in fact it manages to partially exit the analyzed model. Being the opposite of what is observed in Figure D-1, where the arc always remains below the splitter.

However, it must be remembered that for case B2 an external magnetic flux density was imposed, which causes that there is always a movement of the arc. Therefore case B2 can be taken as a good analysis, as long as it is wanted to know the behavior of an arc under the effects of an external magnetic field.

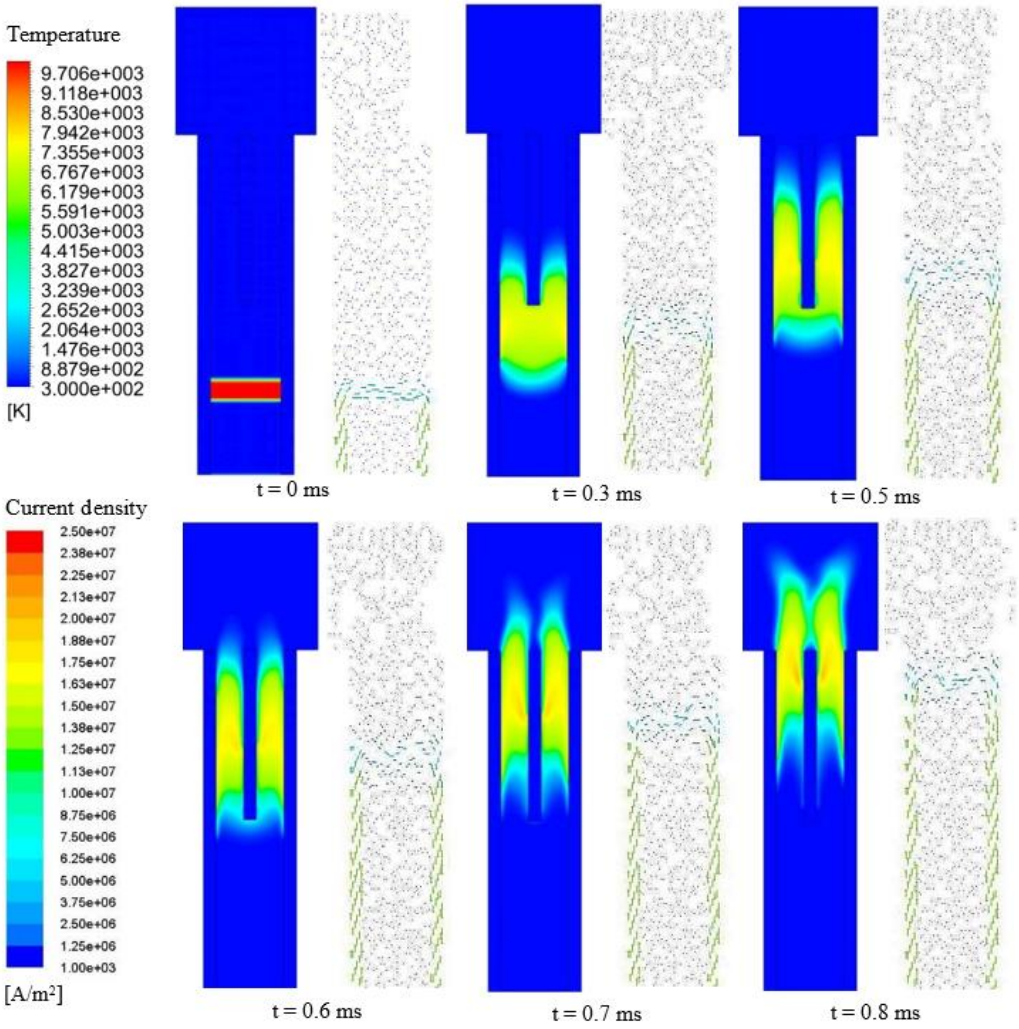

Figure D-3 Arc movement, (temperature and current density) for case B2.

Case C1 vs experimental test

For case C1 (Figure D-4), the times with respect to what is observed in Figure D-1 do not coincide either. However, there is something very interesting for this case. First, the shape of the arc is not uniform, being very similar to Figure D-1. It can also be seen that the arch always remains below the splitter (both cases). This is great news, since the Maxwell-Fluent coupling does better to describe a real-life case. However, it is still necessary to optimize the coupling so that the values can coincide with the real measurements.

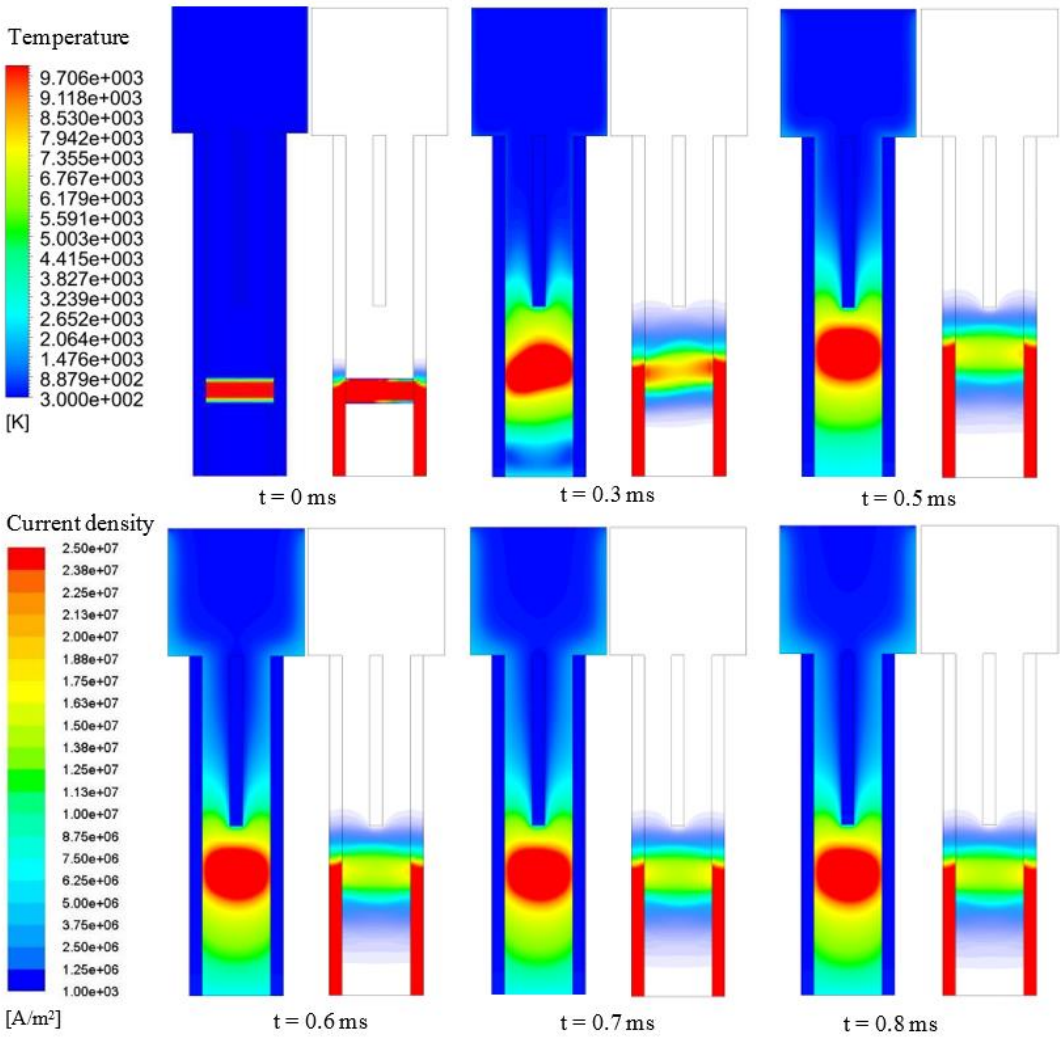

Figure D-4 Arc movement, (temperature and current density) for case C1.

Case E1 vs experimental test

Finally there is the case E1 (Figure D-5), which is very similar to case B1, with the difference of the magnitude of the magnetic flux that is imposed, for this case a fairly small value (0.006T) is assigned. Comparing this result with Figure D-1, it can be observed that the behavior of the arc is very similar, but not the shape of it. For both cases the arc is kept below the splitter, although in the case E1 is very close to it, even touching it. However, like the case B2, the arc will always move, since the magnetic flux is maintained at all times. This analysis can be classified as a good approximation for an arc under the influence of an external magnetic field.

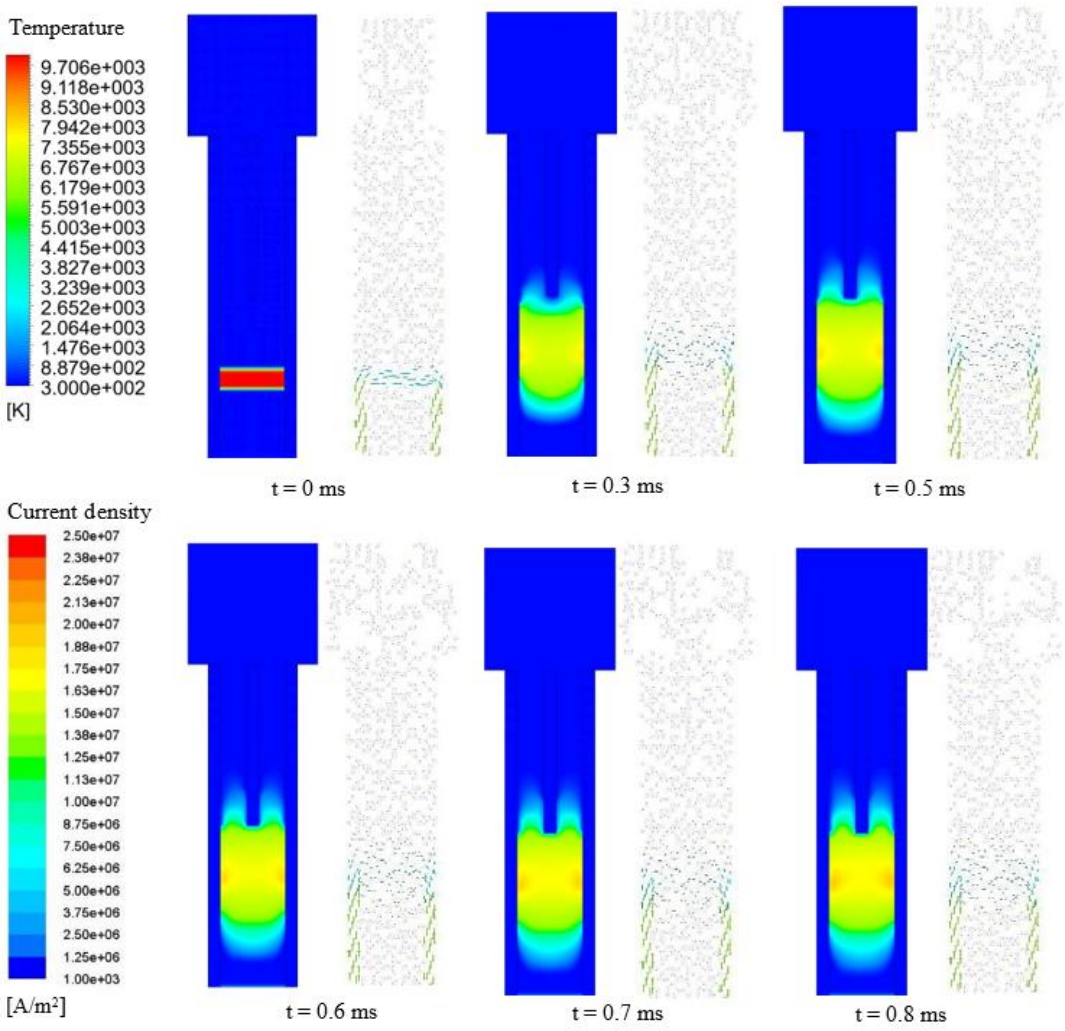

Figure D-5 Arc movement, (temperature and current density) for case E1.

Annex E

Important considerations for simulations

What is covered in this annex is a guide which can help during the simulation process. Some important considerations during the electric arc simulation are as follows:

First, before starting any simulation involving the use of UDFs, it is necessary to check one by one if the coding was done correctly since many errors when compiling in Fluent are caused by bad coding.

It is also important, once correctly coded, to test the UDFs one by one, varying the temperature and measuring if the values calculated in Fluent are equal to what we want to see. Since sometimes there are rounding errors and this can affect the results.

Going to another point, when performing a transient type analysis, it is necessary to start with a very small time-step, since starting with a too large one tends to make a simulation diverge at the beginning, therefore, it is convenient to go increasing the time-steps, until reaching a value that we want. It should be noted that the steps are not the same, should always be calculated based on the type of simulation, geometry, and complexity of the physics to analyze, therefore, this value is more than anything determined by the experience of the engineer.

In addition to the latter, when performing a transient simulation involving many physics, it is convenient to load them one by one, until you see that, with the established conditions, the physicists are able to interact without causing divergence in the simulation.

Finally, when the simulation is initialized and all the physicists interact correctly, they should leave simulating for lapses and check if what is observed is correct.

Julio César Bautista Cruz

Mechanical Engineer.

December 29th, 1992

Monterrey, N.L. México

Julio.bautista.cruz@outlook.es

Julio César Bautista Cruz

EDUCATION AND TRAINING

August 2011 – December 2015

Instituto Tecnológico de Tuxtla Gutiérrez

Tuxtla Gutiérrez, Chiapas.

Mechanical Engineer.

Professional License: 10215876.

Thesis: "Flow Analysis and Structural Optimization in a Wet Membrane Filter"

August 2016 – May 2018

Instituto Tecnológico y de Estudios Superiores de Monterrey

Monterrey, Nuevo León

Master of Science in Energy Engineering.

Specialization area: Electrical and Thermal, (simulations).

Thesis: "Characterization of Arc Extinction in Direct Current Residential Circuit Breakers".

WORK EXPERIENCE

August- December 2015
Querétaro, Qro.

Centro de Ingeniería y Desarrollo Industrial (CIDESI)

Position: Professional internship.

Realization of professional practice in the CIDESI, Querétaro. Conducting the project "Flow Analysis and Structural Optimization in a Wet Membrane Filter".

February – July 2014
Tuxtla Gutiérrez, Chiapas.

Construcciones, Instalaciones de Alta y Baja Tensión, Mantenimientos y Suministros, (CIMAS)

Position: assistant coordinator.

Development of construction budgets in general.

SOFTWARE MANAGEMENT AND COURSES

Intermediate knowledge in analysis of transient phenomena in electrical circuits.
Professional management of SolidWorks.
Professional management of ANSYS Fluent.
Professional management of Altair Flux
Programming in C ++ language
Modeling and simulation of CAD in ANSYS and SolidWorks
Basic course on refrigeration and air conditioning
Programming electrical circuits in SIMULINK-MATLAB
Analysis of steam cycles, gas, combined using EES software
Programming in Arduino
Handling of Office packages at a professional level.

Personal skills

- ***Advanced English (written and spoken).***
- ***Teamwork skills.***
- ***Leadership***

Special acknowledgments

To Instituto Tecnológico de Estudios superiors de Monterrey, since, not only allowed me to study in a prestigious institution, but also made me discover an environment of overcoming and constant improvements, sincerely thanks.

To Schneider-Electric for allowing me to develop a magnificent project, supporting me in each stage of this.

To the support from the *Consejo Nacional de Ciencia y Tecnología* (CONACyT), since this allowed me to support myself throughout my stay in the master's degree.

This thesis has been done in Microsoft Word by Julio César.